
Electronic Thesis and Dissertation Repository

2-7-2017 12:00 AM

Synthesis of Manganese(II) Containing Metal Chalcogen Cluster Complexes from Metal Trimethylsilylthiolate Precursors

Kyle NW Rozic
The University of Western Ontario

Supervisor
John F. Corrigan
The University of Western Ontario

Graduate Program in Chemistry
A thesis submitted in partial fulfillment of the requirements for the degree in Master of Science
© Kyle NW Rozic 2017

Follow this and additional works at: <https://ir.lib.uwo.ca/etd>

 Part of the [Inorganic Chemistry Commons](#)

Recommended Citation

Rozic, Kyle NW, "Synthesis of Manganese(II) Containing Metal Chalcogen Cluster Complexes from Metal Trimethylsilylthiolate Precursors" (2017). *Electronic Thesis and Dissertation Repository*. 4468.
<https://ir.lib.uwo.ca/etd/4468>

This Dissertation/Thesis is brought to you for free and open access by Scholarship@Western. It has been accepted for inclusion in Electronic Thesis and Dissertation Repository by an authorized administrator of Scholarship@Western. For more information, please contact wlsadmin@uwo.ca.

Abstract

The manganese(II)-palladium(II)-sulfide complex $[\text{MnCl}_2(\mu_3\text{-S})_2\text{Pd}_2(\text{dppp})_2]$ **2** has been isolated from the reaction of $[(\text{dppp})\text{PdCl}_2]$ with $[\text{Li}(\text{N,N}'\text{-tmeda})]_2[\text{Mn}(\text{SSiMe}_3)_4]$ **1** in a 2:1 ratio under mild conditions. The trimethylsilyl thiolate complex $[(\text{dppp})\text{Pd}(\text{SSiMe}_3)_2]$ **3** has been synthesized from the reaction of $[(\text{dppp})\text{PdCl}_2]$ with $\text{Li}[\text{SSiMe}_3]$ as well as the reaction of $[(\text{dppp})\text{Pd}(\text{OAc})_2]$ with $\text{Li}[\text{SSiMe}_3]$ under mild conditions. The newly synthesized complex $[(\text{dppp})\text{Pd}(\text{SSiMe}_3)_2]$ **3** was used in reaction with the manganese(II) salt $[(\text{CH}_3\text{CN})_2\text{Mn}(\text{OTf})_2]$ to form the manganese(II)-palladium(II)-sulfide complex $[\text{Mn}(\text{OTf})(\text{thf})_2(\mu\text{-S})_2\text{Pd}_2(\text{dppp})_2]\text{OTf}$ **4**.

The reaction of the trimethylsilyl thiolate complex $[\text{PPh}_3\text{AuSSiMe}_3]$ **5** with the manganese(II) salt $[(\text{CH}_3\text{CN})_2\text{Mn}(\text{OTf})_2]$ was explored and it was found that the previously characterized gold(I) sulfide complex $[\text{S}(\text{AuPPh}_3)_3]\text{Cl}$ **6** was formed as the major product. The reaction of $[\text{Li}(\text{N,N}'\text{-tmeda})]_2[\text{Mn}(\text{SSiMe}_3)_4]$ **1** with ferrocenoyl chloride was explored, however a ferrocene containing manganese(II) sulfide cluster could not be isolated. MS ESI studies revealed the molecular ion $[\text{Mn}(\text{Fc}(\text{C}\{\text{O}\}\text{S}))_3]^-$ to be present in the reaction medium.

Single crystal X-ray crystallography, elemental analysis, NMR spectroscopy, EPR spectroscopy, mass spectrometry, UV-Vis absorption spectroscopy and photoluminescence emission spectroscopy were used as characterization techniques to analyze these complexes.

Keywords:

Silylated reagents, ternary, paramagnetic, chalcogen, chalcogenolate, chalcogenide, manganese, palladium, gold, ferrocene, X-ray crystallography, photoluminescence, UV-Vis absorption, NMR spectroscopy, EPR spectroscopy, mass spectrometry, elemental analysis.

Acknowledgments

I would like to express my sincere thanks to my supervisor Professor John F. Corrigan for his support, guidance and patience during my time at Western University. You have been a great supervisor and your advice and encouragement has helped me enormously during many stressful times.

During my time at Western University, I have been lucky enough to get help and support from many individuals in the chemistry and physics department including Mathew Willans for NMR spectroscopy analyses, Doug Hairsine for mass spectrometry, Tim Goldhawk for SEM/EDX, Paul Bazylewski for EPR spectroscopy, Carolyn Cadogan for photoluminescence emission spectroscopy and Yves Rambour for specialty glassware requests.

I would like to thank all of the members of the Corrigan group that I have had the pleasure of working with over the years, and all of the friends I've made in the department who have made my experience at Western University a great one. I would especially like to thank Bahareh Khalili Najafabadi, Mahmood Azizpoor Fard and Paul Boyle for spending so much time helping with X-ray crystallographic analyses.

Lastly, I would like to thank my friends and my family for their continued support and encouragement over the years. I would not be able to overcome the many challenges I've faced without you.

Co-Authorship Statement

The research discussed in chapters 2 and 3 of this dissertation are the results of experimentation conducted by the author, Kyle Rozic, under the supervision of Prof. John F. Corrigan. The contributions from coworkers at the University of Western Ontario are described here.

Bahareh Khalili Najafabadi performed the crystal structure analysis for complex **2**, found in chapter 2. Mahmood Azizpoor Fard performed the crystal structure analysis for the rest of the structures found in this dissertation. The EDX experiments described in chapter 2 were performed by Paul Bazylewski, and the equipment for the experimentation was supplied by Prof. Giovanni Fanchini. The photoluminescence emission spectroscopy experiments described in chapter 2 were performed by Carolyn Cadogan. Finally, the SEM/EDX experiments described in chapter 3 were performed by Tim Goldhawk at the Western Nanofabrication Facility.

Table of Contents

Abstract	ii
Acknowledgments	iii
Co-Authorship Statement	iv
Table of Contents	v
List of Figures	vii
List of Tables	ix
List of Schemes	x
List of Abbreviations	xi
Chapter One	1
<i>Introduction: Synthetic Technique toward Metal Chalcogen Containing Complexes</i>	
1.1 General Introduction	1
1.2 Synthesis of Metal Chalcogen Containing Complexes	2
1.3 Silylated Precursors	4
1.4 Metal Precursors containing -ESiMe ₃	7
1.5 Ternary Systems	10
1.6 Applications in Semiconductor Doping	13
1.7 Project Summary	15
1.8 References	17
Chapter Two	22
<i>Metal Trimethylsilyl Thiolate Precursors for the Synthesis of Ternary Metal Sulfide Complexes</i>	
2.1 Introduction	22
2.2 Experimental	26
2.2.1. [MnCl ₂ (μ ₃ -S) ₂ Pd ₂ (dppp) ₂] - 2	28
2.2.2. [(dppp)Pd(SSiMe ₃) ₂] - 3	28
2.2.3. [MnOTf(thf) ₂ (μ ₃ -S) ₂ Pd ₂ (dppp) ₂]OTf - 4	29
2.3 Results and Discussion	29
2.3.1 Synthesis of [MnCl ₂ (μ ₃ -S) ₂ Pd ₂ (dppp) ₂] - 2	29
2.3.2 Structural Characterization of [MnCl ₂ (μ ₃ -S) ₂ Pd ₂ (dppp) ₂] - 2	31
2.3.3 Synthesis and Characterization of [(dppp)Pd(SSiMe ₃) ₂] - 3	34

2.3.4	Synthesis of $[\text{MnOTf}(\text{thf})_2(\mu_3\text{-S})_2\text{Pd}_2(\text{dppp})_2]\text{OTf} - \mathbf{4}$	38
2.3.5	UV-Vis Absorption, Emission and EPR Spectroscopy	43
2.4	Conclusion	49
2.5	References	50
Chapter Three		49
<i>Metal Trimethylsilyl Thiolate Precursors for the Formation of Au-S-Mn and FcC{O}-S-Mn Bonding Interactions</i>		
3.1	Introduction	53
3.2	Experimental	55
3.2.1	Attempted Synthesis of $[(\text{NCCH}_3)_2\text{Mn}(\text{SAuPPh}_3)_2]$	57
3.2.2	Attempted Synthesis of $[\text{Mn}(\text{SAuPPh}_3)_4]^{2-}$	57
3.2.3	Attempted Synthesis of $[\text{Mn}(\text{SAuPEt}_3)_4]^{2-}$	58
3.2.4	Attempted Synthesis of $[\text{Mn}(\text{FcC}\{\text{O}\}\text{S})_4]^{2-} - \mathbf{7}$	58
3.3	Results and Discussion	59
3.3.1	Reaction of $[\text{Ph}_3\text{PAuSSiMe}_3] - \mathbf{5}$ with $[(\text{CH}_3\text{CN})_2\text{Mn}(\text{OTf})_2]$	59
3.3.2	Reaction of Reaction of $[\text{Li}(\text{N,N}'\text{-tmeda})]_2[\text{Mn}(\text{SSiMe}_3)_4] - \mathbf{1}$ with $[\text{FcC}\{\text{O}\}\text{Cl}]$	65
3.4	Conclusion	70
3.5	References	71
Chapter Four		68
<i>Summary and Future Work</i>		
4.1	Conclusions	74
4.2	Future Work	75
4.3	References	77
Appendix A		79
Supporting Information for Chapter 2		
Appendix B		81
X-ray Crystallographic Data Parameters for Compounds 2 , 3 and 4		
Curriculum Vitae		96

List of Figures

Figure 1.1.	Common coordination modes of chalcogenide (E^{2-}) ligands	4
Figure 1.2.	Crystal structure of $[Au_2(SeInCl_3)dpppe]_2$ (left) and $[Au_8Se_4In(dppe)_4](InCl_4)_3$ (right). C (grey), Cl (green), In (pink), P (orange), and Se (purple)	11
Figure 1.3.	Molecular structure of $[Mn_{19/20}Ag_{150/148}S_{94}(P^nPr_3)_{30}]$. C (grey), P (green), S (yellow) and Ag (blue)	15
Figure 2.1.	Structure of (clockwise): $[(Ph_2P)_4Pd_2(\mu_3-S)_2Cu(PPh_3)]^+$, $[Cp^{tt_2}Zr(\mu_3-S)_2\{Pd(\eta^3-C_3H_5)\}_2]$, $[(dppp)_2Pd_2(\mu_3-S)_2(SnB_{11}H_{11})]$ and $[PtPd_2(\mu_3-S)_2(dppe)(dppmS-\kappa^2S,P^4)]^{2+}$	24
Figure 2.2.	Molecular structure of complex 2 . Grey spheres represent C, yellow: S, orange: P, blue: Pd, purple: Mn, and green: Cl. Ellipsoids drawn at 50% probability. Hydrogen atoms are omitted for clarity. The molecule resides on a mirror plane which contains the atoms Mn, Pd1, Pd2, Cl1 and Cl2	33
Figure 2.3.	Molecular structure of complex 3 (one of two crystallographically independent molecules). Grey spheres represent C, yellow: S, orange: P, blue: Pd, and beige: Si. Ellipsoids drawn at 50% probability. Hydrogen atoms were omitted for clarity	36
Figure 2.4.	View of molecular structure of 3 showing different geometry of dppp ligand for polymorph A (left) and B (right)	37
Figure 2.5.	Molecular structure of complex 4 . Grey spheres represent C, yellow: S, orange: P, blue: Pd, purple: Mn, red: O, and green: F. Ellipsoids drawn at 50% probability. Hydrogen atoms were omitted for clarity	39
Figure 2.6.	View of molecular structure of 4 showing different P—S—P angles (top) and distortion of square planar geometry around Pd1 (bottom left) and Pd2 (bottom right)	42
Figure 2.7.	UV-Vis absorption spectra of (a) 2 and (b) 4 at different concentrations....	44
Figure 2.8.	Solid state emission spectra of 2 and 4	46
Figure 2.9.	EPR spectrum of 4 in THF. Spectrum parameters: $g = 1.9867$, line width = 3.827, $a = 9.496$ mT	47
Figure 3.1.	Drawing based on the crystallographic data set for $[S(AuPPh_3)_3]_2$	60

Figure 3.2.	EDX analysis and SEM images of crystals acquired from reaction Scheme 3.1	61
Figure 3.3.	(a) Experimental mass spectrum for crystals obtained from reaction Scheme 3.1 (b) Calculated mass spectrum for $[S(AuPPh_3)_3]^+$	63
Figure 3.4.	$^{31}P\{^1H\}$ NMR spectrum of the reaction solution for Scheme 3.1	64
Figure 3.5.	Partial 1H NMR spectrum of the reaction solution outlined in Scheme 3.2	67
Figure 3.6.	(a) Experimental mass spectrum for reaction Scheme 3.3 (b) Calculated mass spectrum for $[Mn(Fc(C\{O\}S))_3]^-$	69

List of Tables

Table 2.1.	Selected bond distances (Å) and angles (deg) for 2	32
Table 2.2.	Selected bond distances (Å) and angles (°) for polymorph A (top) and B (bottom) of complex 3	37
Table 2.3.	Selected bond distances (Å) and angles (deg) for 4	40
Table 2.4.	Electronic Transitions for complexes 2 and 4	43

List of Schemes

Scheme 1.1.	General route for synthesis of various clusters from FcC(O)ESiMe_3 (E= S, Se)	6
Scheme 1.2.	Synthetic route for $\{(\text{dppp})_2\text{Pd}_2\text{-}\mu\text{-}\kappa_2\text{E-[1,2-(ECH}_2)_2\text{C}_6\text{H}_4]\}^{2+}$ (E = S, Se)	7
Scheme 1.3.	Route for preparation of <i>trans</i> - $[\text{Pd}(\text{ESiMe}_3)_2(\text{PnBu}_3)_2]$ complexes	8
Scheme 1.4.	Reaction for the synthesis of $[\text{Li}(\text{N,N}'\text{-tmeda})]_2[\text{Mn}(\text{SSiMe}_3)_4]$	9
Scheme 1.5.	Reaction for synthesis of ternary gold indium selenide cluster $[\text{Au}_2(\text{SeInCl}_3)\text{dpppe}]_2$ (top) and $[\text{Au}_8\text{Se}_4\text{In}(\text{dppe})_4](\text{InCl}_4)_3$ (bottom)	10
Scheme 1.6.	Reaction of $[\text{Pd}(\text{S}_2\text{SiMe}_2)(\text{PEt}_3)_2]$ to yield heterometallic palladium-titanium-sulfide complexes	13
Scheme 2.1.	Reaction of $[(\text{dppf})_2\text{Pd}_2(\mu\text{-S})_2]$ with AgCl to form $[\text{Pd}_2(\text{dppf})_2(\mu_3\text{-S})_2\text{Ag}_2\text{Cl}_2]$	23
Scheme 2.2.	Reaction of <i>cis</i> - $[\text{Pd}(\text{S}_2\text{SiMe}_2)(\text{PEt}_3)_2]$ with $\text{TiCl}_4(\text{thf})_2$ to form $\text{TiCl}_2(\text{S})(\mu_3\text{-S})_2\text{Pd}_2(\text{PEt}_3)_4$	25
Scheme 2.3.	Synthesis of complex 2 $[\text{MnCl}_2(\mu_3\text{-S})_2\text{Pd}_2(\text{dppp})_2]$	30
Scheme 2.4.	Synthesis of complex 3 $[(\text{dppp})\text{Pd}(\text{SSiMe}_3)_2]$	35
Scheme 2.5.	Synthesis of complex 4 $[\text{MnOTf}(\text{thf})_2(\mu\text{-S})_2\text{Pd}_2(\text{dppp})_2](\text{OTf})$	38
Scheme 3.1.	Proposed reaction of $[\text{Ph}_3\text{PAuSSiMe}_3]$ 5 with $[(\text{CH}_3\text{CN})_2\text{Mn}(\text{OTf})_2]$	59
Scheme 3.2.	Proposed reaction of $[\text{R}_3\text{PAuCl}]$ with $[\text{Li}(\text{N,N}'\text{-tmeda})]_2[\text{Mn}(\text{SSiMe}_3)_4]$ 1 ...	65
Scheme 3.3.	Proposed reaction of ferrocenoyl chloride with $[\text{Li}(\text{N,N}'\text{-tmeda})]_2[\text{Mn}(\text{SSiMe}_3)_4]$ 1	66

List of Abbreviations

{ ¹ H}	proton decoupled
{ ¹³ C}	carbon decoupled
{ ³¹ P}	phosphorus decoupled
Å	angstrom
°C	degree Celcius
ε	absorption coefficient
λ	wavelength
A	absorbance
Cl ⁻	chloride anion
dppp	1,2-Bis(diphenylphosphino)ethane (Ph ₂ P(CH ₂) ₂ PPh ₂)
dppf	1,1'-Bis(diphenylphosphino)ferrocene (Ph ₂ P(C ₁₀ H ₈ Fe)PPh ₂)
dpppe	1,5-Bis(diphenylphosphino)pentane (Ph ₂ P(CH ₂) ₅ PPh ₂)
dppp	1,3-Bis(diphenylphosphino)propane (Ph ₂ P(CH ₂) ₃ PPh ₂)
E	any chalcogen atom
EDX	energy-dispersive X-ray spectroscopy
g	gram
<i>J</i>	coupling constant
M	any metal atom
m(NMR)	multiplet
m.p.	melting point
Me	methyl
MHz	MegaHertz
mL	milliliter
mmol	millimole
mol	mole
mT	millitesla
nm	nanometer
NMR	nuclear magnetic resonance
OAc ⁻	acetate
OTf	triflate
Ph	phenyl
ppm	parts per million
ⁱ Pr	propyl
r.t.	room temperature
s(NMR)	singlet
SEM	scanning electron microscopy
THF	tetrahydrofuran solvent
thf	tetrahydrofuran ligand
t(NMR)	triplet

UV-Vis ultraviolet-visible

Chapter One

Introduction: Synthetic Technique toward Metal Chalcogen Containing Complexes

1.1 General Introduction

In order to produce complexes and materials with new and interesting properties, scientists are continually developing different methodologies and synthetic techniques to overcome seemingly impossible feats. In the world of semiconducting clusters and mixed metal coordination complexes, differences in size, elemental composition and coordination about metal centers can produce vast differences in the physical properties of the resulting material. Control over these parameters can prove to be extremely valuable for producing molecules with finely tuned characteristics. In this field, an area of burgeoning materials research involves the chemistry of the Group 16 elements and their interactions with transition metals.¹⁻⁴

The elements oxygen, sulfur, selenium, tellurium, and polonium of Group 16 in the periodic table are generally referred to as “chalcogens”.⁵ Although oxygen is included in this definition, it is often removed from chemical and technological discussions of chalcogen containing materials due to the great differences between the chemical properties of it from that of sulfur and the other, heavier elements. Polonium is of course typically omitted due to its radioactivity and thus less developed chemistry. The chalcogens provide a promising avenue towards diverse and specialized materials due to their ability to both catenate as well as bind to multiple metal centers. When combined with main group and transition metals, metal chalcogenide materials can be produced as precisely defined structures ranging in size from molecular to nanometer scale assemblies. Semiconductor nanomaterials are desirable due to their tunable electronic and photophysical properties which arise from the quantum confinement effect.⁶ Because of the vast range in materials and structures of metal chalcogenides, applications of their properties are found in

various areas including electronics and optics, ion-sensitive electrodes, solar energy harvesting and fuel cells to name a few.⁷⁻¹⁶

The extensive synthetic and structural diversity of metal chalcogenide materials arises due to the ability of chalcogen species to adopt several bridging coordination modes.¹⁷ Though this property provides benefit by allowing diverse structure formation, it also allows for compounds to form bulk solids through numerous reactions of molecular sub-units. Since the electronic and photophysical properties of nanoscale semiconductor systems are dependent on their size and structure, control over both the size and structure of the product through synthetic technique is imperative. The formation of bulk product formation is circumvented by using ancillary ligands such as organochalcogenolate anions, tertiary phosphines or amines to kinetically stabilize both molecular and nanoscale metal-chalcogen assemblies.¹⁸ Modifications in the synthetic approach as well as the precursors involved helps to fine tune the exact composition and structure of the product.

1.2 Synthesis of Metal Chalcogen Containing Complexes

Molecular metal chalcogenides can be synthesized using a number of different methods. Alkali-metal-stabilized chalcogenide anions M^*_2E ($E = S, Se, Te$) have been used to synthesize metal chalcogenides by addition to a ligand-stabilized metal salt L_nM-X .¹⁹

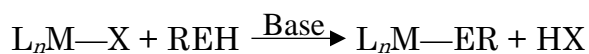


(Eqn 1.1)

The production of a thermodynamically favourable alkali metal halide M^*X drives these reactions forward. The poor solubility of the M^*_2E salt hinders the widespread use of this technique. A similar technique involves the use of chalcogenide anions which are generated in situ from H_2E by deprotonation in a basic solution. This methodology, however, can lead to a multitude of products

and the high toxicity of reagents makes them undesirable to work with.²⁰

Another method involves the use of chalcogenolate anions (RE⁻). These anions can be introduced as either a chalcogenol REH or a diorganodichalcogenide REER (R = alkyl, aryl) (Eqn 1.2 and 1.3). Thermal and photosensitivity of chalcogenol reagents introduce difficulty when using this method with the heavier congeners.²¹ When using a chalcogenol reagent, base is used to neutralize the acid byproduct and increase the yield of the metal chalcogenolate. Diorganochalcogenide reagents don't require base, but do require heat to progress the reaction. Bulky "R" groups also suffer from slow reaction rates.



(Eqn 1.2)



(Eqn 1.3)

Elemental chalcogen inserts directly into a metal-carbon bond, however these reactions normally require high temperatures due to the insolubility of the chalcogen precursor.²²

Both chalcogenide and chalcogenolate ligands are often employed together during the synthesis of metal chalcogenide clusters to simultaneously provide structure to the core (eg. sulfide ligands) and stabilize the surface (eg. thiolate ligands) from further reaction.²³ Chalcogenide ligands have the ability to adopt μ_2 -, μ_3 -, μ_4 - and higher coordination modes allowing multiple metal atoms to be bridged through a single ligand, and when working with larger molecules and/or clusters, serve to provide structure to the core of the complex. The diversity of chalcogenide coordination modes increases with increasing polarizability moving down the periodic table.

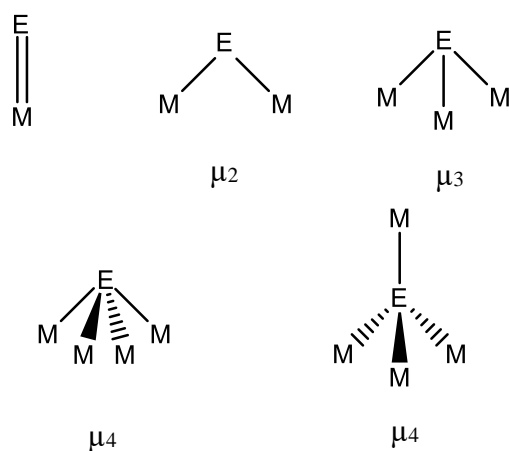
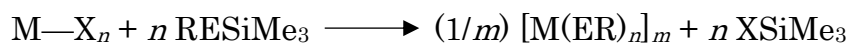


Figure 1.1. Common coordination modes of chalcogenide (E^{2-}) ligands.¹⁹

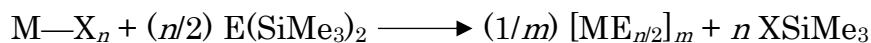
Chalcogenolate ligands (RE^-) tend to bridge metal centers as well, however they do not exhibit the same diverse coordination ability of the electron rich chalcogenide ligands (E^{2-}). Chalcogenolate ligands provide benefit, in that they maintain their organo-substituent in the product and occupy surface sites of the compound. This provides size stabilization by inhibiting bulk material production through condensation reactions and allows for modification of the target complex by altering the electronics and sterics of these “R” substituents. Specific functionality can be employed with the “R” substituent which can be especially useful when synthesizing larger nanometer sized molecules with semiconductor like properties. The techniques described above are useful for the synthesis of metal chalcogenide materials, however they also exhibit drawbacks and leave room for improvement in this chemistry.

1.3 Silylated Precursors

The use of trimethylsilyl (TMS) groups to deliver chalcogen anions to a metal center has been well developed by Fenske and colleagues.²³⁻²⁵ Analogous to the above methodologies, silylated reagents allow for the synthesis of metal chalcogenide systems with structurally diverse architectures. These reagents are ideal because they provide a soluble source of chalcogen for use under mild reaction conditions.



(Eqn 1.4)



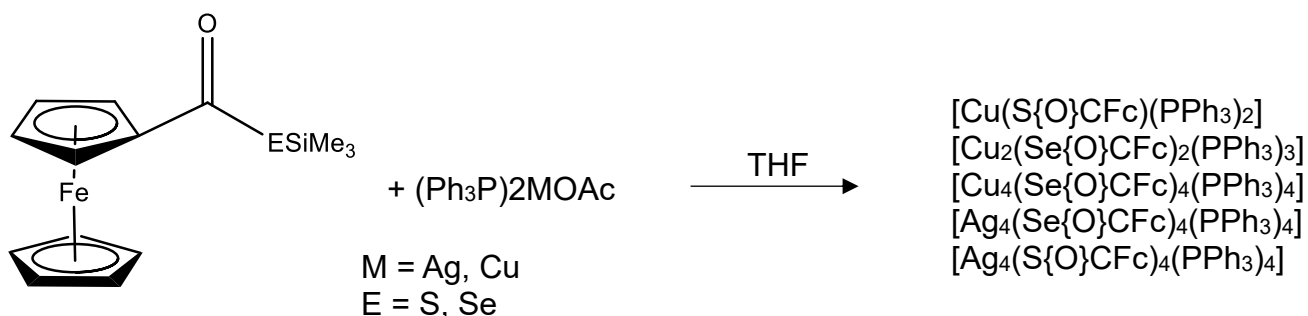
(Eqn 1.5)

The silylated chalcogen reagent $\text{E}(\text{SiMe}_3)_2$ ($\text{E} = \text{S}, \text{Se}, \text{Te}$) can be formed from the reaction of alkali-metal chalcogenide anions M^*_2E with a trimethylsilylhalide such as ClSiMe_3 .²⁶ After reduction of the disulfide RSSR to $\text{M}^*[\text{SR}]$, the reaction of ClSiMe_3 with $\text{M}^*[\text{SR}]$ can produce the RESiMe_3 compound.²⁷ These complexes react readily with various transition metal and main group metal salts to form the corresponding metal chalcogenide (M-E-M) or metal chalcogenolate (M-ER) products (Eqn 1.4 and 1.5).¹⁹ These reactions are driven by the thermodynamically favourable formation of XSiMe_3 ($\text{X}=\text{halide}, \text{acetate}, \text{alkyl}, \text{etc.}$).²⁸ The high solubility of these precursors as well as the silane by-product allows for great control over the formation and crystallization of coordination complexes and nanocluster frameworks.²⁴ These compounds exhibit a long shelf lives and are handled easily, however they do undergo rapid oxidation/hydrolysis with air/moisture to produce toxic H_2S and must be handled and stored under inert conditions.

This method has been utilized to produce binary nanoclusters with sulfur, selenium and tellurium bridging various metal centers including silver, gold, copper, and cadmium to name a few.^{23, 29-32} To synthesize the cluster, a metal salt is generally solubilized in an organic solvent followed by the addition of the chalcogen source at low temperatures. Low temperatures are used to avoid the formation of undesirable polydisperse bulk material. The temperature is then raised, allowing the progression of the reaction to be monitored (qualitatively) through the colour change that accompanies cluster formation, most notably for the group 11 metals.¹⁹

For example, MacDonald and Corrigan have found that a number of polyferrocene functionalized metal chalcogenide structures are accessible through reaction of ferrocenoyl

chalcogenolates with a metal salt.³³ Binary cluster complexes containing ferrocene ligands as the “R” substituent of a chalcogenolate have potential applications in molecular electronics and chemical sensors, causing it to be the focus of much research.³⁴⁻³⁶

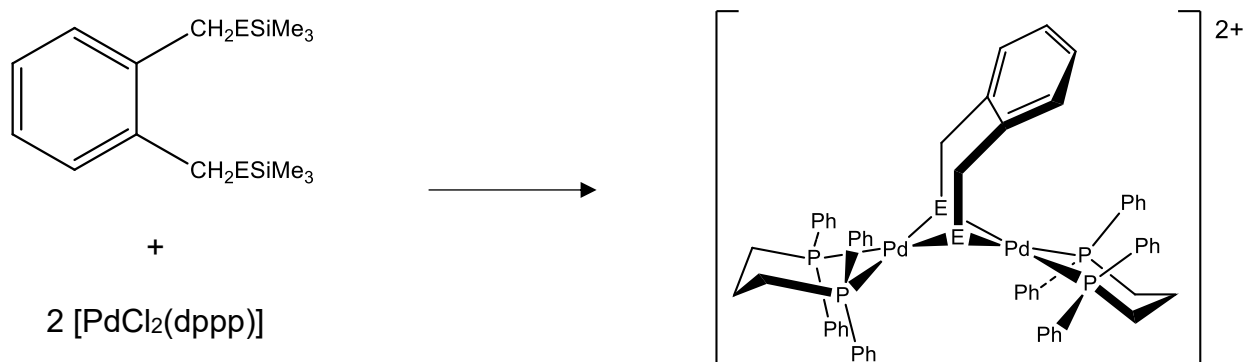


Scheme 1.1. General route for synthesis of various clusters from FcC(O)ESiMe_3 (E = S, Se).³³

Although the ratio of reactants is constant among these reactions, a multitude of structures are observed as products. By altering the chalcogen species and the metal species, different cluster structures form under similar reaction conditions. During the synthesis of the copper(I) selenide complex, it was found that low temperatures were required to produce the dinuclear compound, while room temperature reaction conditions afforded the tetranuclear compound. These reactions display how different structures can be created through a controlled route when utilizing trimethylsilyl chalcogenide precursors.

Recently, Azizpoor Fard and Corrigan have exploited trimethylsilyl organochalcogenolate precursors for the assembly of binary palladium cluster systems.³⁷ Two dinuclear palladium complexes were synthesized, one dithiolate bridged complex $\{(\text{dppp})_2\text{Pd}_2-\mu-\kappa^2\text{S}-[1,2-(\text{SCH}_2)_2\text{C}_6\text{H}_4]\}^{2+}$, and one diselenolate bridged complex $\{(\text{dppp})_2\text{Pd}_2-\mu-\kappa^2\text{Se}-[1,2-(\text{SeCH}_2)_2\text{C}_6\text{H}_4]\}^{2+}$ (dppp = $\text{Ph}_2\text{P}(\text{CH}_2)_3\text{PPh}_2$) (Scheme 1.5). The structural rigidity of the chalcogenolate ligands in these complexes were observed through various types of nuclear magnetic resonance spectroscopy and described in great detail. A third tetranuclear palladium complex $[(\text{dppp})_4\text{Pd}_4-$

$\mu\text{-}\kappa^4\text{S-}\{1,2,4,5\text{-(SCH}_2\text{)}_4\text{C}_6\text{H}_2\}\}^{4+}$ was also synthesized, consisting of an interesting double-butterfly metal-thiolate framework. Since palladium(II) prefers to adopt a *trans* configuration, the chelating dppp ligand is used to force *cis* conformation around the palladium centre which allows the disulfide ligands to bridge the two palladium(II) atoms. This work illustrates that palladium dithiolate bridged butterfly structures are formed through the use of these silylated chalcogenolate precursors, and leaves potential for other related structures to be developed in a similar manner.

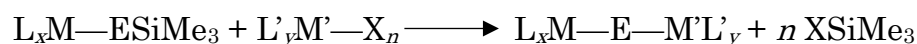


Scheme 1.2. Synthetic route for $\{(\text{dppp})_2\text{Pd}_2\text{-}\mu\text{-}\kappa^2\text{E-}[1,2\text{-(ECH}_2\text{)}_2\text{C}_6\text{H}_4]\}^{2+}$ (E = S, Se).³⁷

1.4 Metal Precursors containing -ESiMe₃

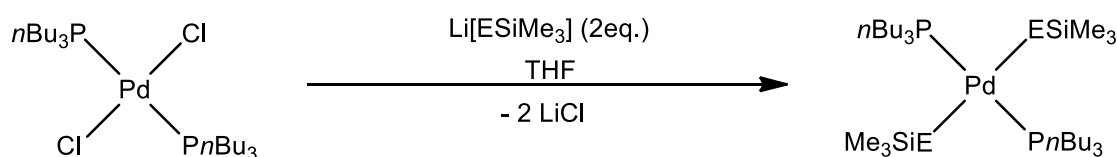
Metal chalcogenolate complexes with TMS functional groups on the chalcogen ligands (M—ESiMe₃) have recently been used to produce ternary metal chalcogenide systems.^{38, 39} These compounds are typically prepared by selectively eliminating a TMS group from E(SiMe₃)₂ by a reaction with a metal salt to form the silyl-functionalized metal chalcogenolate complex. Due to the tendency of chalcogenide (E²⁻) and chalcogenolate (RE⁻) ligands to adopt bridging coordination modes, polynuclear ME systems are often formed under these conditions. Terminal coordination of trimethylsilyl chalcogenolate ligands is especially difficult for late *d*-block metals (i.e. group XI

and XII). The formation of polynuclear species is circumvented by ensuring all available coordination sites around the metal are occupied. This is achieved by the introduction of either chelating phosphine ligands (dppe, dppp) or stronger N-donor ligands. The ligand (L) is introduced in excess prior to reaction with $E(\text{SiMe}_3)_2$.²⁴ Modification of these ligands can affect the reactivity and stability of the metal trimethylsilylchalcogenolate compounds, and different ligands (L') can be used on the secondary metal salt complex $L'M'X$. Depending on the strength of the metal halide bond $M-X$, a more nucleophilic reagent may be required—like an alkali metal trimethylsilyl chalcogenide reagent ($M^*[\text{ESiMe}_3]$, $M^* = \text{alkali metal}$)—to facilitate the displacement of X^- to form the alkali metal salt M^*X as the side product. Lithiated trimethylsilyl chalcogenide compounds can be synthesized by reaction of $E(\text{SiMe}_3)_2$ with $n\text{BuLi}$ to form $\text{Li}[\text{ESiMe}_3]$.²⁶



(Eqn 1.6)

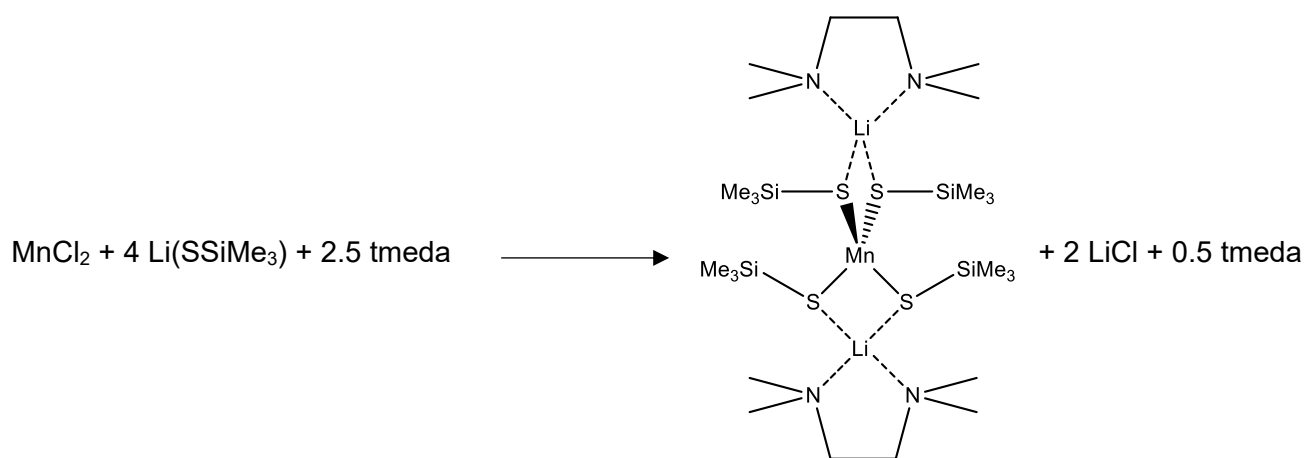
Chalcogenolate functionalized metals can react with other metal salts to produce ternary $MM'E$ systems, as opposed to the extensively studied binary ME systems (Eqn 1.6). The TMS moieties of these complexes react with secondary metal salt precursors to provide the subsequent ternary cluster and $X\text{SiMe}_3$ by-product.^{40, 41}



$E = \text{S, Se}$

Scheme 1.3. Route for preparation of *trans*- $[\text{Pd}(\text{ESiMe}_3)_2(\text{PnBu}_3)_2]$ complexes.⁴²

The Corrigan group has developed this area greatly, and has revealed a wide range of silyl-functionalized metal chalcogenolate complexes in the process.^{42, 43} The square planar silyl-functionalized palladium complex, shown as the product to the reaction in Scheme 1.3, has been produced using this general synthetic route using both sulfur and selenium lithiated precursors (Scheme 1.1).⁴² It is marked as the first trimethylsilyl palladium chalcogenolate complex, and its reactivity with halide precursors was proven with an organic acyl chloride to yield the complex *trans*-[Pd(SeC{O}CH₂CH₃)₂(PⁿBu₃)₂]. Trimethylsilylchalcogenolate functionalization of cobalt and manganese have also been recently explored, with applications in the production of ternary paramagnetic metal chalcogenide systems.⁴⁴



Scheme 1.4. Reaction for the synthesis of $[\text{Li}(\text{N},\text{N}'\text{-tmeda})]_2[\text{Mn}(\text{SSiMe}_3)_4]$.⁴⁴

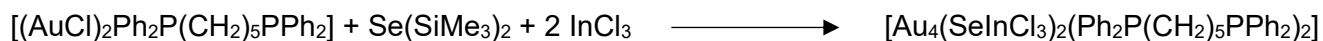
In the reaction of MnCl_2 with LiSSiMe_3 , it was found that the tetrakis(trimethylsilyl)thiolate manganese complex $[\text{Li}(\text{N},\text{N}'\text{-tmeda})]_2[\text{Mn}(\text{SSiMe}_3)_4]$ could be synthesized, having four of its coordination sites occupied by trimethylsilylthiolate ligands. The reagent tmeda was used to allow solvation of manganese(II) dichloride in common solvents. Having coordination sites occupied by $-\text{SSiMe}_3$ opens up the possibility for manganese to be incorporated into the core of a metal chalcogenide cluster for doping applications. These reactions illustrate the ability for the development of reactive trimethylsilylchalcogenolate metal precursors, and their products allow

for the controlled assembly of ternary metal chalcogenide complexes.

1.5 Ternary Systems

Ternary metal chalcogenide systems have not been explored to the extent of their binary counterparts, however some ternary structures have been synthesized using trimethylsilyl functionalized chalcogenide precursors. Depending on the reaction conditions, these materials can range in size from small molecules to large nanoclusters and this allows for the size dependent properties of these materials to be studied.^{45, 46}

Due to their rich photophysical and photochemical properties, gold(I) chalcogenide complexes have received considerable attention in cluster synthesis.⁴⁷⁻⁴⁹ The vast majority of the gold chalcogenide complexes explored have been binary systems due to constraints in conventional synthetic approach.⁵⁰ Through the use of silylated chalcogenide precursors, ternary clusters can also be developed. These heterometallic systems allow for broader control over properties and as such have potential for more applications over binary cluster systems.⁵¹



Scheme 1.5. Reaction for synthesis of ternary gold indium selenide cluster $[\text{Au}_2(\text{SeInCl}_3)\text{dpppe}]_2$ (top) and $[\text{Au}_8\text{Se}_4\text{In}(\text{dppe})_4](\text{InCl}_4)_3$ (bottom).⁵²

In an attempt to expand the field of gold chalcogenide cluster synthesis, Fenske and coworkers have shown that ternary gold chalcogenide clusters are accessible by reaction of $\text{E}(\text{SiMe}_3)_2$ with a combination of metal salts.⁵² In addition to gold-indium-selenide clusters, a gold-

gallium-telluride was also prepared using this methodology. The phosphine ligands provide stabilization to the cluster and prevent the formation of binary gold chalcogenides. Two very different gold indium selenide structures (Figure 1.2) are found to be accessible using this technique through simple modification of the reaction (Scheme 1.5). When the gold precursor is bridged by the phosphine ligand dpppe ($\text{Ph}_2\text{P}(\text{CH}_2)_5\text{PPh}_2$), reaction with InCl_3 results in a four centered gold cluster with two InCl_3 units located on the surface, bonded directly to the bridging $\mu_3\text{-Se}^{2-}$ ligands. However, when the gold precursor is bridged by the phosphine ligand dppe ($\text{Ph}_2\text{P}(\text{CH}_2)_2\text{PPh}_2$) as shown in Scheme 1.5 (bottom), reaction with InCl_3 results in a larger gold selenide structure templated around a central indium atom.

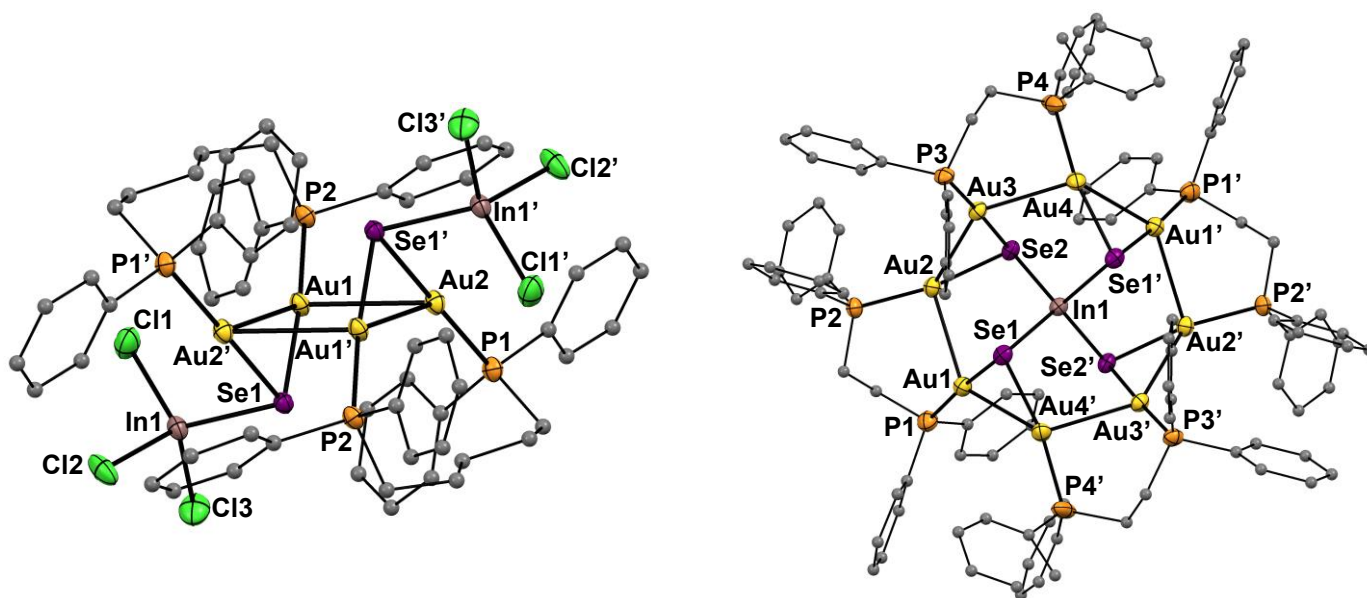


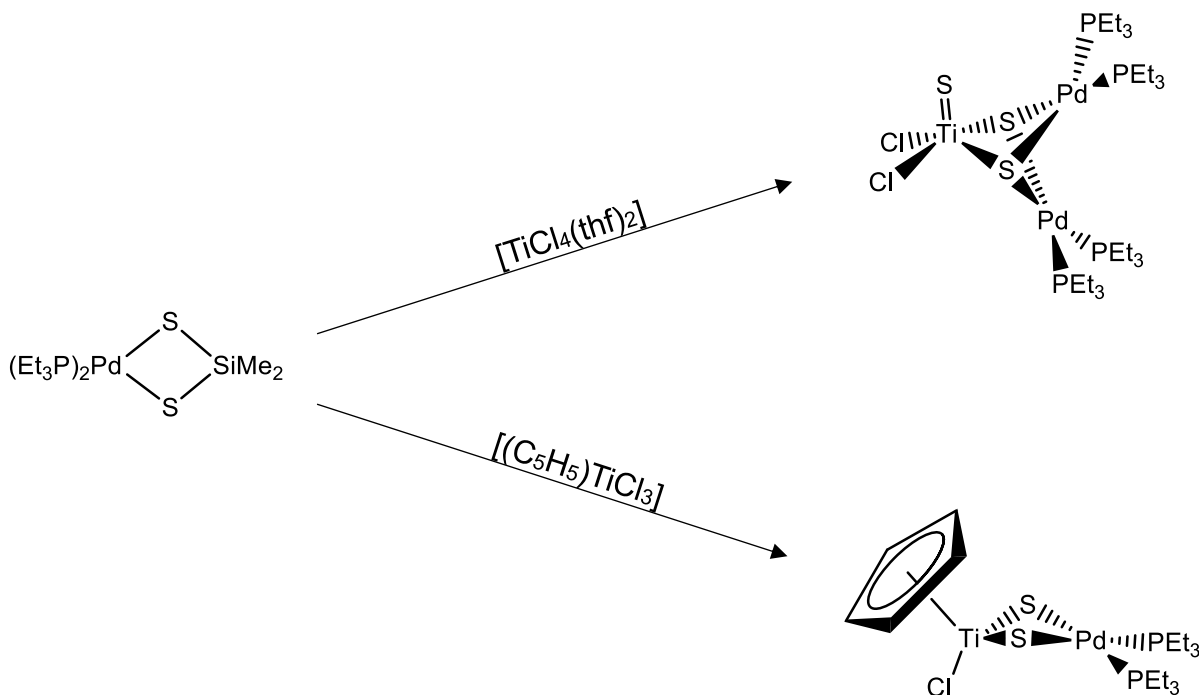
Figure 1.2. Crystal structure of $[\text{Au}_2(\text{SeInCl}_3)\text{dpppe}]_2$ (left) and $[\text{Au}_8\text{Se}_4\text{In}(\text{dppe})_4](\text{InCl}_4)_3$ (right). C (grey), Cl (green), In (pink), P (orange), and Se (purple).⁵²

These reactions illustrate the large number of possibilities of metal chalcogenide structures attainable when using trimethylsilyl functionalized precursors. Although some ternary clusters have been accessed through chalcogenide and organochalcogenolate precursors, silylated metals as precursors have not been explored to the same extent and utilization of these complexes will allow for a more controlled introduction of the different metal species.

Another area of metal chalcogenide chemistry that has received a considerable amount of research focus is the platinum group metal chalcogenide clusters. The Lewis basicity of the chalcogen centers of $M_2(\mu-E)_2(P-P)_2$ ($M = Pd, Pt$; $E = S, Se$; $P-P =$ diphosphine or monophosphine) have allowed ternary clusters to be formed through this precursor.⁵³ The platinum containing adduct has been explored greatly, and many ternary metal chalcogenide clusters have been synthesized from this precursor.⁵⁴ The palladium adduct, however, has not seen nearly the same amount of progress toward ternary metal chalcogenide systems, likely due to difficulties in solubility, lability, polymerization and dissociation of palladium units.⁵⁵

Palladium precursors such as $[Pd_2(\mu-S)_2(PPh_3)_4]$ are, relatively, poorly characterized, and their chemistry left unexplored, due to the lability of the phosphine ligands. This problem can be circumvented through the use of chelating phosphine ligands. By restricting coordination to the *cis* configuration, bridged dinuclear palladium(II) sulfide complexes are made more accessible.^{53, 54, 56}

Another interesting methodology that allows access to ternary palladium sulfide bridged clusters involves the use of the dimethylsilanedithiolato complex $[Pd(S_2SiMe_2)(PEt_3)_2]$, shown in Scheme 1.6. This disulfide ligand restricts the coordination geometry to *cis*.⁵⁷ The reactivity of this dimethylsilanedithiolato precursor was illustrated with two titanium chloride precursors, revealing that ternary palladium sulfide bridged clusters are conveniently accessible in this fashion under mild conditions. By utilizing silylchalcogen metal precursors in conjunction with phosphine bridged palladium salts, other ternary palladium sulfide bridged structures can be obtained.



Scheme 1.6. Reaction of $[\text{Pd}(\text{S}_2\text{SiMe}_2)(\text{PEt}_3)_2]$ to yield heterometallic palladium-titanium-sulfide complexes.⁵⁷

1.6 Applications in Semiconductor Doping

Semiconductor materials can benefit in a number of ways by having an impurity doped into the semiconductor structure. Some examples include modification of catalytic processes in electrocatalysis as well as fine tuning emission wavelengths of quantum dots. The emission of quantum dots, or semiconductor nanostructures, can be controlled through size modifications due to the quantum confinement effect. Introducing an impurity into the structure in a controlled manner can vary the energy of possible emission, providing further functionality. For example, manganese(II) doping of quantum dots results in a significant red shift in the emission properties of the material. This change in emission arises due to the acceptance of an excited electron from the conduction band of the semiconductor to the Mn^{2+} .⁵⁸ Different elements bring different properties, and as such, doping the semiconductor with different species brings rise to vast possibilities in applications.

When introduced into a quantum dot, paramagnetic species such as Mn^{2+} , Co^{2+} and Ni^{2+} can bring new functionality, such as magneto-optical effects. These materials are referred to as dilute magnetic semiconductors (DMS).⁵⁹⁻⁶³ Manganese doped III-V compounds such as (Ga, Mn)As semiconductors have gained attention due to their magneto-optical properties, which allows semiconductor properties of the material to be manipulated through an external magnetic field. An unpaired paramagnetic electron can exist in one of two different spin states: spin up or spin down. This unique property can enhance semiconductor systems to allow for applications in areas ranging from solar cells to spintronics.^{29, 64-69} Conventional electronics make use of silicon based semiconductor material, where changes of the materials conductivity is used to communicate electrical information. Spintronic devices are based on the theory that the spin state of an unpaired electron, as opposed to the conductivity of the material, may be used to communicate electrical information.^{67, 70} Typically these DMS contain between %1–%10 manganese content relative to the amount of the primary metal content.⁷¹ These semiconductor systems require precise control over structure and site specific coordination in order to maintain their desirable properties. This has prompted the investigation of trimethylsilyl chalcogenolate precursors for use in the synthesis of ternary metal chalcogenide clusters containing manganese.

Previous work by C. B. Khadka has shown that it is possible to dope silver sulfide nanoclusters with manganese by method of TMS functionalized metal chalcogenolate complexes.⁷² The manganese containing compounds $[Li(N,N'-tmeda)]_2[Mn(SSiMe_3)_4]$ and $[Li(N,N'-tmeda)]_2[(N,N'-tmeda)Mn_5(SSiMe_3)_6(S)_3]$ have been used to produce the clusters $[Mn_{19/20}Ag_{150/148}S_{94}(P^nPr_3)_{30}]$ and $[Mn_{35/36}Ag_{118/116}S_{94}(P^nPr_3)_{30}]$ respectively.⁷² The presence of manganese was initially determined through the use of EDX analysis of single crystals, while the molecular formula was determined by elemental analysis. Although difficult to do, single crystals of both clusters were produced and evaluated using X-ray diffraction analysis. A complete crystallographic data set was collected for $[Mn_{19/20}Ag_{150/148}S_{94}(P^nPr_3)_{30}]$ although localization of the manganese(II) sites was not possible due to extensive site disorder within the cluster (Figure 1.3).

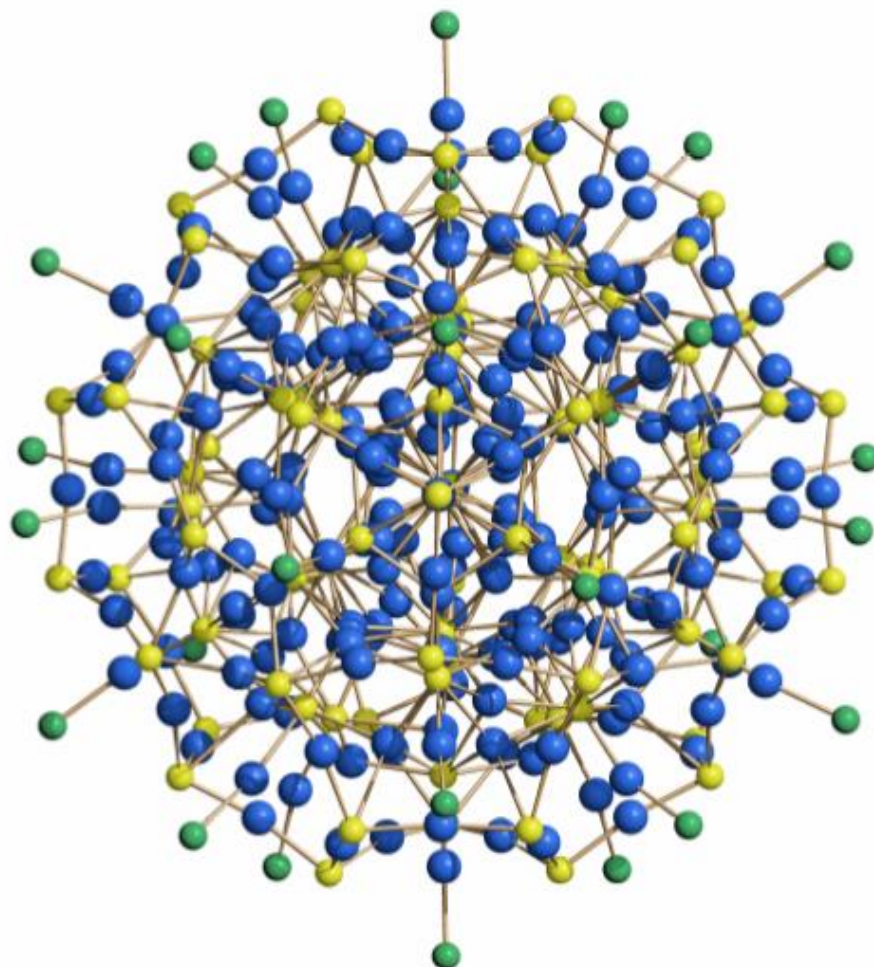


Figure 1.3. Molecular structure of $[\text{Mn}_{19/20}\text{Ag}_{150/148}\text{S}_{94}(\text{P}^n\text{Pr}_3)_{30}]$. C (grey), P (green), S (yellow) and Ag (blue).⁷²

1.7 Project Summary

Recently, ternary zinc manganese chalcogenide structures have been obtained through the use of metal trimethylsilylchalcogenolate complexes. By employing the zinc(II) chalcogenolate precursor $(N,N'\text{-tmeda})[\text{Zn}(\text{ESiMe}_3)_2]$ ($E = \text{S}, \text{Se}$), multiple ternary clusters of the formula $(N,N'\text{-tmeda})_6[\text{Zn}_{14-x}\text{Mn}_x\text{E}_{13}\text{Cl}_2]$ were prepared, where x ranges from ~ 2 to ~ 8 .⁷³ This methodology allows strict control over structure and elemental composition of the products, which made

possible the observation that the replacement of manganese with zinc prefers specific sites depending on how many manganese atoms are introduced into the cluster. Attempts to impart manganese within the cluster core of quantum dots has proven very difficult, often resulting in manganese diffusing toward the surface or being expelled completely.⁷⁴ This ability to observe the mechanisms behind manganese doping, as well as the mechanisms involved with incorporation of manganese into ternary cluster systems could prove to be very useful for determining what favourable conditions may be needed to promote manganese doping into larger semiconductor clusters.

The focus of this thesis is to explore ternary metal chalcogenide cluster synthesis, particularly ternary manganese metal chalcogenide clusters. Chapter 2 describes the reaction of $[\text{Li}(\text{N},\text{N}'\text{-tmeda})]_2[\text{Mn}(\text{SSiMe}_3)_4]$ **1** with $[(\text{dppp})\text{PdCl}_2]$ and $[(\text{dppp})\text{Pd}(\text{OAc})_2]$. Both reactions yield the novel ternary complex $[\text{MnCl}_2(\mu\text{-S})_2\text{Pd}_2(\text{dppp})_2]$ **2**. The synthesis of the new palladium dithiolate complex $[(\text{dppp})\text{Pd}(\text{SSiMe}_3)_2]$ **3** from both $[(\text{dppp})\text{PdCl}_2]$ and $[(\text{dppp})\text{Pd}(\text{OAc})_2]$ is also described. The reactivity of this complex is tested through a reaction with $[(\text{CH}_3\text{CN})_2\text{Mn}(\text{OTf})_2]$, yielding the new complex $[\text{Mn}(\text{OTf})(\text{thf})_2(\mu\text{-S})_2\text{Pd}_2(\text{dppp})_2]\text{OTf}$ **4**. Chapter 3 describes reactions of $[\text{Li}(\text{N},\text{N}'\text{-tmeda})]_2[\text{Mn}(\text{SSiMe}_3)_4]$ **1** with various phosphine gold chlorides, gold triflate, as well as ferrocenoyl chloride. Reactions of $[(\text{CH}_3\text{CN})_2\text{Mn}(\text{OTf})_2]$ with $[\text{PPh}_3\text{AuSSiMe}_3]$ **5** are also described. Synthesized compounds were characterized using multiple methods including melting point, elemental analysis, single crystal X-ray crystallography, NMR spectroscopy, EPR spectroscopy, EDX spectroscopy, mass spectrometry, SEM, UV-Vis absorption and photoluminescence spectroscopy.

1.8 References

1. J.F. Corrigan, O. Fuhr, and D. Fenske; *Advanced Materials*, **2009**. 21(18): p. 1867-1871.
2. I. Dance and K. Fisher, *Metal Chalcogenide Cluster Chemistry*, in *Progress in Inorganic Chemistry*. John Wiley & Sons, Inc. **2007**; p. 637-803.
3. H.-W. Hou, X.-Q. Xin, and S. Shi; *Coordination Chemistry Reviews*, **1996**. 153: p. 25-56.
4. Q.-F. Zhang, W.-H. Leung, and X. Xin; *Coordination Chemistry Reviews*, **2002**. 224(1-2): p. 35-49.
5. M. Bouroushian, *Chalcogens and Metal Chalcogenides*, in *Electrochemistry of Metal Chalcogenides*. Springer: Heidelberg, Berlin. **2010**; p. 1-56.
6. B.O. Dabbousi, J. Rodriguez-Viejo, F.V. Mikulec, J.R. Heine, H. Mattoussi, R. Ober, K.F. Jensen, and M.G. Bawendi; *The Journal of Physical Chemistry B*, **1997**. 101(46): p. 9463-9475.
7. S.L. Li, K. Tsukagoshi, E. Orgiu, and P. Samori; *Chemical Society Reviews*, **2016**. 45(1): p. 118-151.
8. K. Surana, R.M. Mehra, B. Bhattacharya, H.W. Rhee, A.R. Polu, and P.K. Singh; *Renewable & Sustainable Energy Reviews*, **2015**. 52: p. 1083-1092.
9. A. Klein; *Journal of Physics-Condensed Matter*, **2015**. 27(13): p. 24.
10. R.J. Gui, H. Jin, Z.H. Wang, and L.J. Tan; *Coordination Chemistry Reviews*, **2015**. 296: p. 91-124.
11. M.R. Gao, J. Jiang, and S.H. Yu; *Small*, **2012**. 8(1): p. 13-27.
12. Y.J. Feng, A. Gago, L. Timperman, and N. Alonso-Vante; *Electrochimica Acta*, **2011**. 56(3): p. 1009-1022.
13. X. He and D. Antonelli; *Angewandte Chemie-International Edition*, **2002**. 41(2): p. 214-229.
14. T.I. Levchenko, C. Kubel, D. Wang, B.K. Najafabadi, Y.N. Huang, and J.F. Corrigan; *Chemistry of Materials*, **2015**. 27(10): p. 3666-3682.
15. Y. Liu, B. Khalili Najafabadi, M. Azizpoor Fard, and J.F. Corrigan; *Angewandte Chemie*, **2015**. 127(16): p. 4914-4917.
16. S.M. Hosseinpour-Mashkani, A. Sadeghinia, Z. Zarghami, and K. Motevalli; *Journal of*

- Materials Science-Materials in Electronics*, **2016**. 27(1): p. 365-374.
17. A. Müller and E. Diemann, *Polysulfide Complexes of Metals*, in *Advances in Inorganic Chemistry*, H.J. Emeléus and A.G. Sharpe, Editors. Academic Press. **1987**; p. 89-122.
 18. S. Dehnen, A. Eichhofer, J.F. Corrigan, and D. Fenske, *Synthesis and characterization of Ib-VI nanoclusters.*, in *Nanoparticles*, G. Schmid, Editor. VCH: Weinheim, Germany. **2004**; p. 107-185.
 19. D.G. MacDonald and J.F. Corrigan; *Philosophical Transactions of the Royal Society A: Mathematical Physical and Engineering Sciences*, **2010**. 368(1915): p. 1455-1472.
 20. L.C. Roof and J.W. Kolis; *Chemical Reviews*, **1993**. 93(3): p. 1037-1080.
 21. K. Hamada and H. Morishita; *Japanese Journal of Applied Physics*, **1976**. 15(4): p. 748-748.
 22. K. McGregor, G.B. Deacon, R.S. Dickson, G.D. Fallon, R.S. Rowe, and B.O. West; *Journal of the Chemical Society-Chemical Communications*, **1990**. 1990(19): p. 1293-1294.
 23. S. Dehnen, A. Eichhofer, and D. Fenske; *European Journal of Inorganic Chemistry*, **2002**. 2002(2): p. 279-317.
 24. M.W. DeGroot and J.F. Corrigan; *Zeitschrift Fur Anorganische Und Allgemeine Chemie*, **2006**. 632(1): p. 19-29.
 25. D. Fenske, in *Clusters and Colloids, from Theory to Applications*, G. Schmid, Editor. VCH: Weinheim, Germany. **1994**; p. 212-297.
 26. D. Taher, A.I. Wallbank, E.A. Turner, H.L. Cuthbert, and J.F. Corrigan; *European Journal of Inorganic Chemistry*, **2006**. 2006(22): p. 4616-4620.
 27. I. Kuwajima and T. Abe; *Bulletin of the Chemical Society of Japan*, **1978**. 51(7): p. 2183-2184.
 28. D. Fenske and F. Simon; *Angewandte Chemie International Edition in English*, **1997**. 36(3): p. 230-233.
 29. T.I. Levchenko, C. Kubel, Y.N. Huang, and J.F. Corrigan; *Chemistry-A European Journal*, **2011**. 17(51): p. 14394-14398.
 30. C.B. Khadka, B.K. Najafabadi, M. Hesari, M.S. Workentin, and J.F. Corrigan; *Inorganic Chemistry*, **2013**. 52(12): p. 6798-6805.
 31. D.G. MacDonald, C. Kubel, and J.F. Corrigan; *Inorganic Chemistry*, **2011**. 50(8): p. 3252-

3261.

32. W. Yu, O. Fuhr, and D. Fenske; *Journal of Cluster Science*, **2012**. 23(3): p. 753-766.
33. D.G. MacDonald and J.F. Corrigan; *Dalton Transactions*, **2008**. 2008(37): p. 5048-5053.
34. V. Chandrasekhar, S. Nagendran, S. Bansal, M.A. Kozee, and D.R. Powell; *Angewandte Chemie-International Edition*, **2000**. 39(10): p. 1833-1835.
35. G.L. Zheng, J.F. Ma, Z.M. Su, L.K. Yan, J. Yang, Y.Y. Li, and J.F. Liu; *Angewandte Chemie-International Edition*, **2004**. 43(18): p. 2409-2411.
36. M.A. Fard, A.R. Kenaree, P.D. Boyle, P.J. Ragona, J.B. Gilroy, and J.F. Corrigan; *Dalton Transactions*, **2016**. 45(7): p. 2868-2880.
37. M.A. Fard, M.J. Willans, B.K. Najafabadi, T.I. Levchenko, and J.F. Corrigan; *Dalton Transactions*, **2015**. 44(17): p. 8267-8277.
38. T. Komuro, T. Matsuo, H. Kawaguchi, and K. Tatsumi; *Dalton Transactions*, **2004**. 2004(10): p. 1618-1625.
39. T. Komuro, T. Matsuo, H. Kawaguchi, and K. Tatsumi; *Angewandte Chemie International Edition*, **2003**. 42(4): p. 465-468.
40. M.W. DeGroot, K.M. Atkins, A. Borecki, H. Rosner, and J.F. Corrigan; *Journal of Materials Chemistry*, **2008**. 18(10): p. 1123-1130.
41. H. Sommer, A. Eichhöfer, N. Drebov, R. Ahlrichs, and D. Fenske; *European Journal of Inorganic Chemistry*, **2008**. 2008(32): p. 5138-5145.
42. T. Niebel, D.G. MacDonald, C.B. Khadka, and J.F. Corrigan; *Zeitschrift Fur Anorganische Und Allgemeine Chemie*, **2010**. 636(6): p. 1095-1099.
43. M.W. DeGroot and J.F. Corrigan; *Organometallics*, **2005**. 24(14): p. 3378-3385.
44. C.B. Khadka, D.G. Macdonald, Y.H. Lan, A.K. Powell, D. Fenske, and J.F. Corrigan; *Inorganic Chemistry*, **2010**. 49(16): p. 7289-7297.
45. M.L. Fu, I. Issac, D. Fenske, and O. Fuhr; *Angewandte Chemie-International Edition*, **2010**. 49(38): p. 6899-6903.
46. C.E. Anson, A. Eichhofer, I. Issac, D. Fenske, O. Fuhr, P. Sevillano, C. Persau, D. Stalke, and J. Zhang; *Angewandte Chemie-International Edition*, **2008**. 47(7): p. 1326-1331.

47. M. Ganguly, J. Jana, A. Pal, and T. Pal; *RSC Advances*, **2016**. 6(21): p. 17683-17703.
48. H.Y. Yang, Y. Wang, A.J. Edwards, J.Z. Yan, and N.F. Zheng; *Chemical Communications*, **2014**. 50(92): p. 14325-14327.
49. H. Wen, Y.R. Liu, K.M. Xu, T. Huang, C.J. Hu, W.J. Zhang, and W. Huang; *Rsc Advances*, **2014**. 4(29): p. 15066-15076.
50. J.P. Eussner and S. Dehnen; *Chemical Communications*, **2014**. 50(77): p. 11385-11388.
51. A.M. Polgar, C.B. Khadka, M. Azizpoor Fard, B. Nikkel, T. O'Donnell, T. Neumann, K. Lahring, K. Thompson, C. Cadogan, F. Weigend, and J.F. Corrigan; *Chemistry – A European Journal*, **2016**: p. n/a-n/a.
52. J. Olkowska-Oetzel, P. Sevillano, A. Eichhofer, and D. Fenske; *European Journal of Inorganic Chemistry*, **2004**. 2004(5): p. 1100-1106.
53. G. Li, C.-K. Lam, S.W. Chien, T.C.W. Mak, and T.S. Andy Hor; *Journal of Organometallic Chemistry*, **2005**. 690(4): p. 990-997.
54. J. Li and T.S.A. Hor; *Dalton Transactions*, **2008**. 2008(42): p. 5708-5711.
55. S.W. Audi Fong and T. S. Andy Hor; *Journal of the Chemical Society, Dalton Transactions*, **1999**. 1999(5): p. 639-652.
56. J. S. L. Yeo, G. Li, W.-H. Yip, W. Henderson, T. C. W. Mak, and T. S. Andy Hor; *Journal of the Chemical Society, Dalton Transactions*, **1999**. 1999(3): p. 435-442.
57. T. Komuro, T. Matsuo, H. Kawaguchi, and K. Tatsumi; *Chemical Communications*, **2002**. 2002(9): p. 988-989.
58. R. Beaulac, Y. Feng, J.W. May, E. Badaeva, D.R. Gamelin, and X. Li; *Physical Review B*, **2011**. 84(19): p. 195324.
59. S.C. Erwin, L. Zu, M.I. Haftel, A.L. Efros, T.A. Kennedy, and D.J. Norris; *Nature*, **2005**. 436(7047): p. 91-94.
60. R.N. Bhargava, D. Gallagher, X. Hong, and A. Nurmikko; *Physical Review Letters*, **1994**. 72(3): p. 416-419.
61. V. Proshchenko and Y. Dahnovsky; *Journal of Physical Chemistry C*, **2014**. 118(48): p. 28314-28321.

62. D.J. Norris, N. Yao, F.T. Charnock, and T.A. Kennedy; *Nano Letters*, **2000**. 1(1): p. 3-7.
63. P. Tang, D. Kuang, S. Yang, and Y. Zhang; *Journal of Alloys and Compounds*, **2015**. 622: p. 194-199.
64. I.J. Kramer and E.H. Sargent; *Chemical Reviews*, **2014**. 114(1): p. 863-882.
65. P.K. Santra and Y.S. Chen; *Electrochimica Acta*, **2014**. 146: p. 654-658.
66. J.T. Arantes, G.M. Dalpian, and A. Fazzio; *Physical Review B*, **2008**. 78(4): p. 1-5.
67. J.R. Chelikowsky, E. Kaxiras, and R.M. Wentzcovitch; *Physica Status Solidi B-Basic Solid State Physics*, **2006**. 243(9): p. 2133-2150.
68. V.A. Fonoberov, K.A. Alim, A.A. Balandin, F.X. Xiu, and J.L. Liu; *Physical Review B*, **2006**. 73(16): p. 1-9.
69. Z.H. Sun, X.Y. Yang, C. Wang, T. Yao, L. Cai, W.S. Yan, Y. Jiang, F.C. Hu, J.F. He, Z.Y. Pan, Q.H. Liu, and S.Q. Wei; *ACS Nano*, **2014**. 8(10): p. 10589-10596.
70. F.D. Natterer, K. Yang, W. Paul, P. Willke, T. Choi, T. Greber, A.J. Heinrich, and C.P. Lutz; *Nature*, **2017**. 543(7644): p. 226-228.
71. T. Dietl; *Nat Mater*, **2010**. 9(12): p. 965-974.
72. C.B. Khadka, *Transition metal complexes with reactive trimethylsilylchalcogenolate ligands precursors for the preparation of ternary nanoclusters*. School of Graduate and Postdoctoral Studies, University of Western Ontario, London, Ont. **2011**. p. xvii, 178 leaves ill.
73. C.B. Khadka, A. Eichhofer, F. Weigend, and J.F. Corrigan; *Inorganic Chemistry*, **2012**. 51(5): p. 2747-2756.
74. G.M. Dalpian and J.R. Chelikowsky; *Physical Review Letters*, **2006**. 96(22): p. 4.

Chapter Two

Metal Trimethylsilyl Thiolate Precursors for the Synthesis of Ternary Metal Sulfide Complexes

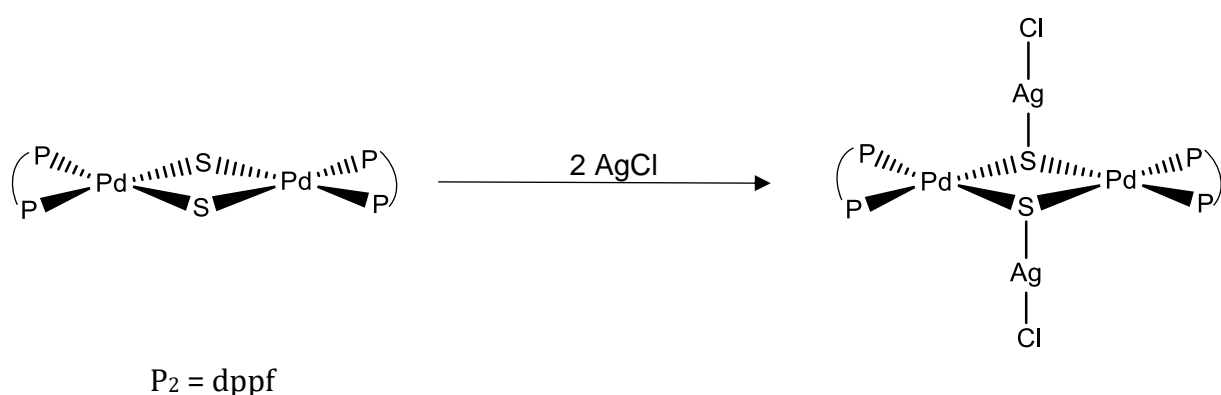
2.1 Introduction

Metal chalcogenide clusters are of increasing interest due to the wide array of properties attainable, and the subsequent applications of these materials.^{1,2} Within this field, it is well known that sulfide (S^{2-}) bridges support the formation of clusters varying in size, nuclearity, and coordination making them a very useful ligand type.³⁻⁸ These possibilities arise due to a sulfide ligands ability to coordinate both in a terminal, bridging and encapsulated fashion, catenate into polysulfido ligand chains, and stabilize a variety of cluster species.⁷ In order to explore this field to the fullest extent, great efforts have been made to achieve controlled construction of chalcogenide clusters, which has led to the development of a wide range of methods and subsequently the development of complex metal sulfide clusters of defined structure and elemental composition.⁶

Platinum group metals have been shown to have a high affinity for chalcogen based ligands, giving rise to a variety of platinum and palladium based chalcogenide (E^{2-}) and chalcogenolate (RE^-) complexes. Unlike some other metal chalcogenides, platinum(II) and palladium(II) based complexes do not develop metal-metal bonding interactions to support the complex framework.¹ The structural complexity of these systems depends entirely on the metal-chalcogen bridging interactions, as well as additional ligand-metal bonding to provide stability to the structure.

The main building block for many of these complexes is the dinuclear complex $[(R_3P)_2M(\mu-E)_2M(R_3P)_2]$ ($M = Ni, Pd, Pt; E = S, Se, Te$).⁹ The metal centres of these dinuclear complexes maintain a distorted square planar geometry with the ligands in a *cis* configuration. Although it is possible to synthesize a dinuclear complex of this fashion with monodentate phosphine ligands, there is a

tendency for the metal centre to adopt a *trans* configuration.¹⁰ The lability of the phosphine ligands is especially problematic in palladium based compounds, and adoption of the *trans* configuration inhibits the formation of the dinuclear dichalcogenide bridged compound. The diversity of palladium sulfide compounds thus accessible has suffered due to this; however, it has been found that the use of chelating phosphines restricts coordination to the *cis* configuration and facilitates bridging between metals to ultimately produce larger, more complex systems.



Scheme 2.1. Reaction of $[(\text{dppf})_2\text{Pd}_2(\mu\text{-S})_2]$ with AgCl to form $[\text{Pd}_2(\text{dppf})_2(\mu_3\text{-S})_2\text{Ag}_2\text{Cl}_2]$.

Dinuclear chalcogenide-bridged palladium(II) complexes have been used as a precursor to easily produce larger complexes containing a variety of metals. In one reaction, Hor and co-workers showed that the precursor complex $[(\text{dppf})_2\text{Pd}_2(\mu\text{-S})_2]$ ($\text{dppf} = 1,1'$ -bis(diphenylphosphino)ferrocene) could be used to produce $[\text{Pd}_2(\text{dppf})_2(\mu_3\text{-S})_2\text{Ag}_2\text{Cl}_2]$ through reaction with AgCl (Scheme 2.1).^{10, 11} The core of this molecule maintains a planar $\{\text{Pd}_2\text{S}_2\}$ structure, while openly bridging two AgCl moieties through the nucleophilic sulfur ligands. This precursor framework has also proven useful in the production of complexes with a triangular $\{\text{Pd}_3\text{S}_2\}$ core, such as that seen in $[\text{Pd}_3\text{Cl}(\text{dppf})_2(\text{PPh}_3)(\mu_3\text{-S})_2]\text{Cl}$. In this case, introduction of $\text{PdCl}_2(\text{PPh}_3)_2$ leads to the dissociation of a PPh_3 ligand and Cl^- to afford the trinuclear complex.

Since monodentate phosphine ligands are known to be more labile in palladium systems, ligand migrations can lead to the formation of positional isomers in this complex although the characteristic shape of the core is maintained.

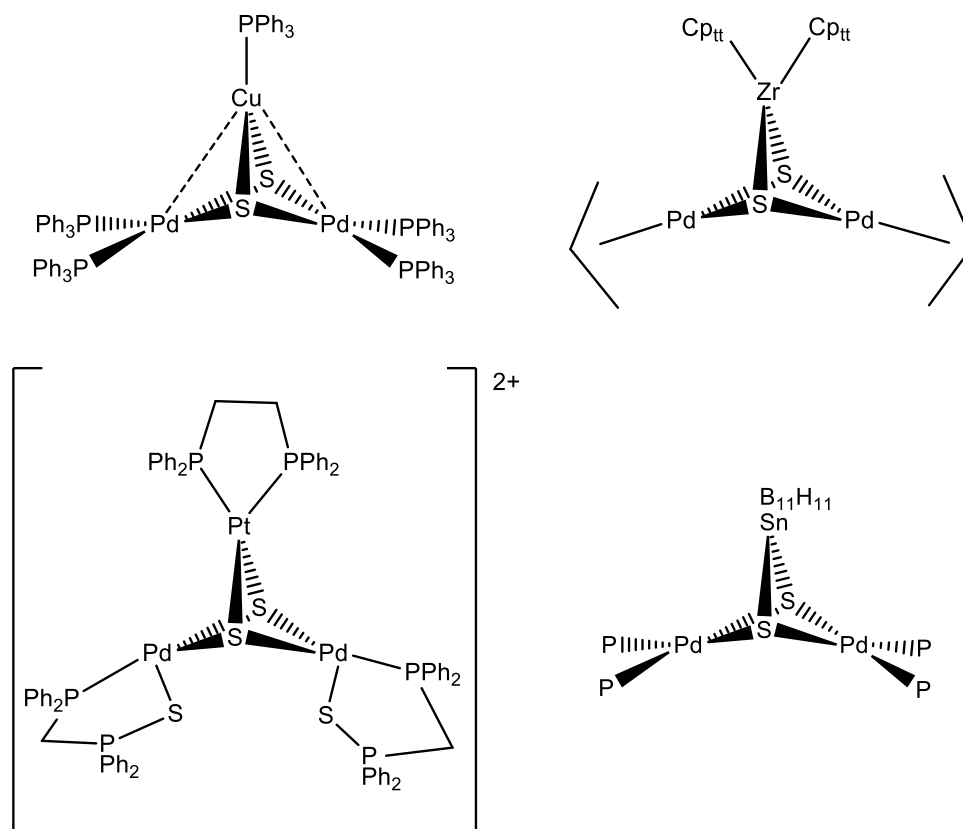
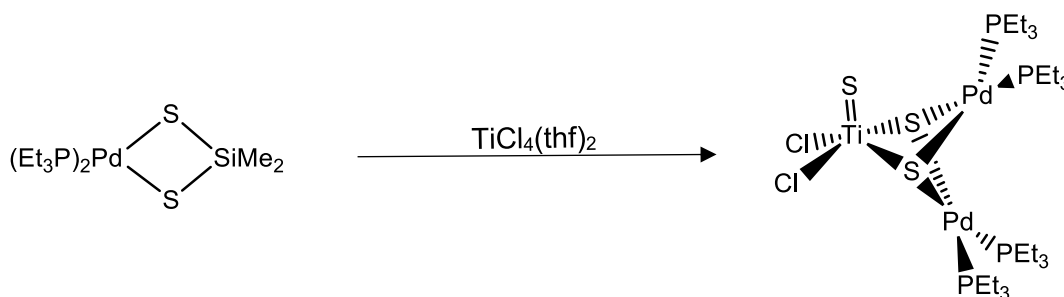


Figure 2.1. Structure of (clockwise): $[(\text{Ph}_2\text{P})_4\text{Pd}_2(\mu_3\text{-S})_2\text{Cu}(\text{PPh}_3)]^+$, $[\text{Cp}^{\text{tt}}_2\text{Zr}(\mu_3\text{-S})_2\{\text{Pd}(\eta^3\text{-C}_3\text{H}_5)\}_2]$, $[(\text{dppp})_2\text{Pd}_2(\mu_3\text{-S})_2(\text{SnB}_{11}\text{H}_{11})]$ and $[\text{PtPd}_2(\mu_3\text{-S})_2(\text{dppe})(\text{dppmS-}\kappa^2\text{S,P}^4)]^{2+}$.¹³⁻¹⁵

The same triangular structure is seen in heterometallic adducts with a $\{\text{Pd}_2\text{MS}_2\}$ core, even when not prepared from a palladium precursor containing the $\{\text{Pd}_2\text{S}_2\}$ unit. For example, $[(\text{Ph}_2\text{P})_4\text{Pd}_2(\mu_3\text{-S})_2\text{Cu}(\text{PPh}_3)]^+$ was synthesized from a mixture of $[\text{Pd}(\text{PPh}_3)_4]$ and $[\text{Cu}_2\text{-(PPh}_3)_3(\mu\text{-OS}_3)]$.¹² Some other structures with a similar $\{\text{Pd}_2\text{MS}_2\}$ include $[\text{Cp}^{\text{tt}}_2\text{Zr}(\mu_3\text{-S})_2\{\text{Pd}(\eta^3\text{-C}_3\text{H}_5)\}_2]$ ($\text{Cp}^{\text{tt}} = \eta^5\text{-1,3-di-tert-butylcyclopentadienyl}$), $[\text{PtPd}_2(\mu_3\text{-S})_2(\text{dppe})(\text{dppmS-}\kappa^2\text{S,P}^4)]$ [PF_6]₂ ($\text{dppe} = \text{bis(diphenylphosphino)ethane}$), and more recently, $[(\text{dppp})_2\text{Pd}_2(\mu_3\text{-S})_2(\text{SnB}_{11}\text{H}_{11})]$ ($\text{dppp} =$

bis(diphenylphosphino)propane).¹³⁻¹⁵ This triangular system is the resulting structure of many different reaction routes, likely due to the thermodynamic stability of the framework.

The use of silylated chalcogen reagents has been proven to be a convenient approach towards the synthesis of a range of metal chalcogenide coordination complexes as well as metal chalcogenide cluster systems. The reactivity of the $-\text{ESiMe}_3$ group of the chalcogenolate precursor allows for convenient reaction with metal salt precursors to facilitate the formation of metal-chalcogen bonds. The thermodynamically favourable formation of XSiMe_3 ($\text{X} = \text{Cl}, \text{OAc}, \text{OTf}$) drives the formation of the $\text{M}-\text{E}$ bond ($\text{E} = \text{S}, \text{Se}$). This method has previously been used to synthesize palladium sulfide complexes of varying structure.



Scheme 2.2. Reaction of $\text{cis}[\text{Pd}(\text{S}_2\text{SiMe}_2)(\text{PEt}_3)_2]$ with $\text{TiCl}_4(\text{thf})_2$ to form $\text{TiCl}_2(\text{S})(\mu_3\text{-S})_2\text{Pd}_2(\text{PEt}_3)_4$.¹⁶

The use of silylated-chalcogen precursors to access these palladium(II) chalcogenide complexes has only recently been employed. One of the first methods used the silanedithiolato complex $\text{cis}[\text{Pd}(\text{S}_2\text{SiMe}_2)(\text{PEt}_3)_2]$ as a precursor along with $\text{TiCl}_4(\text{thf})_2$ to form $\text{TiCl}_2(\text{S})(\mu_3\text{-S})_2\text{Pd}_2(\text{PEt}_3)_4$ (Scheme 2.2).¹⁶ This complex allowed controlled reactivity with the titanium chloride reactant while maintaining *cis* configuration about palladium. In a different fashion, Azizpoor Fard and Corrigan have utilized chelating diphosphine ligands to control geometry about the palladium metal, and trimethylsilyl functionalized organochalcogenolate reagents as the source of the bridging chalcogen ligand to form palladium(II) thiolate complexes.¹⁷ The palladium salt $[(\text{dppp})\text{PdCl}_2]$ was reacted with $1,2\text{-(Me}_3\text{SiECH}_2)_2\text{C}_6\text{H}_4$ ($\text{E} = \text{S}, \text{Se}$) to produce the dinuclear

palladium(II) complexes $\{(dppp)_2Pd_2-\mu-\kappa^2S-[1,2(SCH_2)_2C_6H_4]\}^{2+}$, and $\{(dppp)_2Pd_2-\mu-\kappa^2Se-[1,2-(SeCH_2)_2C_6H_4]\}^{2+}$ and with 1,2,4,5-(Me₃SiSCH₂)₄C₆H₂ to produce the tetranuclear complex $[(dppp)_4Pd_4-\mu-\kappa^4S-\{1,2,4,5-(SCH_2)_4C_6H_2\}]^{4+}$. These reactions show that the palladium(II) dithiolate bridged butterfly structures can be achieved through the use of silylated chalcogen precursors, and can allow for the production of unique dinuclear {Pd₂R₂S₂} and trinuclear {Pd₂MS₂} complexes.

In order to expand this area, we set out to develop new heterometallic palladium(II) chalcogenide complexes by using silylated metal precursor reagents. To date, there have been no palladium chalcogenide complexes synthesized that contain paramagnetic heteroatoms. Previous work performed by Khadka led to the development of the convenient complex $[Li(N,N'-tmeda)]_2[Mn(SSiMe_3)_4]$ **1** which allows reaction with other metal salts to produce ternary metal chalcogenide clusters.^{18, 19} This, combined with the paramagnetic properties of manganese in its common Mn²⁺ state make this complex an ideal reagent for the introduction of a paramagnetic species into butterfly palladium(II) disulfide complexes. This complex and the newly synthesized trimethylsilyl palladium(II) dithiolate complex $[(dppp)Pd(SSiMe_3)_2]$ **3** were combined with palladium and manganese salt reagents respectively to afford the new triangular MnCl₂(μ₃-S)₂Pd₂(dppp)₂ **2** and $[MnOTf(thf)_2(\mu_3-S)_2Pd_2(dppp)_2]OTf$ **4** (OTf = CF₃SO₃⁻).

2.2 Experimental

All experimental procedures were performed using standard double manifold Schlenk line techniques under an atmosphere of dried nitrogen gas or in nitrogen filled glove boxes. The non-chlorinated solvents (pentane, hexanes, THF, toluene), purchased from Caledon (HPLC grade), were dried and collected using an MBraun MB-SP Series solvent purification system with tandem activated alumina (THF, toluene) and activated alumina/copper redox catalyst (hydrocarbons)²⁰. Dichloromethane (CH₂Cl₂), purchased from Caledon, was dried and distilled over P₂O₅. *N,N,N',N'*-tetramethylethylenediamine (TMEDA), purchased from Sigma Aldrich, was dried and distilled

over CaH₂. Spectral grade solvent chloroform CDCl₃, purchased from Cambridge Isotope Laboratories, was dried and distilled over P₂O₅. Celite® was dried by heating at 120 °C under vacuum for 48 hours. Chemicals were used as received from Alfa Aesar and/or Sigma Aldrich without further purification. Starting reagents S(SiMe₃)₂,²¹ Li[SSiMe₃],²¹ [Li(N,N'-tmeda)]₂[Mn(SSiMe₃)₄],¹⁸ and [Mn(OTf)₂(CH₃CN)₂]²² were synthesized using literature procedure.

For precursor materials, ¹H and ³¹P{¹H} NMR spectra were recorded on a Varian Mercury 400 MHz spectrometer with an operating frequency of 400.08 MHz and the chemical shifts were referenced internally to signals from residual H relative to SiMe₄ (¹H) or 85% H₃PO₄ (³¹P). For the rest of the materials, ¹H and ³¹P{¹H} NMR spectra were recorded on an Inova 400 MHz with an operating frequency of 399.76 MHz and internally referenced to the residual proton peak in CDCl₃ relative to SiMe₄ (¹H) or 85% H₃PO₄ (³¹P). Electron paramagnetic resonance (EPR) experiments were run on a JEOL JES-FA200 EPR spectrometer. Complex [4]⁺ was dissolved in THF and measurements were taken at 20 °C using 0.4 mm quartz tubes.

X-ray data were collected on either a Bruker APEXII (**2**, **4**) or a Nonius KappaCCD (**3**) diffractometer. Single crystals were mounted on a Mitegen polyimide micromount with a small amount of Paratone N oil. The structures were solved using direct methods and refined by the full-matrix least-squares procedure of SHELXTL.^{23, 24} All non-hydrogen atoms were refined with anisotropic thermal parameters. Hydrogen atoms were introduced at idealized positions and were allowed to ride on the parent atom.

Elemental analysis of **2** and **4** was performed by Laboratoire d'Analyse Élémentaire de l'Université de Montréal (Quebec, Canada). A uniform sample of **3** could not be prepared and elemental analysis experiments were not performed. UV-Vis absorption studies were performed at room temperature on a Varian Cary 300 spectrometer.

2.2.1 [MnCl₂(μ₃-S)₂Pd₂(dppp)₂] - 2

[(dppp)PdCl₂] (0.1500 g, 0.254 mmol) was dissolved in 12 mL CH₂Cl₂. A solution of [Li(*N,N'*-tmeda)]₂[Mn(SSiMe₃)₄] **1** (0.0918 g, 0.127 mmol) in 12 mL CH₂Cl₂ was added at room temperature to immediately create a transparent bright orange mixture with a small amount of precipitate. The reaction was left to stir for three hours at this temperature to produce a clear red-brown coloured mixture with a small amount of light beige precipitate. The solution was filtered over dried Celite® through a glass frit, and the brown coloured solution was reduced in volume to ~12 mL under vacuum. The solution was cooled to -30 °C and layered with 40 mL of pentane. Deep red prisms of **2** deposited after 4 days. The mother liquor was removed via pipette and the crystals were washed with 5x20 mL of pentane and dried *in vacuo*. Yield 62 % (0.097 g); m.p. 228 °C (dec).

Anal. Calcd for C₅₄H₅₂Cl₂MnP₄Pd₂S₂·0.3CH₂Cl₂: C 52.04, H 4.23, S 5.12; found C 52.07, H 4.35, S 4.89%.

UV-Vis λ_{max} (ε /M⁻¹cm⁻¹): 268 (16700), 275 (17100), 283 (17500), 320 (9250), 410 (1130), 531 (254) nm.

Solid State PL: ~900 nm

2.2.2 [(dppp)Pd(SSiMe₃)₂] - 3

[(dppp)Pd(OAc)₂] (0.1768 g, 0.278 mmol) and freshly prepared Li[SSiMe₃] (0.556 mmol) were each dissolved in THF (5 mL each) to produce a yellow suspension and a colourless solution, respectively. The two solutions were mixed at room temperature and stirred to immediately produce a deep orange solution. The solvent was then removed *in vacuo* and 15 mL of toluene was added to solubilize product **3**. This mixture was filtered over dried Celite® through a glass frit. The solvent was removed under vacuum to yield a bright orange oily solid. A concentrated solution of **3** in pentane was prepared by evaporating pentane until the solution began to precipitate out, followed by a filtration of this mixture over dried Celite®. This solution was left in a glove box in a container with a small opening to allow slow evaporation. After 3 days approximately half of the solvent had evaporated, leaving amorphous non-crystalline material in the bottom of the vial. After

7 days the solvent had completely evaporated and a few deep orange prisms were present in the bottom of the vial, along with amorphous, greasy product. Yield 84 % (0.170 g).

^1H NMR (399.76 MHz, CDCl_3 , 25 °C): δ 7.80 – 7.75 (m, 8 H, Ar-*H*), 7.47 – 7.37 (m, 12 H, Ar-*H*), 2.35 (m, 4 H, PCH_2), 2.02 (m, 2 H, PCH_2CH_2), 0.01 (s, 18H, SiCH_3) ppm.

$^{13}\text{C}\{^1\text{H}\}$ NMR (150.74 MHz, CDCl_3 25 °C): δ 134.3 (t, $J = 4.5$ Hz), 130.5 (s), 128.3 (t, $J = 5.0$ Hz), 29.1 (t, PCH_2 , $J = 15.1$ Hz), 20.5 (PCH_2CH_2), 6.6 (Si-CH_3) ppm.

$^{31}\text{P}\{^1\text{H}\}$ NMR (161.97 MHz, CDCl_3 , 25 °C): δ 3.4 ppm (s, PPh_2).

2.2.3 $[\text{MnOTf}(\text{thf})_2(\mu_3\text{-S})_2\text{Pd}_2(\text{dppp})_2]\text{OTf} - 4$

$[(\text{dppp})\text{Pd}(\text{SSiMe}_3)_2] \mathbf{2}$ (0.0805 g, 0.110 mmol) was dissolved in 5 mL THF. A solution of freshly prepared $\text{Mn}(\text{OTf})_2(\text{CH}_3\text{CN})_2$ (0.055 mmol) in 5 mL THF was then added at room temperature, resulting in no change to the solution colour. After 2 hours of stirring, a fine white precipitate formed along with a darkening of the liquid to a dark red colour. The mixture was filtered over dried Celite® through a glass frit to yield a dark red solution. The solution was cooled to -70 °C, layered with 30 mL of pentane and stored at -25 °C. Dark red prisms deposited after 2 days. The mother liquor was removed via pipette and the crystals were washed with 5x20 mL of pentane and dried *in vacuo*. Yield 45 % (0.040 g); m.p. (>260 °C).

Anal. Calcd. for $\text{C}_{64}\text{H}_{68}\text{F}_6\text{MnO}_8\text{P}_4\text{Pd}_2\text{S}_4$: C 48.07, H 4.29, S 8.02; Found C 47.18, H 4.25, S 7.69.

UV-Vis λ_{max} ($\epsilon / \text{M}^{-1}\text{cm}^{-1}$): 275 (72500), 350 (36700), 406 (16600) nm.

Solid State PL: >1000 nm

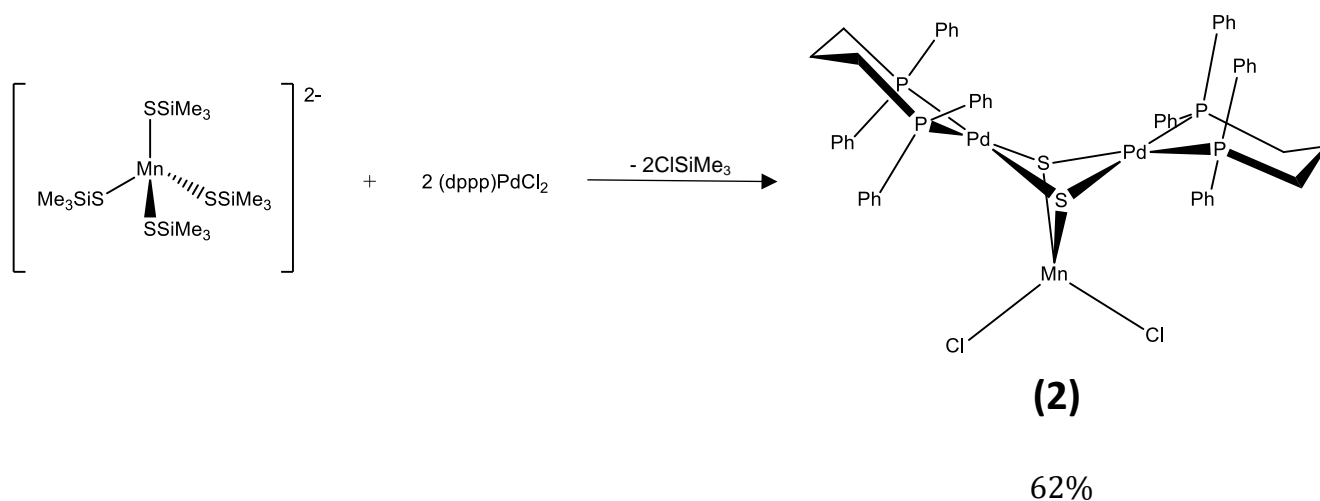
EPR: $g = 1.9867$, line width = 3.827, $a = 9.496$ mT

2.3 Results and Discussion

2.3.1 Synthesis of $[\text{MnCl}_2(\mu_3\text{-S})_2\text{Pd}_2(\text{dppp})_2] (\mathbf{2})$

The chalcogenolate precursor $[\text{Li}(\text{N,N}'\text{-tmeda})]_2[\text{Mn}(\text{SSiMe}_3)_4] \mathbf{1}$ was prepared according to a previously published methodology by Khadka.¹⁸ Treatment of this compound with other MX metal salts has been proven to yield heterometallic chalcogenolate compounds with varying

structure and properties, showing the potential for the manganese chalcogenolate complex to act as a convenient precursor to other heterometallic chalcogenolate precursors.^{18, 19} The reactivity of **1** towards small cluster formation was tested with the palladium(II) complex [(dppp)PdCl₂] (dppp = 1,3-bis(diphenylphosphino)propane). The reaction of the chalcogenolate coordination complex [Li(N,N'-tmeda)]₂[Mn(SSiMe₃)₄] **1** with two equivalents of [(dppp)PdCl₂] afforded the isolation of the ternary complex [MnCl₂(μ-S)₂Pd₂(dppp)₂] (62%) **2** (Scheme 2.3). The Pd—S bonds formed as a result of the production of ClSiMe₃. The reaction completed after 3 hours at room temperature, with a colour change from light orange to deep red-brown taking place. Layering the solution with pentane as a counter solvent afforded the product in the form of deep red crystals. Complex **2** is highly soluble in CH₂Cl₂, and sparingly soluble in THF. In solid crystalline form, the compound is stable in air at room temperature; however, the complex exhibits some sensitivity to air in solution.



Scheme 2.3. Synthesis of complex **2** ([MnCl₂(μ₃-S)₂Pd₂(dppp)₂]).

2.3.2 Structural Characterization of $[\text{MnCl}_2(\mu_3\text{-S})_2\text{Pd}_2(\text{dppp})_2]$ (**2**)

The molecular structure of **2** was determined through X-ray diffraction analysis (Figure 2.2). The compound crystallizes in the monoclinic space group $P2_1/m$ with $Z = 2$. Crystallographic parameters are reported in Appendix B. Each palladium is coordinated by one dppp and two sulfide ligands in a distorted square planar geometry. The 4-coordinate geometry index differs between the two Pd atoms, with $\tau_4 = 0.062$ for Pd1 and $\tau_4 = 0.080$ for Pd2. The S—Pd—S angles ($84.45(7)^\circ$ and $84.43(7)^\circ$) are statistically identical and smaller than that of the P—Pd—P angles ($91.44(8)^\circ$ and $95.26(8)^\circ$), which are quite different. The two palladium atoms of the structure are bridged by the two sulfide ligands forming a $\{\text{Pd}_2\text{S}_2\}$ moiety which has been observed in many other $\{\text{Pd}_2\text{S}_2\}$ and Pt_2S_2 containing compounds.¹⁰ This Pd_2S_2 ring folds along the two sulfur ligands to form the iconic butterfly shaped structure known for these compounds. The dihedral angle between the two PdS_2 moieties is $132.30(5)^\circ$ for complex **2**, which is comparable to measurements found in similar structures.¹⁰

The manganese centre is also coordinated to the two bridging sulfides as well as two chloride ligands in a distorted tetrahedral geometry with $\tau_4 = 0.899$ ($\tau_4' = 0.896$). The angles about the manganese centre vary significantly with an S—Mn—S angle of $79.69(7)^\circ$ and an Cl—Mn—Cl of $108.68(10)^\circ$. The “pinching” of S—Mn—S is likely due to the square planar geometry about the two palladium centres which are also bonded to the two sulfides. The average manganese-sulfide bond length ($2.4713(17) \text{ \AA}$) is comparable to that of other similar manganese sulfide compounds.¹⁸ The distances between manganese and palladium ($2.9423(17) \text{ \AA}$ and $3.1983(17) \text{ \AA}$) are too large for any metal-metal bonding interaction to be suggested as is the distance between the two palladium centres ($3.1574(15) \text{ \AA}$).

Table 2.1. Selected bond distances (Å) and angles (deg) for **2**.

	Distance (Å)		Angle (°)
Mn1-Pd1	2.9423(17)	S1-Mn1-S1	79.69(7)
Mn1-Pd2	3.1983(17)	Cl1-Mn1-Cl2	108.68(10)
Pd1-Pd2	3.1574(15)	S1-Pd1-S1	84.45(7)
Mn1-S1	2.4713(17)	P1-Pd1-S1	91.99(6)
Mn1-Cl1	2.337(3)	P1-Pd1-P1	91.44(8)
Mn1-Cl2	2.366(3)	S1-Pd2-S1	84.43(7)
Pd1-S1	2.3561(15)	S1-Pd2-P2	90.14(5)
Pd1-P1	2.2716(15)	P2-Pd2-P2	95.26(8)
Pd2-S1	2.3567(14)	P1-S1-P2	132.30(5)
Pd2-P2	2.2719(15)		

Since chlorine and sulfur have similar electron densities, it is difficult to distinguish them from one another from X-ray diffraction data. To prove that chlorine had replaced the sulfur ligands present on the manganese thiolate precursor, combustion elemental analysis of crystals of **2** was performed. It was found that **2** contained 4.89% sulfur, correlating strongly with the theoretical value of 5.17%. Substitution of the sulfur ligands for chlorine results in a total charge of zero for the molecule; the observed Mn—Cl bond distances are shorter than those for Mn—S and thus closer to those previously reported for Mn—Cl.²⁵ These data confirmed that the sulfide ligands were displaced, resulting in the presence of chloride ligands in the final product to form a neutral complex.

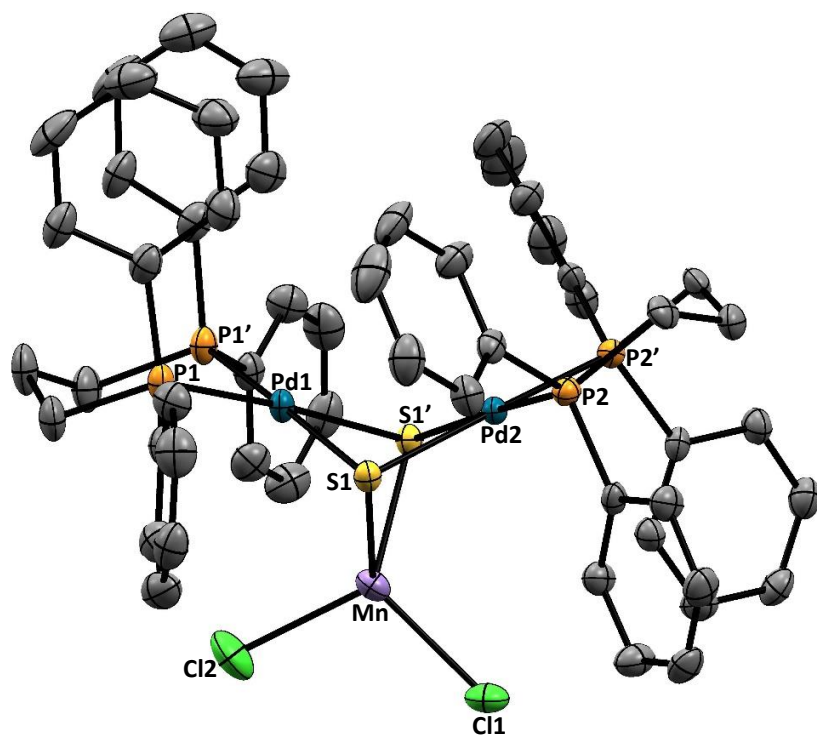
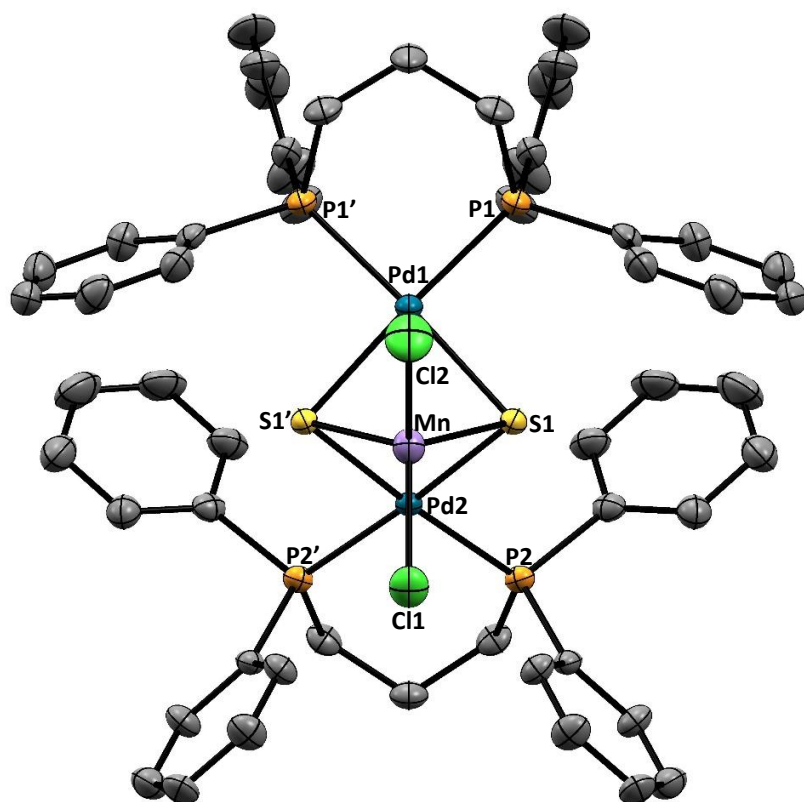


Figure 2.2. Molecular structure of complex 2 shown with two different perspectives. Grey spheres represent C, yellow: S, orange: P, blue: Pd, purple: Mn, and green: Cl. Ellipsoids are depicted at 50% probability. Hydrogen atoms are omitted for clarity. The molecule resides on a mirror plane which contains the atoms Mn, Pd1, Pd2, Cl1 and Cl2.

Since complex **1** ($[\text{Li}(\text{N,N}'\text{-tmeda})]_2[\text{Mn}(\text{SSiMe}_3)_4]$) initially contained, potentially, four reactive chalcogenolate sites, a reaction with a higher stoichiometric amount of $[(\text{dppp})\text{PdCl}_2]$ was performed to probe the synthesis of a larger complex. The chalcogenolate coordination complex **1** was reacted with $[(\text{dppp})\text{PdCl}_2]$ in a 1:3 ratio at room temperature over a period of 2.5 h. A colour change from light orange to gold-brown was observed. Single crystals of deep red nature were obtained by layering the CH_2Cl_2 solution with heptane in a 2:1 ratio. The crystals were not suitable to collect a full data set with single X-ray diffraction, however the unit cell volume of 2739.10 \AA^3 is similar to that of complex **2** ($2732.0(19) \text{ \AA}^3$) revealing that the change in ratio did not result in a cluster of higher nuclearity. A similar reaction was tested with the between **1** and $[(\text{dppp})\text{Pd}(\text{OAc})_2]$ with THF as a solvent to avoid the presence of chlorine. Here, too, the trinuclear complex **2** was identified through X-ray diffraction, likely due to traces of lithium chloride that remain present with complex **1**.

2.3.3 Synthesis and Characterization of $[(\text{dppp})\text{Pd}(\text{SSiMe}_3)_2]$ (**3**)

The complex $[(\text{dppp})\text{Pd}(\text{SSiMe}_3)_2]$ **3** was prepared by treatment of $[(\text{dppp})\text{Pd}(\text{OAc})_2]$ with lithio(trimethylsilyl)-thiolate $[\text{LiSSiMe}_3]$ in a 2:1 ratio, in THF at room temperature. The complex was then dissolved in toluene and solid LiOAc was removed through filtration. The solvent was removed and the product was dissolved in pentane. Evaporation of pentane resulted in the formation of a mixture of vibrant orange crystalline and amorphous material. The yield was found to be 84 % yield (Scheme 2.4). The complex can also be prepared from $[(\text{dppp})\text{PdCl}_2]$ to produce LiCl , however the acetate adduct was used to avoid complications caused by the presence of Cl^- , which have caused the repeated formation of complex **3**. Complex **3** is highly soluble in common organic solvents, and stable in solution for several days if stored at low temperature and under inert atmosphere. The compound is stable for longer periods if stored in solid form under the same conditions.



Scheme 2.4. Synthesis of complex 3 [(dppp)Pd(SSiMe₃)₂].

(3)

Complex 3 was characterized through ¹H NMR, ¹³C{¹H} NMR and ³¹P{¹H} NMR spectroscopy. The chemical shifts of the -Si(CH₃)₃ groups resonate at high field in both the ¹H and ¹³C{¹H} NMR spectra at 0.01 ppm and 6.6 ppm respectively. The phenyl rings of the dppp ligand give rise to two multiplets in the ¹H NMR spectrum at 7.78 and 7.41 ppm which agree with chemical shifts for similar compounds.²⁶ There are likely three signals, with two of the signals overlapping which would give rise to two observable signals in the spectrum. The methylene groups in the ligand are observed as two signals due to the symmetry of the propyl chain. These signals appear at 2.35 and 2.02 ppm in the ¹H NMR spectrum and 29.1 and 20.5 ppm in the ¹³C{¹H} NMR spectrum. The ³¹P{¹H} chemical shift displayed a singlet at 3.4 ppm, upfield from the chemical shift for the precursor [(dppp)Pd(OAc)₂] (11.2 ppm) due to increased shielding at the phosphorus site.

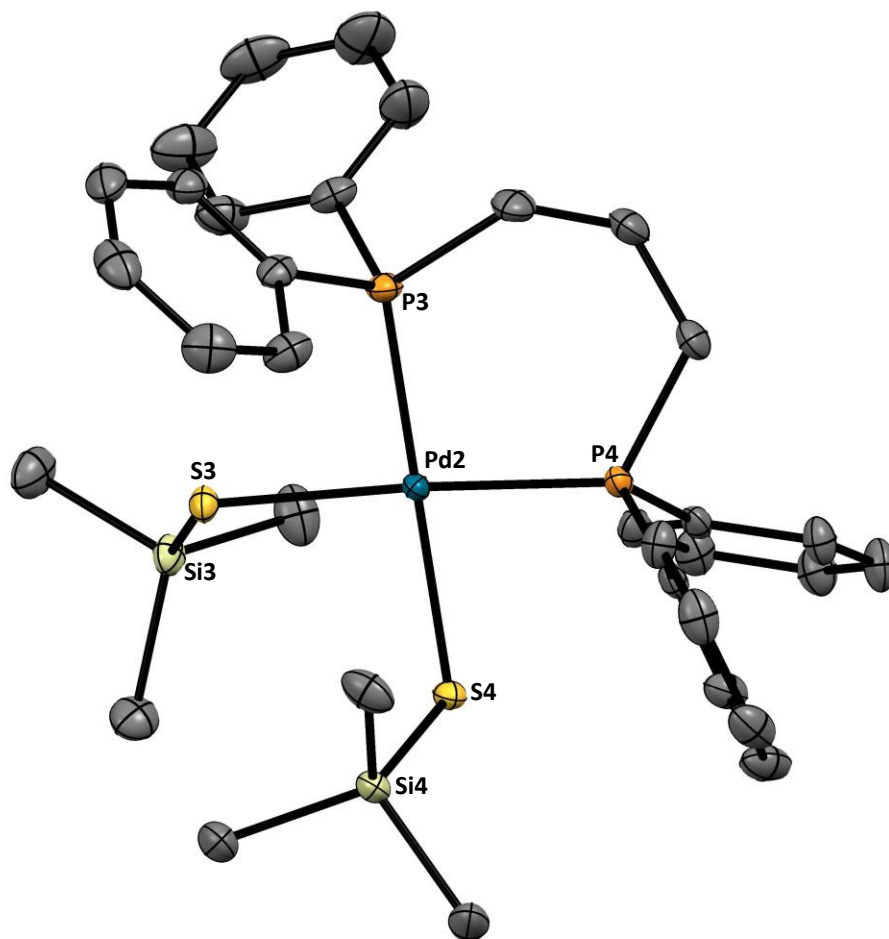


Figure 2.3. Molecular structure of complex **3** (one of two crystallographically independent molecules). Grey spheres represent C, yellow: S, orange: P, blue: Pd, and beige: Si. Ellipsoids are depicted at 50% probability. Hydrogen atoms were omitted for clarity.

Single crystals of **3** suitable for X-ray diffraction studies were obtained by slow evaporation of a pentane solution at room temperature under inert atmosphere. The structure of **3** is illustrated in Figure 2.3 and selected bond length and angles are summarized in Table 2.2. Crystallographic parameters are reported in the Appendix B. The complex crystallizes in the space group $P 2_1/n$ with $Z = 8$, and the crystal contains two similar yet crystallographically independent molecules in the asymmetric unit. The two conformations have similar Pd—P distances (2.2735(7) – 2.293(1) Å), while the Pd—S distances for **3-A** (2.3539(7) and 2.369(1) Å) are slightly shorter

than the Pd—S distances for **3-B** (2.3895(6) and 2.395(1) Å). In contrast, the S—Pd—S angles are quite similar (92.24(3) and 93.76(2)°) while the P—Pd—P angles differ greatly (91.06(3) and 96.38(3)°). Both structures exhibit a distorted square planar geometry around the palladium(II) centre, however the angles of **3-B** deviate from 90° to a greater extent than they do for **3-A**. The 4-coordinate geometry index of $\tau_4 = 0.058$ ($\tau'_4 = 0.050$) for **3-A** is higher than the index of $\tau_4 = 0.042$ ($\tau'_4 = 0.032$) for **3-B**, indicating that the geometry around Pd in **3-B** is closer to square planar. The propyl chain of the dppp ligand in **3-B** is shown to be more symmetrical than the propyl chain in **3-A** (Figure 2.4).

Table 2.2. Selected bond distances (Å) and angles (°) for conformation **A** (top) and **B** (bottom) of complex **3**.

	Distance (Å)		Angle (°)
Pd1-P1	2.293(1)	S1-Pd1-S2	92.24(3)
Pd1-P2	2.2735(7)	S1-Pd1-P1	91.50(3)
Pd1-S1	2.3539(7)	S2-Pd1-P2	85.14(3)
Pd1-S2	2.369(1)	P1-Pd1-P2	91.06(3)
Pd2-P3	2.283(1)	S3-Pd2-S4	93.76(2)
Pd2-P4	2.2827(6)	S3-Pd2-P3	86.15(3)
Pd2-S3	2.3895(6)	S4-Pd2-P4	83.81(2)
Pd2-S4	2.395(1)	P3-Pd2-P4	96.38(3)

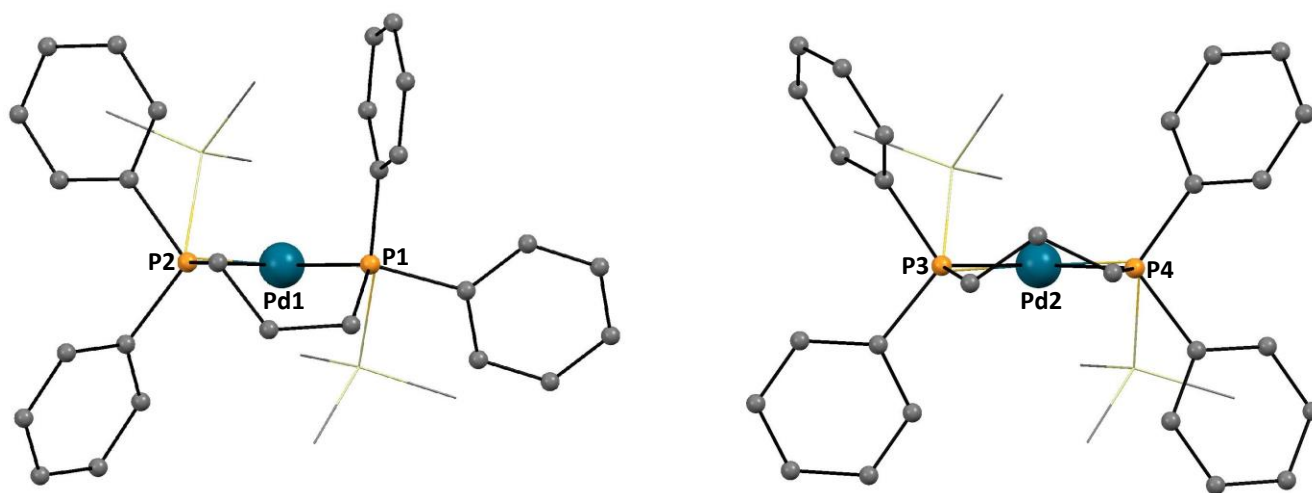
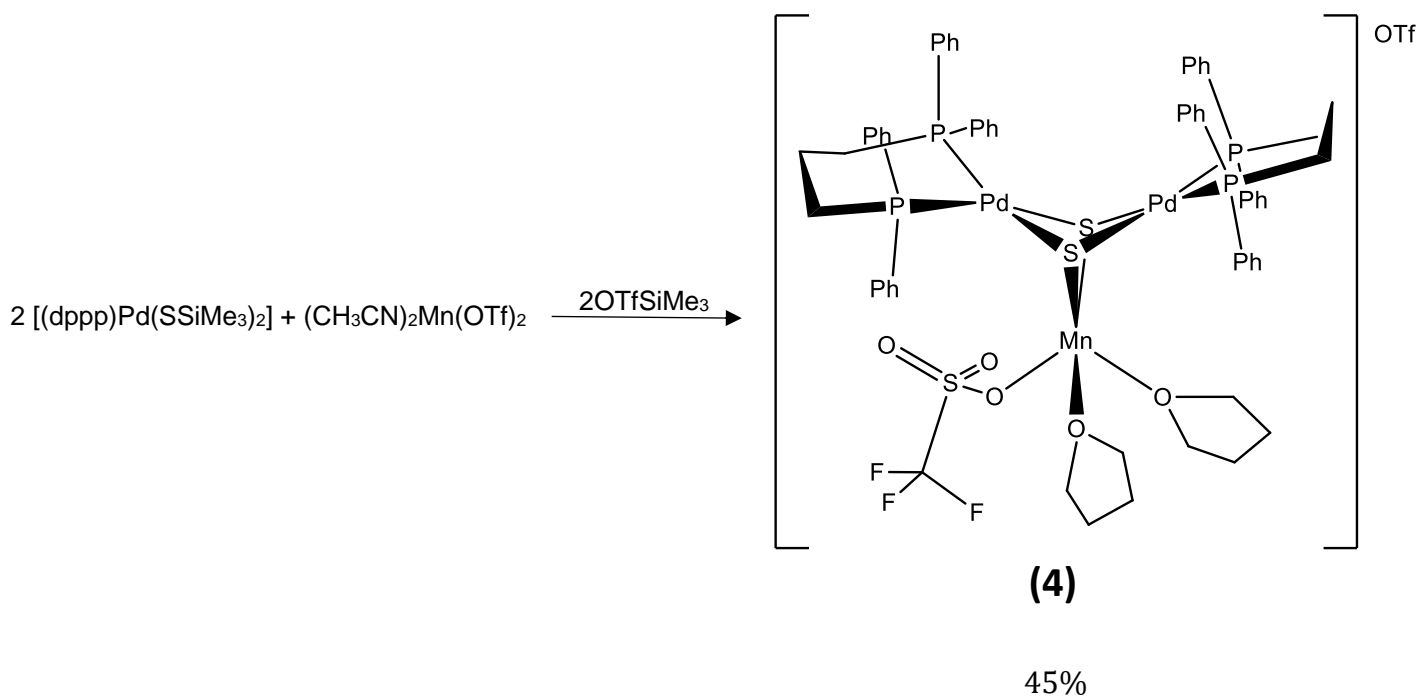


Figure 2.4. View of molecular structure of **3** showing different geometry of dppp ligand for conformation **A** (left) and **B** (right).

2.3.4 Synthesis of $[\text{MnOTf}(\text{thf})_2(\mu\text{-S})_2\text{Pd}_2(\text{dppp})_2]\text{OTf}$ (**4**)

A freshly prepared solution of $[(\text{dppp})\text{Pd}(\text{SSiMe}_3)_2]$ **3** was reacted with $[\text{Mn}(\text{OTf})_2]$ in THF at room temperature. The reaction took place over a period of 2 hours to form a deep red mixture with a white precipitate. After filtration, the product was collected by layering the solution with a counter-solvent and letting the mixture settle at $-25\text{ }^\circ\text{C}$ for two days. The complex $[\text{MnOTf}(\text{thf})_2(\mu\text{-S})_2\text{Pd}_2(\text{dppp})_2]\text{OTf}$ **4** was obtained as deep red crystals in 45% yield (Scheme 2.5). Compared to complex **2**, these crystals are very fragile and difficult to handle, making single crystal X-ray crystallography a challenge. It was found that the crystals of complex **4** degrade when left in the mother liquor for more than 1 day after formation. This complex is stable in air when in the solid state, however some decomposition in the form of black precipitate is noticeable when a solution of the complex is left exposed to air. This compound is soluble in THF and sparingly soluble in diethyl ether. It is also soluble in CH_2Cl_2 , however it is unknown whether the presence of chlorine will affect the structure over time. Therefore, contact with chlorinated solvents was avoided.



Scheme 2.5. Synthesis of complex **4** $[\text{MnOTf}(\text{thf})_2(\mu\text{-S})_2\text{Pd}_2(\text{dppp})_2](\text{OTf})$.

The molecular structure of **4** was determined through X-ray diffraction analysis and is depicted in Figure 2.5. The compound crystallized in the monoclinic space group P-1 with $Z = 2$ and no molecular symmetry. Crystallographic parameters are reported in Appendix B. As with **2**, the complex contains two dppp containing palladium moieties that are bridged through two central sulfide ligands.

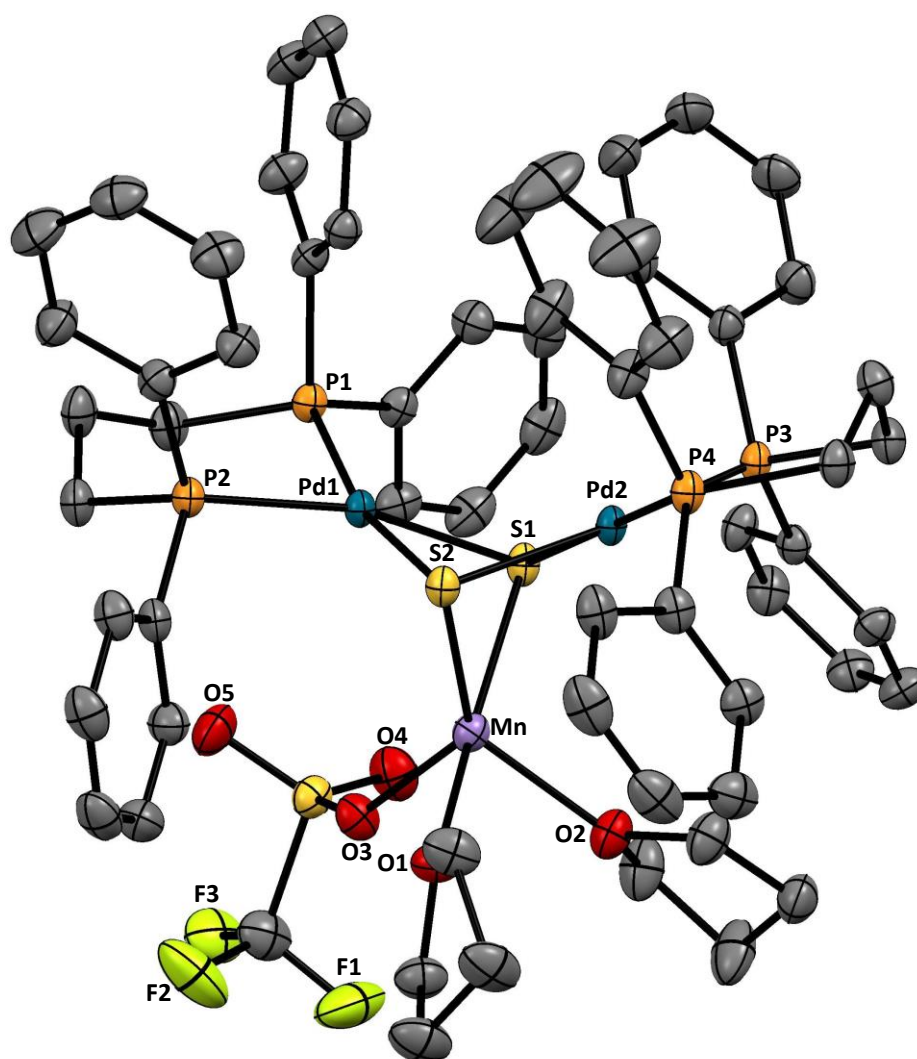


Figure 2.5. Molecular structure of complex **4**. Grey spheres represent C, yellow: S, orange: P, blue: Pd, purple: Mn, red: O, and green: F. Ellipsoids are depicted at 50% probability. Hydrogen atoms were omitted for clarity.

Table 2.3. Selected bond distances (Å) and angles (deg) for **4**.

	Distance (Å)		Angle (°)
Mn1-Pd1	3.0227(9)	S1-Mn1-S2	79.55(3)
Mn1-Pd2	3.093(1)	S1-Mn1-O2	98.62(7)
Pd1-Pd2	3.1818(8)	S1-Mn1-O3	103.66(7)
S1-S2	3.172(1)	S1-Mn1-O1	169.46(6)
Mn1-S1	2.506(1)	O1-Mn1-S2	91.30(6)
Mn1-S2	2.452(1)	O1-Mn1-O2	83.51(9)
Mn1-O1	2.203(2)	O1-Mn1-O3	86.28(9)
Mn1-O2	2.137(2)	S2-Mn1-O2	131.70(7)
Mn1-O3	2.113(3)	S2-Mn1-O3	131.20(7)
Pd1-S1	2.3427(9)	O2-Mn1-O3	96.47(9)
Pd1-S2	2.368(1)	S1-Pd1-S2	84.66(3)
Pd1-P1	2.2797(9)	S1-Pd1-P1	91.40(3)
Pd1-P2	2.2865(9)	S2-Pd1-P2	93.59(3)
Pd2-S1	2.336(1)	P1-Pd1-P2	93.15(3)
Pd2-S2	2.3737(9)	Pd1-S1-Pd2	85.71(2)
Pd2-P3	2.2775(9)	Pd1-S2-Pd2	84.30(2)
Pd2-P4	2.275(1)	S1-Pd2-S2	84.68(3)
		S1-Pd2-P3	86.44(3)
		S2-Pd2-P4	91.59(3)
		P3-Pd2-P4	97.30(3)
		P1-S1-P3	120.83(3)
		P2-S2-P4	141.59(3)

Similar to **2**, the manganese centre is also coordinated to the two bridging sulfur ligands. However, two THF ligands as well as a triflate ligand are bound to manganese as opposed to the two chloride ligands. The two THF are coordinated to manganese through oxygen with Mn—O distances (2.203(2) Å and 2.137(3) Å) that are short enough to confirm bonding interactions. The triflate ligand is bonded to manganese through oxygen as well with a Mn—O distance of 2.113(3) Å. The geometry around the manganese(II) centre forms a distorted trigonal bipyramidal structure where the S1 sulfide ligand and the O1 of THF define the axial ligands, while the remaining triflate, THF and sulfide represent the equatorial ligands. The 5-coordinate geometry index of $\tau_5 = 0.629$ for manganese(II) indicates that there is a significant amount of square planar character exhibited in the geometry. The S1—Mn—O1 angle deviates slightly from the expected angle of 180° by ~10° with an angle of 169.46(6)°. The S2—Mn—O2 and S2—Mn—O3 equatorial

angles ($131.20(7)^\circ - 131.70(7)^\circ$) are much larger than the O2—Mn—O3 angle of $96.47(9)^\circ$, both deviating from the expected value of 120° .

The geometry around the two palladium structures differs between each other, however both exhibit a distorted square planar structure. The 4-coordinate geometry index differs between the two Pd atoms, with $\tau_4 = 0.191$ ($\tau_4' = 0.188$) for Pd1 and $\tau_4 = 0.094$ ($\tau_4' = 0.076$) for Pd2. The S—Pd—S angles ($84.66(3)^\circ$ and $84.68(3)^\circ$) are statistically identical and very similar to the values found for complex **2** ($84.45(7)^\circ$ and $84.43(7)^\circ$). The P—Pd—P angles ($93.15(3)^\circ$ and $97.30(3)^\circ$) however, deviate to a larger extent than they do for **2** ($91.44(8)^\circ$ and $95.26(8)^\circ$). Although the P3—Pd2—P4 angle ($97.30(3)^\circ$) deviates from 90° more than the P1—Pd1—P2 angle ($93.15(3)^\circ$), the P3 and P4 atoms remain in plane with the square planar geometry while the P1 and P2 atoms do not remain in plane (Figure 2.6). The twisted dppp ligated to Pd1 gives rise to differing P—S—P angles ($120.83(3)^\circ$ and $141.59(3)^\circ$), rather than the symmetrical P—S—P angles seen in **2**. The phenyl groups of the dppp ligands are likely strained due to the bulk introduced by the large triflate ligand bound to the manganese(II) centre, which is supported by the space filling model. The $\{\text{Pd}_2\text{S}_2\}$ moiety forms a similar ring structure that folds along the two sulfur ligands forming the butterfly shaped. The angle across the S...S vector for the Pd—S₂—Pd arrangement is observed to be 132.09° for **4**. The Pd—Pd ($3.1818(8) \text{ \AA}$) and Mn—Pd ($3.0227(9) \text{ \AA}$ and $3.093(1) \text{ \AA}$) distances are too large for any bonding interactions to be suggested. The S—S ($3.172(1) \text{ \AA}$) distance is similar to that seen for other $\{\text{Pd}_2\text{S}_2\}$ butterfly structures, however the distance is too long for any bonding interactions to be described. The length of the bridging Pd—S bonds ($2.336(1) - 2.3737(9) \text{ \AA}$) are within range of reported values for other palladium-sulfide bonding interactions.^{10, 27}

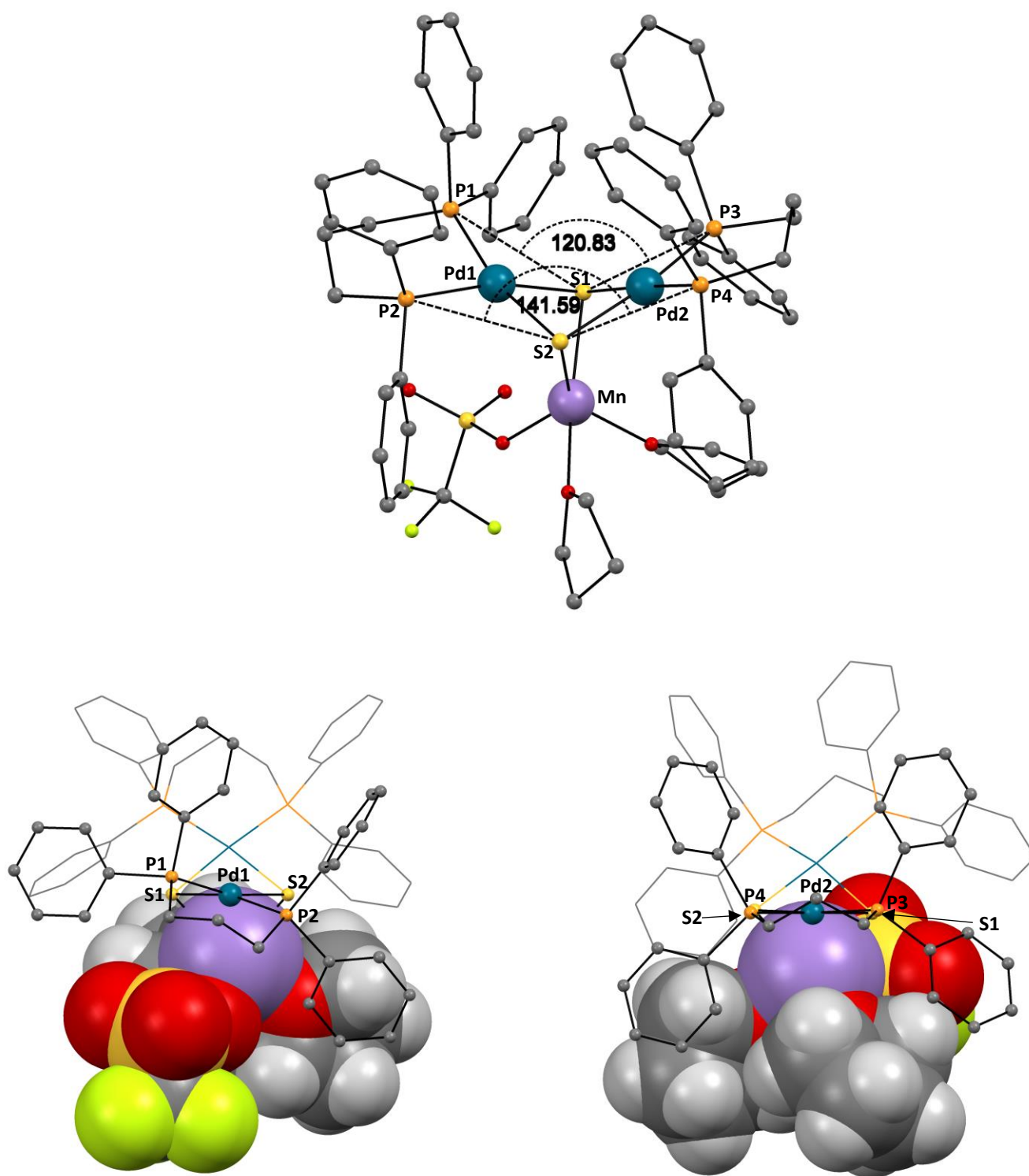


Figure 2.6. View of molecular structure of **4** showing different P—S—P angles (top) and distortion of square planar geometry around Pd1 (bottom left) and Pd2 (bottom right). The bottom perspectives depict the thf and OTf ligands with spacefilling models to show the proximity of the Ph of dppp to these ligands.

Similar reactions were conducted as with complex **3** in an attempt to synthesize a compound with a larger and/or smaller number of dppp containing palladium(II) moieties. $[(\text{dppp})\text{Pd}(\text{SSiMe}_3)_2]$ was reacted with $[\text{Mn}(\text{OTf})_2]$ in a 1:1 and 3:1 ratio in a similar manner to that described for the preparation of **4**. Crystallization attempts were made, however the mixture was unable to produce suitable crystals for X-ray diffraction studies.

2.3.5 UV-Vis Absorption, Emission and EPR Spectroscopy

Electronic spectroscopy studies for complexes **2** and **4** were performed in CH_2Cl_2 and THF respectively in various concentrations. Complex **2** was not completely soluble in THF so CH_2Cl_2 was used, and complex **4** was run in THF to avoid any Cl^- contamination that may occur from CH_2Cl_2 . The data gathered from these spectra are summarized in Table 2.4 and the spectra themselves are displayed in Figure 2.7. The spectrum of **2** shows two peaks at 283 and 531 nm and two shoulders at 320 and 410 nm. The peak at 283 nm has two small but noticeable shoulders at 268 and 275 nm. The spectrum for **4** reveals 2 peaks at 350 and 275 nm and a shoulder at 406 nm with the low energy absorbance above 500 nm not being present. The peak at 275 nm appears to contain a similar set of shoulder absorbances, however the overlap with the absorbance from THF makes it difficult to accurately describe.

Table 2.4. Electronic transitions for complexes **2** and **4**.

	2	4
$\lambda_{\text{max}}/\text{nm}$ ($\epsilon / \text{M}^{-1}\text{cm}^{-1}$)	268 (16700)	275 (72500)
	275 (17100)	350 (36700)
	283 (17500)	406 (16600)
	320 (9250)	
	410 (1130)	
	531 (254)	

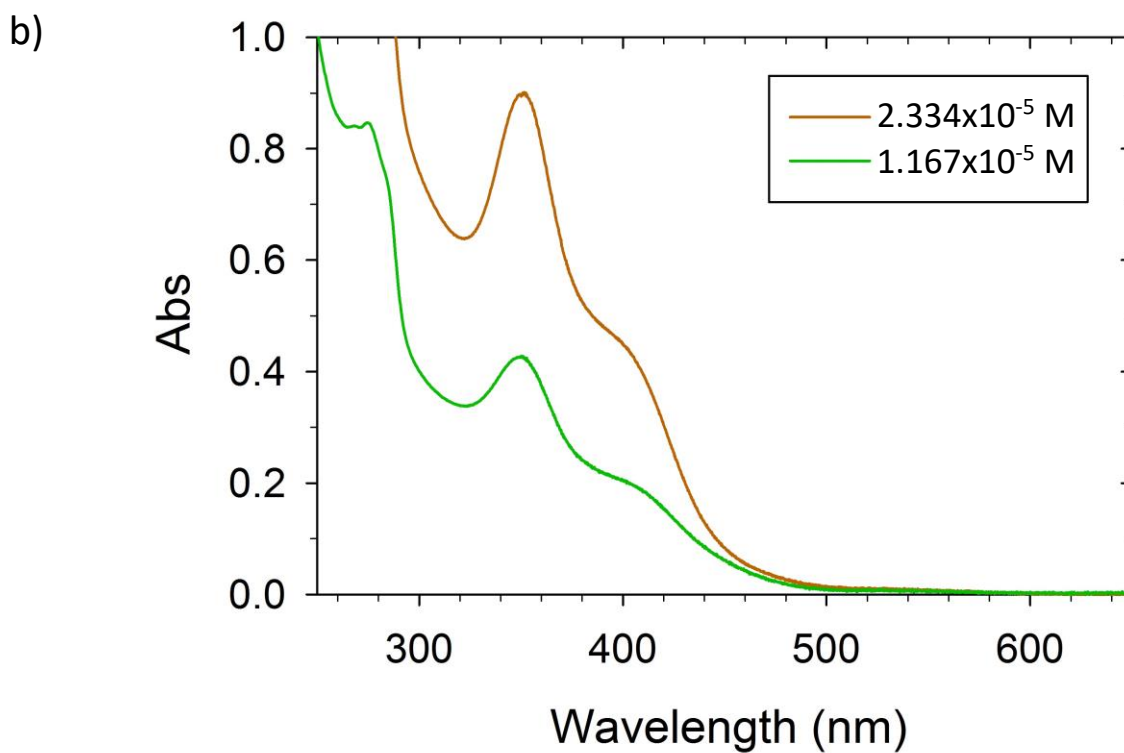
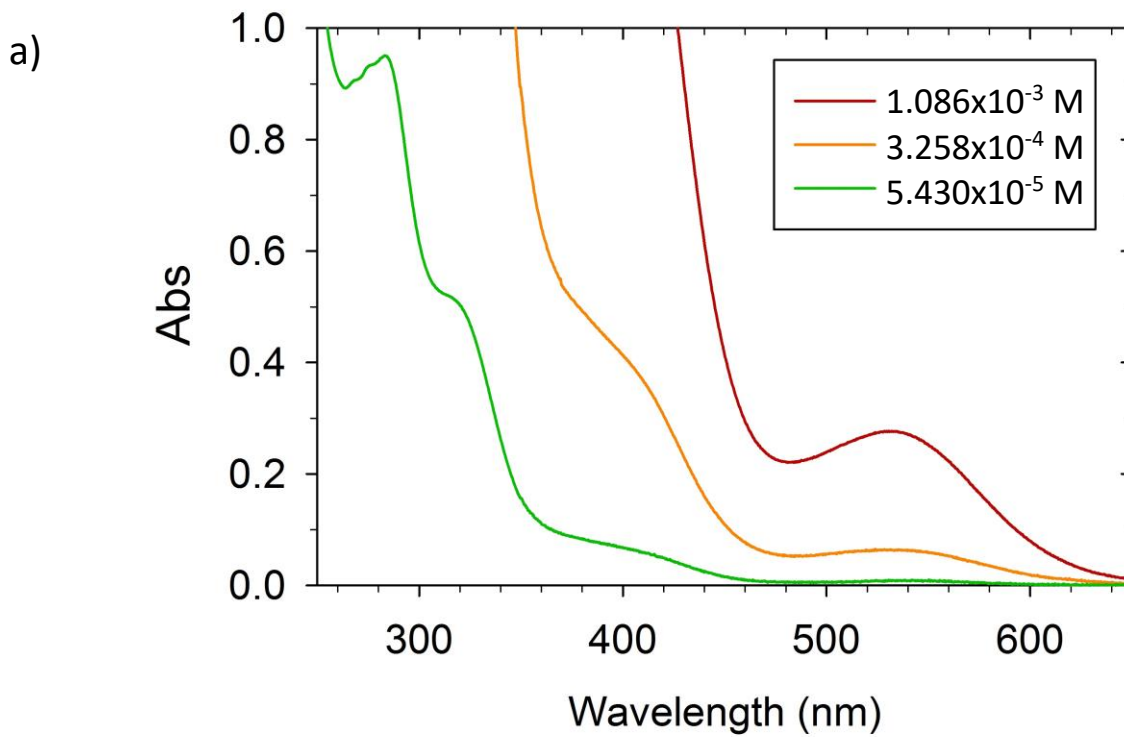


Figure 2.7. UV-Vis absorption spectra of (a) **2** and (b) **4** at different concentrations.

The absorbances below 300 nm are due to the dppp ligands and have been observed for other diphosphine palladium(II) complexes.¹⁷ The shoulders at 320 and 410 nm for **3** and the peak at 350 and shoulder at 406 nm for **4** dominate the rest of the spectrum and trail out towards lower energy regions. Transitions observed between 300 and 400 nm have previously been assigned to sulfur-to-palladium LMCT transitions, which is likely the case for these four transitions.²⁸ The higher wavelength band for **2** at 531 nm is of much weaker absorption, and can be attributed to manganese(II) d-d transition. Transitions of this nature have been described for other manganese(II) species and are typically observed above 400 nm as a very weak absorbance.²⁹

Solid state emission studies were performed on **2** and **4** as well. The samples were mounted on a crystalline silicon wafer and irradiated with a 400 nm light source. The resulting spectra, displayed in Figure 2.8, reveal a weak emission in the infrared region below 700 nm. Unfortunately, the detector used is not sensitive enough to observe the details of the emission, however the emission for **2** appears to exhibit a peak at ~950 nm. A weak artifact emission at ~450 nm is present in both spectra, likely due to preferential scattering from the sample plate. Solution emission spectra were attempted at room temperature, however there were no noticeable emissions in the infrared region. Previous reports have shown manganese(II) coordination complexes to emit at ~700 nm, however emission from these complexes is quite rare.³⁰ Palladium(II) complexes typically do not exhibit photoluminescent properties at room temperature due to nonradiative deactivation of the low energy metal-centered excited state via molecular distortion.³¹

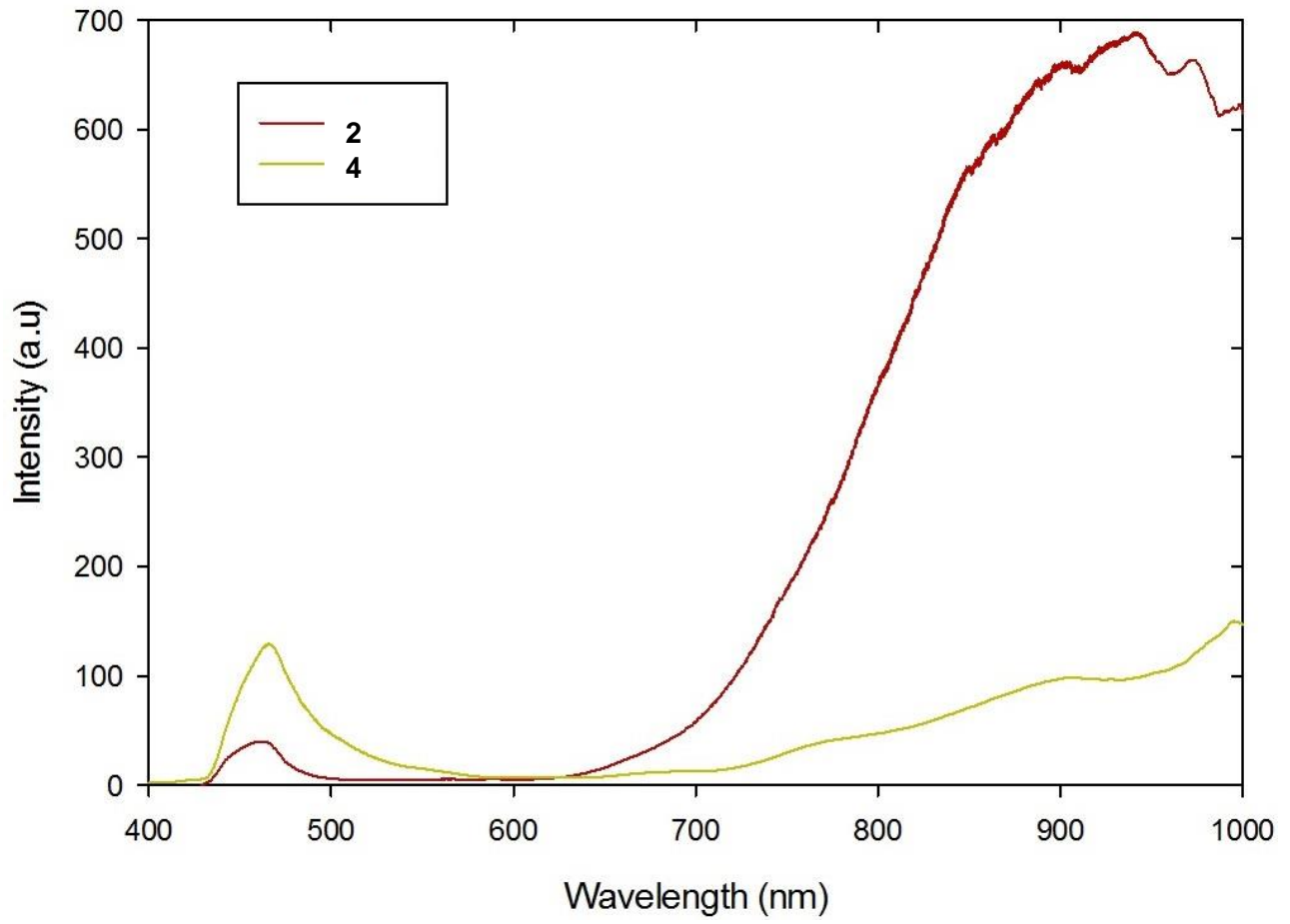


Figure 2.8. Solid state emission spectra of **2** and **4**.

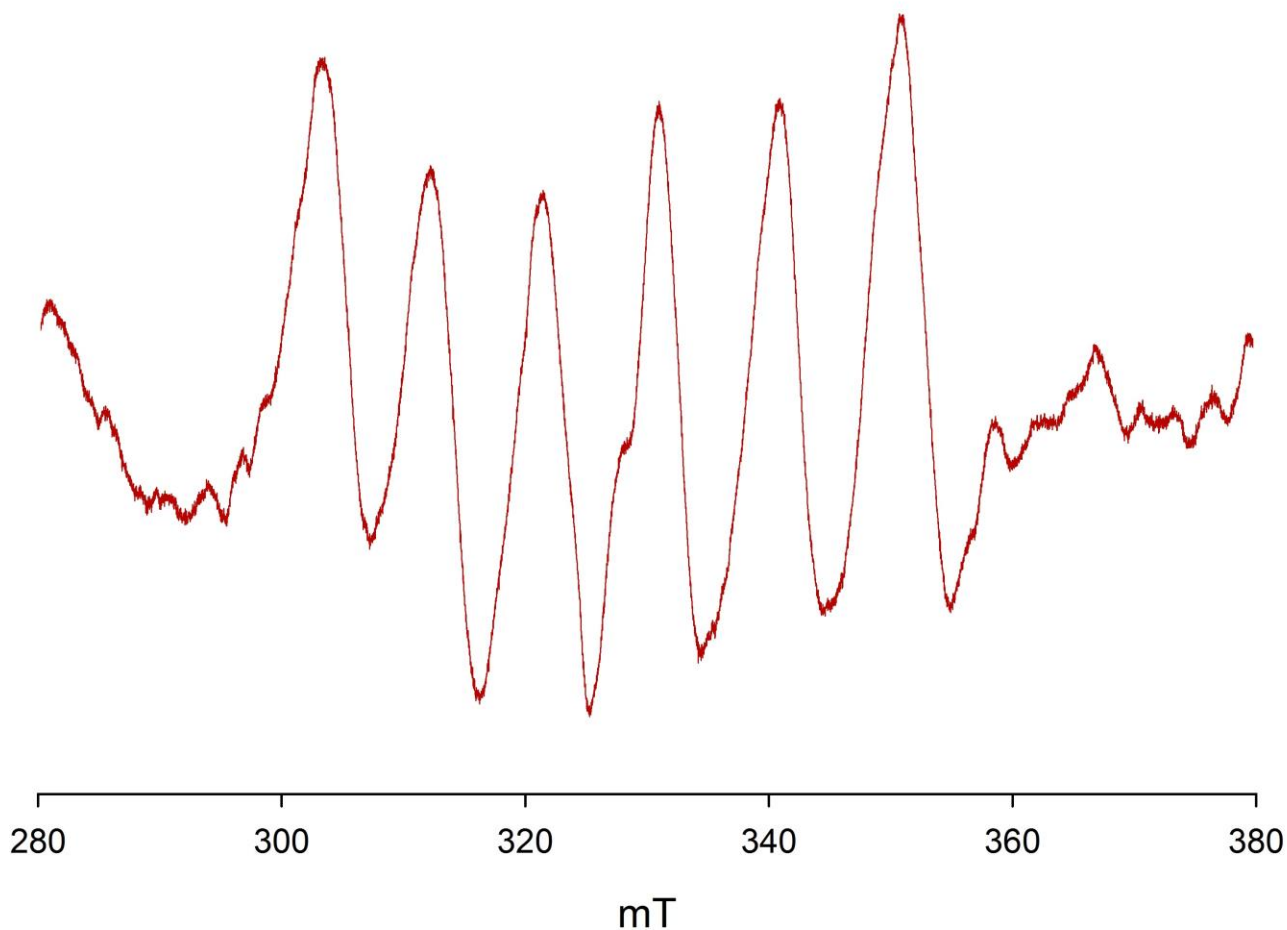


Figure 2.9. EPR spectrum of **4** in THF. Spectrum parameters: $g = 1.9867$, line width = 3.827, $a = 9.496$ mT

^1H , $^{13}\text{C}\{^1\text{H}\}$ and $^{31}\text{P}\{^1\text{H}\}$ NMR spectroscopy studies were performed on compounds **2** and **4** however there were no clearly visible signals present in the spectra collected. Unpaired electrons around the manganese centre exhibit a magnetic moment due to their charge and spin, causing each unpaired electron to act as a miniature bar magnet. This perturbs the uniformity of the magnetic field induced by the NMR spectrometer and makes it very difficult to observe signals from nuclei in the vicinity of these unpaired electrons due to broadening of their signals.³² The analogous method of electron paramagnetic resonance (EPR) spectroscopy can be used instead to study the nature of the unpaired electrons about the manganese(II) metal. EPR spectroscopy was

performed on a solution of **4** in THF. The data were collected under a steady microwave radiation source of 9148 MHz while the magnetic field was varied from 280 to 380 mT with a hyperfine coupling constant of 9.496 mT. The spectrum, displayed in Figure 2.9, reveals a signal containing six peaks which spans ~ 60 mT. The signal exhibits a g value of 1.9867 which falls into the acceptable range of g values for other manganese(II) run at room temperature ($\sim 1.97 - 2.07$).³³⁻³⁶ Manganese(II) contains a nuclear spin of $5/2$, and the interaction of one unpaired electron spins with the nucleus will result in six different absorbances, as the 1st derivative spectrum reveals. A high-spin manganese(II) d^5 metal centre often results in a complex spectrum consisting of overlapping signals.³⁷ The spectrum exhibits some weak shouldering on the primary signal, however due to the low intensity of the spectrum it could not be determined whether it was noise or an overlapping signal. Low-spin manganese(II) complexes are quite rare, and ligands with very strong ligand fields are typically present in high-spin manganese(II) complexes.³⁸ Only high-spin complexes have been reported for trigonal bipyramidal manganese(II) systems, with one report exhibiting a similar six peak signal.³⁹⁻⁴¹ It is likely that manganese(II) is high-spin here, though the resolution is too low to confirm. There is no visible coupling to the phosphorus nuclei which indicates they are too far to have any interaction.

2.4 Conclusions

The reaction of $[(dppp)PdCl_2]$ with $[Li(N,N'-tmeda)]_2[Mn(SSiMe_3)_4]$ **1** was performed in a 2:1 ratio, yielding the new manganese(II) containing metal sulfide complex $[MnCl_2(\mu-S)_2Pd_2(dppp)_2]$ **2** in relatively good yield and under mild reaction conditions. Similar reactions with an increased ratio of $[(dppp)PdCl_2]:[Mn(SSiMe_3)_4]^{2+}$ only produced **2**, even if $[(dppp)Pd(OAc)_2]$ was used with non-chlorinated solvents. This is likely due to the presence of LiCl in the crystals of the complex $[Li(N,N'-tmeda)]_2[Mn(SSiMe_3)_4]$ **1**. In order to completely avoid contact with chlorine, the new trimethylsilyl chalcogenolate $[(dppp)Pd(SSiMe_3)_2]$ **3** was synthesized by reaction of $Li[SSiMe_3]$ with $[(dppp)Pd(OAc)_2]$ in a 2:1 ratio. This compound exhibited relatively good temperature stability and surprisingly good solution stability compared to the analogous metal thiolates such as $[Li(N,N'-tmeda)]_2[Mn(SSiMe_3)_4]$ **1**. The reaction of $[(dppp)Pd(SSiMe_3)_2]$ with $[Mn(OTf)_2]$ in a 2:1 ratio produced the new complex $[MnOTf(thf)_2(\mu-S)_2Pd_2(dppp)_2]OTf$ **4** under mild conditions. Although the lack of chlorine led to the synthesis of a new coordination complex, differing Pd:Mn ratio complexes (1:1, 3:1) were still unattainable. Since complex **4** was shown to exhibit steric crowding between the phenyl groups of the dppp ligand and the triflate and thf ligands, it is possible that larger Pd:Mn ratios were inaccessible due to sterics preventing coordination of manganese to another palladium unit. Smaller chelating phosphine ligands may produce higher nuclearity complexes. Complexes were characterized through multiple techniques including NMR spectroscopy, EPR spectroscopy, elemental analysis, X-ray crystallography, UV-Vis absorption and solid state emission spectroscopy. These reactions illustrate the difficulties associated with the synthesis of large and diverse manganese(II) containing coordination complexes.

2.5 References

1. M.N. Sokolov and P.A. Abramov; *Coordination Chemistry Reviews*, **2012**. 256(17–18): p. 1972-1991.
2. O. Fuhr, S. Dehnen, and D. Fenske; *Chemical Society Reviews*, **2013**. 42(4): p. 1871-1906.
3. S. Dehnen, A. Eichhofer, and D. Fenske; *European Journal of Inorganic Chemistry*, **2002**. 2002(2): p. 279-317.
4. T.I. Levchenko, C. Kubel, D. Wang, B.K. Najafabadi, Y.N. Huang, and J.F. Corrigan; *Chemistry of Materials*, **2015**. 27(10): p. 3666-3682.
5. Y. Liu, B. Khalili Najafabadi, M. Azizpoor Fard, and J.F. Corrigan; *Angewandte Chemie*, **2015**. 127(16): p. 4914–4917.
6. D.G. MacDonald and J.F. Corrigan; *Philosophical Transactions of the Royal Society A: Mathematical Physical and Engineering Sciences*, **2010**. 368(1915): p. 1455-1472.
7. M. Bouroushian, *Chalcogens and Metal Chalcogenides*, in *Electrochemistry of Metal Chalcogenides*. Springer: Heidelberg, Berlin. **2010**; p. 1-56.
8. C.E. Anson, A. Eichhofer, I. Issac, D. Fenske, O. Fuhr, P. Sevillano, C. Persau, D. Stalke, and J. Zhang; *Angewandte Chemie-International Edition*, **2008**. 47(7): p. 1326-1331.
9. V.K. Jain and L. Jain; *Coordination Chemistry Reviews*, **2005**. 249(24): p. 3075-3197.
10. S.W. Audi Fong and T. S. Andy Hor; *Journal of the Chemical Society, Dalton Transactions*, **1999**. 1999(5): p. 639-652.
11. G.M. Li, S. Li, A.L. Tan, W.H. Yip, T.C.W. Mak, and T.S.A. Hor; *Journal of the Chemical Society-Dalton Transactions*, **1996**(23): p. 4315-4316.
12. B. Wu, W.-J. Zhang, S.-Y. Yu, T.-L. Sheng, and X.-T. Wu; *Journal of Organometallic Chemistry*, **1997**. 545–546: p. 587-589.
13. M.A.F. Hernandez-Gruel, I.T. Dobrinovitch, F.J. Lahoz, L.A. Oro, and J.J. Perez-Torrente; *Organometallics*, **2007**. 26(25): p. 6437-6446.
14. J. Li and T.S.A. Hor; *Dalton Transactions*, **2008**(42): p. 5708-5711.

15. J.-A. Dimmer, M. Hornung, F. Weigend, and L. Wesemann; *Dalton Transactions*, **2010**. 39(32): p. 7504-7512.
16. T. Komuro, T. Matsuo, H. Kawaguchi, and K. Tatsumi; *Chemical Communications*, **2002**. 2002(9): p. 988-989.
17. M.A. Fard, M.J. Willans, B.K. Najafabadi, T.I. Levchenko, and J.F. Corrigan; *Dalton Transactions*, **2015**. 44(17): p. 8267-8277.
18. C.B. Khadka, D.G. Macdonald, Y.H. Lan, A.K. Powell, D. Fenske, and J.F. Corrigan; *Inorganic Chemistry*, **2010**. 49(16): p. 7289-7297.
19. C.B. Khadka, *Transition metal complexes with reactive trimethylsilylchalcogenolate ligands precursors for the preparation of ternary nanoclusters*. School of Graduate and Postdoctoral Studies, University of Western Ontario, London, Ont. **2011**. p. xvii, 178 leaves ill.
20. A.B. Pangborn, M.A. Giardello, R.H. Grubbs, R.K. Rosen, and F.J. Timmers; *Organometallics*, **1996**. 15(5): p. 1518-1520.
21. D. Taher, A.I. Wallbank, E.A. Turner, H.L. Cuthbert, and J.F. Corrigan; *European Journal of Inorganic Chemistry*, **2006**. 2006(22): p. 4616-4620.
22. P.J. Riedel, N. Arulsamy, and M.P. Mehn; *Inorganic chemistry communications*, **2011**. 14(5): p. 734-737.
23. G. Sheldrick; *Acta Crystallographica Section A*, **2008**. 64(1): p. 112-122.
24. G.M. Sheldrick; *Acta Crystallographica. Section C, Structural Chemistry*, **2015**. 71(Pt 1): p. 3-8.
25. M. Nippe, J. Wang, E. Bill, H. Hope, N.S. Dalal, and J.F. Berry; *Journal of the American Chemical Society*, **2010**. 132(40): p. 14261-14272.
26. T.J. Mooibroek, E. Bouwman, M. Lutz, A.L. Spek, and E. Drent; *European Journal of Inorganic Chemistry*, **2010**(2): p. 298-310.
27. B.C. Tzeng, S.C. Chan, M.C.W. Chan, C.M. Che, K.K. Cheung, and S.M. Peng; *Inorganic Chemistry*, **2001**. 40(26): p. 6699-6704.
28. W. Su, R. Cao, M. Hong, D. Wu, and J. Lu; *Journal of the Chemical Society, Dalton Transactions*, **2000**(9): p. 1527-1532.

29. C.A. Téllez S, A.C. Costa Jr, M.A. Mondragón, G.B. Ferreira, O. Versiane, J.L. Rangel, G.M. Lima, and A.A. Martin; *Spectrochimica Acta Part A: Molecular and Biomolecular Spectroscopy*, **2016**. 169: p. 95-107.
30. O. Siiman, M. Wrighton, and H.B. Gray; *Journal of Coordination Chemistry*, **1972**. 2(2): p. 159-161.
31. R.C. Evans, P. Douglas, and C.J. Winscom; *Coordination Chemistry Reviews*, **2006**. 250(15-16): p. 2093-2126.
32. R. Pigliapochi, A.J. Pell, I.D. Seymour, C.P. Grey, D. Ceresoli, and M. Kaupp; *Physical Review B*, **2017**. 95(5): p. 11.
33. C. Duboc, V. Astier-Perret, H. Chen, J. Pécaut, R.H. Crabtree, G.W. Brudvig, and M.-N. Collomb; *Inorganica Chimica Acta*, **2006**. 359(5): p. 1541-1548.
34. S. Chandra and L.K. Gupta; *Spectrochimica Acta Part A: Molecular and Biomolecular Spectroscopy*, **2005**. 61(11-12): p. 2549-2554.
35. S. Chandra and L.K. Gupta; *Spectrochimica Acta Part A: Molecular and Biomolecular Spectroscopy*, **2004**. 60(8-9): p. 1751-1761.
36. S. Krishnan, K. Laly, and M.R. Prathapachandra Kurup; *Spectrochimica Acta Part A: Molecular and Biomolecular Spectroscopy*, **2010**. 75(2): p. 585-588.
37. A.R. Coffino and J. Peisach; *Journal of Magnetic Resonance, Series B*, **1996**. 111(2): p. 127-134.
38. D. Basumatary, R.A. Lal, and A. Kumar; *Journal of Molecular Structure*, **2015**. 1092: p. 122-129.
39. L.M. Brines, J. Shearer, J.K. Fender, D. Schweitzer, S.C. Shoner, D. Barnhart, W. Kaminsky, S. Lovell, and J.A. Kovacs; *Inorganic Chemistry*, **2007**. 46(22): p. 9267-9277.
40. C.P. Berlinguette, D. Vaughn, C. Cañada-Vilalta, J.R. Galán-Mascarós, and K.R. Dunbar; *Angewandte Chemie*, **2003**. 115(13): p. 1561-1564.
41. H.-L. Wu and Y.-C. Gao; *Journal of Coordination Chemistry*, **2006**. 59(2): p. 137-146.

Chapter Three

Metal Trimethylsilylthiolate Precursors for the Formation of Au—S—Mn and FcC{O}—S—Mn Bonding Interactions

3.1 Introduction

The successful synthesis of ternary metal sulfide complexes $[\text{MnCl}_2(\mu\text{-S})_2\text{Pd}_2(\text{dppp})_2]$ **2** and $[\text{MnOTf}(\text{thf})_2(\mu\text{-S})_2\text{Pd}_2(\text{dppp})_2]$ **4** by reaction of the metal trimethylsilylthiolates $[\text{Li}(\text{N,N}'\text{-tmeda})]_2[\text{Mn}(\text{SSiMe}_3)_4]$ **1** and $[(\text{dppp})\text{Pd}(\text{SSiMe}_3)_2]$ **3** with metal salts $[(\text{dppp})\text{PdCl}_2]$ and $[\text{Mn}(\text{OTf})_2(\text{CH}_3\text{CN})_2]$, respectively, illustrate the potential for these new metal complexes with reactive trimethylsilylchalcogenolate ligands to act as precursors for the synthesis of unique ternary MM'E (E = S, Se, Te) complexes. Continuing with the goal of developing manganese(II) sulfide coordination chemistry, this chapter employs metal trimethylsilylthiolate complexes as precursors toward the formation of Au—S—Mn and FcC{O}—S—Mn (Fc = Ferrocene) bonding interactions.

Manganese(II) has been utilized as a dopant in various ternary metal chalcogenide systems due to its desirable paramagnetic and luminescent properties.^{1,2} Various methods have been employed to incorporate manganese(II) into these semiconductor systems, however the product often takes the form of bulk solid or polydisperse nanoscale solid.³ In an effort to control the structure and chemical composition of these ternary metal chalcogenide systems, Eichhofer and co-workers employed bis-trimethylsilylamide transition metal complexes $\text{Cd}(\text{N}(\text{SiMe}_3)_2)_2$ and $\text{Mn}(\text{N}(\text{SiMe}_3)_2)_2$ with HSePh and $\text{E}(\text{SiMe}_3)_2$ (E = S, Se) to form $[\text{Cd}_4\text{Mn}_6\text{Se}_4(\text{SePh})_{12}(\text{P}^n\text{Pr}_3)_4]$ and $[\text{Cd}_4\text{Mn}_4\text{S}(\text{SePh})_{14}(\text{P}^n\text{Pr}_3)_2]$.⁴ The synthesis of these ternary complexes marks the first examples of these systems in a size form that allows for proper structural characterization. Expanding on this development, Khadka and co-workers synthesized and structurally characterized the ternary nanoclusters $[(\text{N,N}'\text{-tmeda})_6\text{Zn}_{14-x}\text{Mn}_x\text{S}_{13}\text{Cl}_2]$ and $[(\text{N,N}'\text{-tmeda})_6\text{Zn}_{14-x}$

$x\text{Mn}_x\text{Se}_{13}\text{Cl}_2$] (tmeda = $(\text{CH}_3)_2\text{NCH}_2\text{CH}_2\text{N}(\text{CH}_3)_2$) from the reaction of the metal chalcogenolate precursor $[(\text{tmeda})\text{Zn}(\text{ESiMe}_3)_2]$ (E = S, Se) with manganese(II) and zinc(II) salts.⁵ These metal chalcogenolate complexes are ideal precursors for the formation of ternary M—E—M' bonding interactions due to the preformed metal-chalcogen bond, their high solubility in common organic solvents and the reactivity of the $-\text{ESiMe}_3$ ligands towards ligand stabilized metal salts.⁶

Ligand stabilized gold(I) salts have previously been used along with trimethylsilylchalcogenolate functionalized precursors to produce metal chalcogenide clusters and coordination complexes. Many of the gold compounds synthesized in this method have been binary systems, however ternary systems should theoretically be accessible by reaction of a metal trimethylsilylthiolate complex with a second type of metal salt. Mixed gold-indium-selenide clusters have been prepared utilizing $\text{Se}(\text{SiMe}_3)_2$ as an Se^{2-} source along with the subsequent metal chloride salts.⁷ This methodology, however, does not provide rigid control over the reaction products. The ternary clusters received through this method contain Au_2Se and Au_3Se subunits. This indicates that the Se^{2-} source likely facilitates the formation of stable binary units which interact with the heterometal through the $\mu_2\text{-Se}^{2-}$ and $\mu_3\text{-Se}^{2-}$ ligands respectively to form the subsequent ternary clusters. Gold-silver-chalcogenide clusters containing similar Au_3S subunits in its structure have also been reported.⁸ Although no manganese containing gold sulfide clusters have been synthesized, spin-polarized DFT computations have been performed to investigate the electronic and magnetic properties of various gold sulfide clusters.⁹⁻¹¹ It has been observed that electronic and magnetic properties are affected by the quantity of paramagnetic atoms introduced into a cluster, as well as the location of these atoms within the framework. These data indicate that if these materials are to be used in molecular spintronics devices, strict site control over magnetic doping is essential.

Ferrocene has the potential to be employed in metal chalcogenide complexes to functionalize phosphido and chalcogenolate surface ligands. Ferrocene introduces electrochemical properties to cluster complexes, which allows for applications in redox-active and/or luminescent sensors as well as electrode materials.^{12, 13} Recently, a silver sulfide

nanocluster decorated with ferrocene-based dithiolate units $[\text{Ag}_{74}\text{S}_{19}(\text{dppp})_6(\text{Fc}(\text{C}\{\text{O}\}\text{OCH}_2\text{CH}_2\text{S})_2)_{18}]$ has been synthesized by treating a silver(I) thiolate coordination polymer $[\text{Fc}(\text{C}\{\text{O}\}\text{OCH}_2\text{CH}_2\text{SAg})_2]_n$ with the S^{2-} source $\text{S}(\text{SiMe}_3)_2$.¹⁴ This method conveniently allows ferrocene to be incorporated into the cluster as a functional group. Ferrocene has been incorporated into the manganese(II) thiolate complex $[(\text{Mn}(\text{CO})_3)_2(\mu\text{-SPh})_2(\mu\text{-dppfe})]$ through phosphine ligation with the ferrocene containing diphosphine dppfe (dppfe = 1,1'-bis(diphenylphosphino)ferrocene).¹⁵ However, the redox properties of this compound were not observable due to decomposition during cyclic voltammetry (CV) measurements. The synthesis of a manganese(II) complex containing a ferrocene unit bonded through a thiolate ligand has yet to be reported, and a complex of this nature may exhibit interesting redox chemistry.

Successful implementation of metal trimethylsilylchalcogenolate complexes as a metal and chalcogen source can allow for the controlled synthesis of chemically unique and structurally diverse manganese(II) containing complexes. This chapter explores the reaction of metal trimethylsilylthiolate complexes $[\text{Li}(\text{N},\text{N}'\text{-tmeda})]_2[\text{Mn}(\text{SSiMe}_3)_4]$ **1** and $[\text{Ph}_3\text{PAuSSiMe}_3]$ **5** with the ligand stabilized metal salts $[\text{R}_3\text{PAuX}]$ ($\text{R} = \text{Et}_3, \text{Ph}_3$; $\text{X} = \text{Cl}, \text{OTf}$) and $[(\text{CH}_3\text{CN})_2\text{Mn}(\text{OTf})_2]$, respectively, as well the reaction of **1** with ferrocenoyl chloride in an effort to facilitate Au—S—Mn and $\text{FcC}\{\text{O}\}\text{—S—Mn}$ bonding interactions.

3.2 Experimental

All experimental procedures were performed using standard double manifold Schlenk line techniques under an atmosphere of dried nitrogen gas or in nitrogen filled glove boxes. The nonchlorinated solvents (pentane, hexanes, THF, toluene), purchased from Caledon (HPLC grade), were dried and collected using an MBraun MB-SP Series solvent purification system with tandem activated alumina (THF, toluene) and activated alumina/copper redox catalyst (hydrocarbons)¹⁶. Dichloromethane (CH_2Cl_2), purchased from Caledon, was dried and distilled

over P₂O₅. *N,N,N',N'*-tetramethylethylenediamine (TMEDA), purchased from Sigma Aldrich, was dried and distilled over CaH₂. Spectral grade solvent chloroform CDCl₃, purchased from Cambridge Isotope Laboratories, was dried and distilled over P₂O₅. Chemicals were used as received from Alfa Aesar and/or Sigma Aldrich without further purification. Starting reagents S(SiMe₃)₂,¹⁷ Li[SSiMe₃],¹⁷ [Ph₃PAuCl],¹⁸ [FcC{O}OH],¹⁹ [FcC{O}Cl],²⁰ [Li(N,N'-tmeda)]₂[Mn(SSiMe₃)₄],⁶ and [(CH₃CN)₂Mn(OTf)₂]²¹ were synthesized using literature procedure. Celite® was dried by heating at 120 °C under vacuum for 48 hours.

For precursor materials, ¹H and ³¹P{¹H} NMR spectra were recorded on a Varian Mercury 400 MHz spectrometer with an operating frequency of 400.08 MHz and the chemical shifts were referenced internally to signals from residual H relative to SiMe₄ (¹H) or 85% H₃PO₄ (³¹P). For the rest of the materials, ¹H and ³¹P{¹H} NMR spectra were recorded on an Inova 400 MHz with an operating frequency of 399.76 MHz and internally referenced to the residual proton peak in CDCl₃ relative to SiMe₄ (¹H) or 85% H₃PO₄ (³¹P). Mass spectrometry and exact mass determinations were performed on a Bruker micrOTOF II instrument. Calculated patterns were produced using Scientific Instrument Services Inc. (SIS) Isotope Distribution Calculator and Mass Spec Plotter.

Energy Dispersive X-ray (EDX) analysis on product mixture from gold manganese sulfide reactions were performed at Western Nanofabrication Facility, London, Ontario. A Quartz XOne EDX analysis system coupled to a Leo 440 SEM equipped with a Gresham light element detector was used to obtain semiquantitative analysis of gold and manganese. The single crystal X-ray measurement was made on a Bruker Kappa Axis Apex2 diffractometer at a temperature of 110 K. Crystals were mounted on a Mitegen polyimide micromount with a small amount of Paratone N oil. The molecular structure of [S(AuPPh₃)₃]Cl was solved via direct methods using the SHELX suite of crystallographic programs (Sheldrick, G. M., Madison, WI).²²

3.2.1 Attempted Synthesis of $[(\text{NCCH}_3)_2\text{Mn}(\text{SAuPPh}_3)_2]$

$[\text{Ph}_3\text{PAuSSiMe}_3]$ (0.0600 g, 0.1057 mmol) was dissolved in 6 mL THF to form a clear and colourless solution. A colourless solution of $[(\text{CH}_3\text{CN})_2\text{Mn}(\text{OTf})_2]$ (0.023 g, 0.053 mmol) in 6 mL THF was added at room temperature to immediately yield a transparent, pale beige coloured solution. The reaction was left to stir for 2 hours at this temperature to produce a mixture of a pale beige liquid and a very fine, colourless precipitate. The mixture was filtered over dried Celite® through a glass frit. Crystallization was performed on the resulting solution by layering with 25 mL of pentane and cooling to $-25\text{ }^\circ\text{C}$ for storage. Clear, colourless, needle-shaped crystals were deposited after 2 days. X-ray diffraction studies on the crystals proved the compound to be the previously characterized complex $[\text{S}(\text{AuPPh}_3)_3]\text{Cl}$ **6** as a new crystallographic polymorph.²³ EDX and mass spectrometry studies were also performed to confirm the identity of the complex.

3.2.2 Attempted Synthesis of $[\text{Mn}(\text{SAuPPh}_3)_4]^{2-}$

1. $[\text{Ph}_3\text{PAuCl}]$ (0.095 g, 0.192 mmol) was dissolved in 10 mL THF to form a colourless solution. A light beige solution of $[\text{Li}(\text{N,N}'\text{-tmeda})_2][\text{Mn}(\text{SSiMe}_3)_4]$ **1** (0.035 g, 0.048 mmol) dissolved in 10 mL THF was added at rt with no immediate change. After 2.5 h a small amount of colourless ppt was observed. The mixture was filtered over dried Celite® through a glass frit, and the solution was layered with 40 mL heptane. Amorphous white solid was collected. No crystals were successfully grown. An ^1H NMR and $^{31}\text{P}\{^1\text{H}\}$ NMR spectra were run; however no signal was observed, likely due to sufficient broadening due to the presence of paramagnetic manganese(II).
2. $[\text{PPh}_3\text{AuOTf}]$ (0.068 g, 0.112 mmol) was dissolved in 10 mL THF to give a colourless solution. A light beige solution of $[\text{Li}(\text{N,N}'\text{-tmeda})_2][\text{Mn}(\text{SSiMe}_3)_4]$ **1** (0.020 g, 0.028 mmol) dissolved in 10 mL THF was added at rt to form a slight purple solution. After 2.5 h a purple precipitate had formed. The mixture was filtered over dried Celite® through a glass frit, and the solution was layered with 40 mL heptane. Amorphous white solid was collected. No crystals were successfully

grown. An ^1H NMR and $^{31}\text{P}\{^1\text{H}\}$ NMR spectra were run, however no signal was observed, likely due to sufficient broadening due to the presence of paramagnetic manganese(II).

3.2.3 Attempted Synthesis of $[\text{Mn}(\text{SAuPEt}_3)_4]^{2-}$

$[\text{PEt}_3\text{AuCl}]$ (0.097 g, 0.277 mmol) was dissolved in 10 mL THF to form a clear and colourless solution. A light beige solution of $[\text{Li}(N,N'\text{-tmeda})]_2[\text{Mn}(\text{SSiMe}_3)_4]$ **1** (0.050 g, 0.069 mmol) dissolved in 10 mL THF was added at 0 °C with no immediate change. The mixture was left to warm to rt over 2 h, which produced a colourless ppt with a slight yellow solution. The solid was filtered over dried Celite® through a glass frit, and the solution was layered with 40 mL heptane. A pale yellow amorphous solid was formed and was shown to luminesce as yellow/green under UV light. No crystals were successfully grown. An ^1H NMR and $^{31}\text{P}\{^1\text{H}\}$ NMR spectra were run, however no signal was observed, likely due to sufficient broadening due to the presence of paramagnetic manganese(II).

3.2.4 Attempted Synthesis of $[\text{Mn}(\text{FcC}\{\text{O}\}\text{S})_4]^{2-}$ (7)

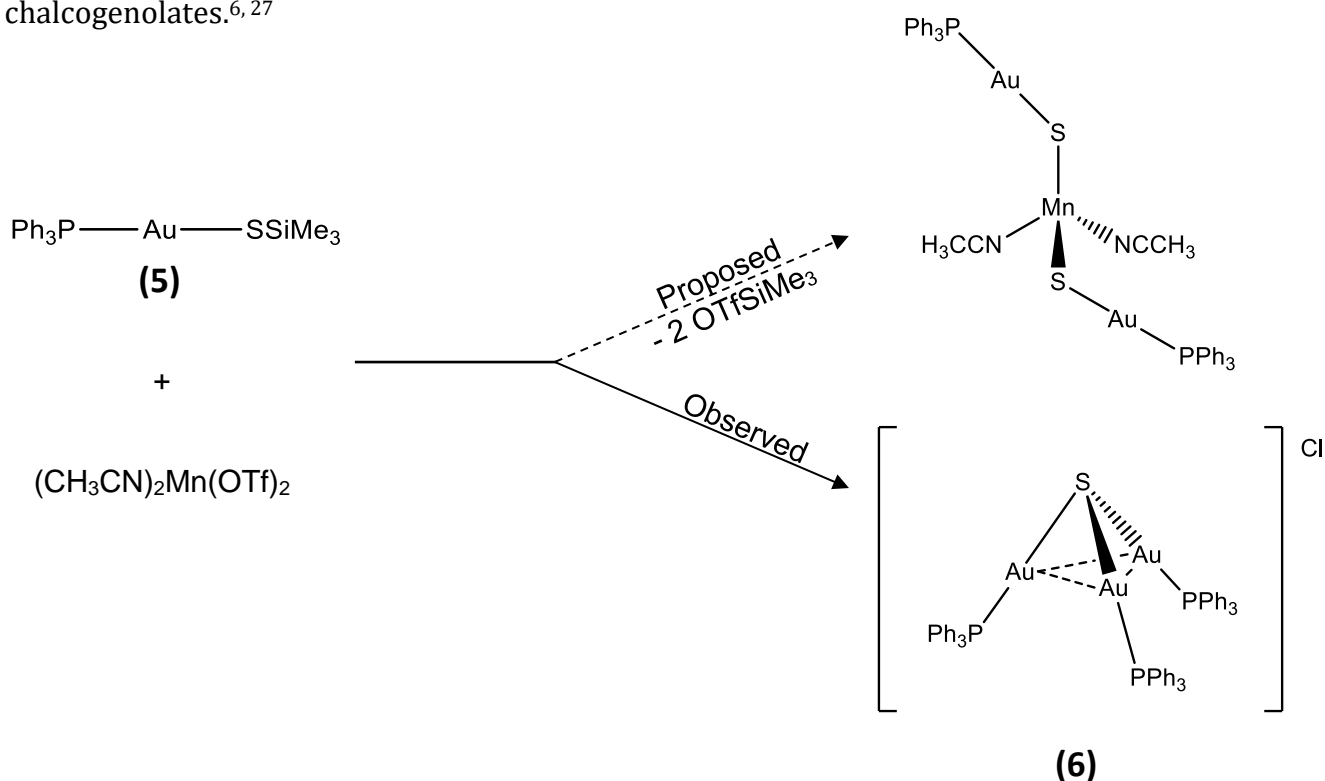
$[\text{FcC}\{\text{O}\}\text{Cl}]$ (0.0275 g, 0.1108 mmol) was dissolved in 10 mL THF to form a deep red solution. A light beige solution of $[\text{Li}(N,N'\text{-tmeda})]_2[\text{Mn}(\text{SSiMe}_3)_4]$ **1** (0.020 g, 0.028 mmol) dissolved in 10 mL THF was added at room temperature. A dark brown precipitate was immediately produced and the reaction was left to stir for 3 hours. The mixture was filtered over dried Celite® through a glass frit, and the solution was reduced until the mixture contained a very slight amount of precipitate. The mixture was filtered over dried Celite® once again to produce a concentrated deep red solution. Crystallization was performed by layering with 40 mL pentane, resulting in a mixture of small red crystals and a pale orange precipitate. The mixture was then stored at -25 °C, producing larger red crystals. X-ray diffraction studies on the crystals revealed the compound to be the previously characterized complex $[(\text{FcC}\{\text{O}\}\text{S})_2]$ through unit cell comparison.²⁴ ^1H NMR

studies support this conclusion, and reveal the formation of the related complexes $[(\text{FcC}\{\text{O}\})_2\text{S}]$ and $[\text{FcC}\{\text{O}\}\text{SSiMe}_3]$ as well.^{25, 26}

3.3 Results and Discussion

3.3.1 Reaction of $[\text{Ph}_3\text{PAuSSiMe}_3]$ (5) with $[(\text{CH}_3\text{CN})_2\text{Mn}(\text{OTf})_2]$

Recently trimethylsilylchalcogenolate functionalized gold(I) phosphine complexes $[\text{Ph}_3\text{PAuESiMe}_3]$ (E = S, Se) have been prepared from the reaction of nucleophilic $\text{Li}[\text{ESiMe}_3]$ with the gold(I) complex $[\text{Ph}_3\text{PAuCl}]$.²⁷ The reaction is driven by the thermodynamic formation of LiCl salt which results in the generation of a $\text{Au}-\text{S}$ bond. In some reactions, the presence of Cl^- ions cause unpredictable interactions with metal salt precursors and intervenes with the formation of targeted products. This is avoided by filtering the LiCl salt before subsequent reactions. This method is commonly applied to metal salts to produce silyl functionalized metal chalcogenolates.^{6, 27}



Scheme 3.1. Proposed reaction of $[\text{Ph}_3\text{PAuSSiMe}_3]$ 5 with $[(\text{CH}_3\text{CN})_2\text{Mn}(\text{OTf})_2]$.

The reaction of triphenylphosphinogold(I) trimethylsilylthiolate with diacetonitrile manganese(II) ditriflate was explored and the results are described here. (Scheme 3.1) Manganese(II) ditriflate is typically coordinated to a nitrogen containing species such as acetonitrile or *N,N'*-tmeda to facilitate its dissolution in common solvents.²¹ For this reaction, manganese(II) ditriflate was suspended in THF with excess acetonitrile to allow coordination. The mixture became a clear and colourless solution after one hour and the THF and excess acetonitrile was then removed *in vacuo*. This compound can be easily dissolved in THF to form a clear colourless solution which facilitated reaction with a clear colourless solution of gold(I) chalcogenolate [$\text{Ph}_3\text{PAuSSiMe}_3$] **5** precursor dissolved in THF. Upon mixing at room temperature, the solution became very pale beige in colour, and after 2 hours a small amount of very fine colourless precipitate had formed. The precipitate was filtered, and the reaction was subsequently layered with pentane in a 2:1 ratio. Unfortunately, there was very little precipitate and it was too fine to attempt characterization.

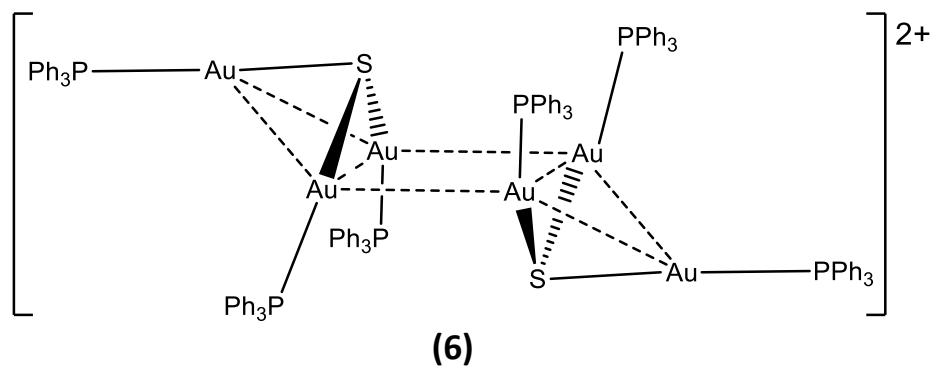


Figure 3.1. Drawing based on the crystallographic data set for $[\text{S}(\text{AuPPh}_3)_3]_2\text{Cl}_2$.

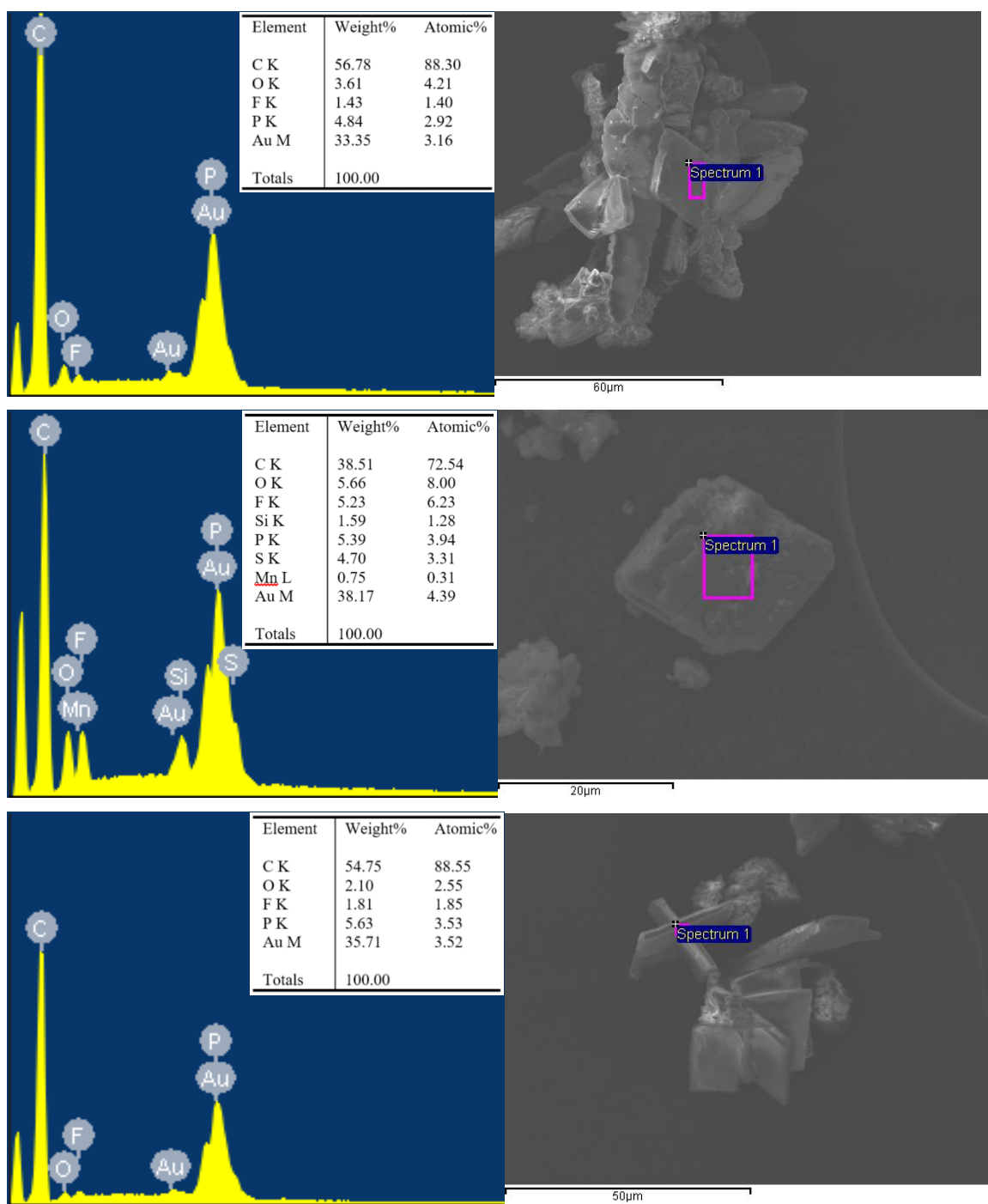


Figure 3.2: EDX analysis and SEM images of crystals acquired from reaction Scheme 3.1.

Crystallization of the filtered solution was performed at -25 °C. After two days, needle shaped crystals of sufficient quality for X-ray analysis were formed. A data set was collected for the crystal, which proved to be the known compound $[S(AuPPh_3)_3]Cl$ **6** as a new crystallographic polymorph.²³ The molecule is present as the dimer $[S(AuPPh_3)_3]_2Cl_2$ (Figure 3.1) in the solid state and crystallizes in the triclinic space group P-1 with Z = 2. The crystallographic data set clearly depicts the core $\{Au_3S\}$ structure and reveals the absence of manganese in the complex. Due to disorder amongst the phenyl rings of the PPh_3 ligands, a drawing of the complex (Figure 3.1) is displayed in place of the crystal structure. These compounds containing three gold centers coordinated to a single sulfide ligand have been extensively explored in gold sulfide cluster chemistry, and many different methodologies have been found to produce this structure due to the structural stability of the molecule.²⁸ It is likely that the Cl^- anion arises from $LiCl$ that may be present in the crystalline material of complex **1**, since there is no other source of Cl^- present during the reaction methodology.

In addition to the needle shaped crystals, there also appeared to be square plate crystals present within the reaction mixture. None of these square plate crystals were of sufficient quality for diffraction studies to be performed, however SEM/EDX studies were utilized to detect if there was any manganese present in the crystals. Two crystals of square/rhombus plate structures were imaged with SEM, and their elemental composition determined through EDX (Figure 3.2). One crystal showed the presence of manganese (0.31%) in the EDX spectrum (Figure 3.1 c) however the small amount may come from the amorphous material coating the surface of the crystal as seen in the SEM image (Figure 3.1 d). None of the other crystals showed any trace of manganese present in the material. What appeared to be needle shaped crystals under optical microscopy was determined to be clusters of square plate crystals, giving the appearance of a needle shaped star structure.

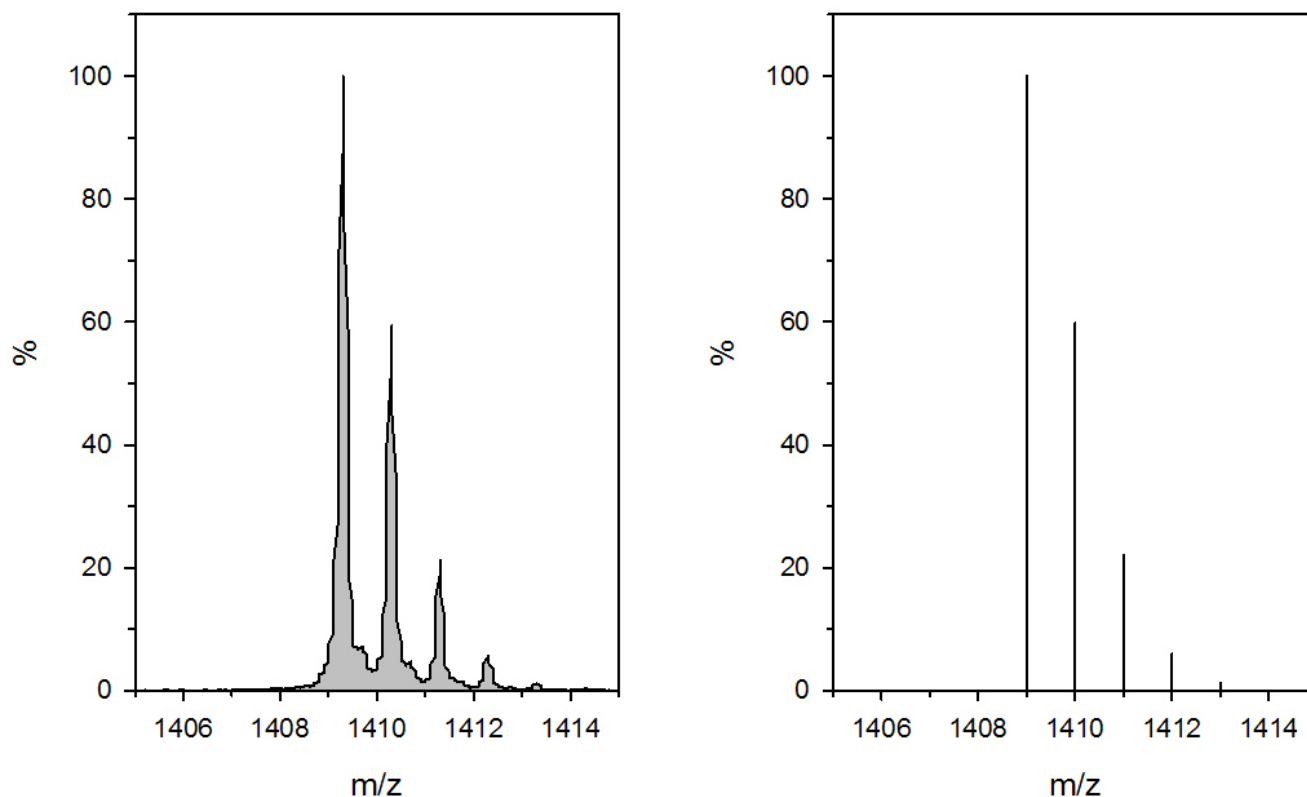


Figure 3.3. (a) Experimental mass spectrum for crystals obtained from reaction Scheme 3.1 (b) Calculated mass spectrum for $[S(AuPPh_3)_3]^+$.

Mass spectrometry was also performed on crystals obtained from the reaction outlined in Scheme 3.1 in the positive ion polarity mode, which showed the presence of a major molecular fraction at 1409.3 m/z (Figure 3.3a). The m/z value of this signal closely matches the theoretical value of 1409.0 m/z for the molecular ion $[S(AuPPh_3)_3]^+$. The experimental spectrum shows six isotopes corresponding to the molecular ion, with relative percentage abundances of 100.0%, 59.38%, 21.29%, 5.65%, 1.21% and 0.34%. These isotopic abundances are very similar to those that were calculated for the theoretical model of the spectrum (Figure 3.3b). Other fractions of lower mass value can also be observed, however their identity remains unknown. The full spectrum for this sample can be found in the Appendix. Other anion complexes of the gold cluster may have been present, however the chloride adduct was the only complex observed through X-ray crystallography.

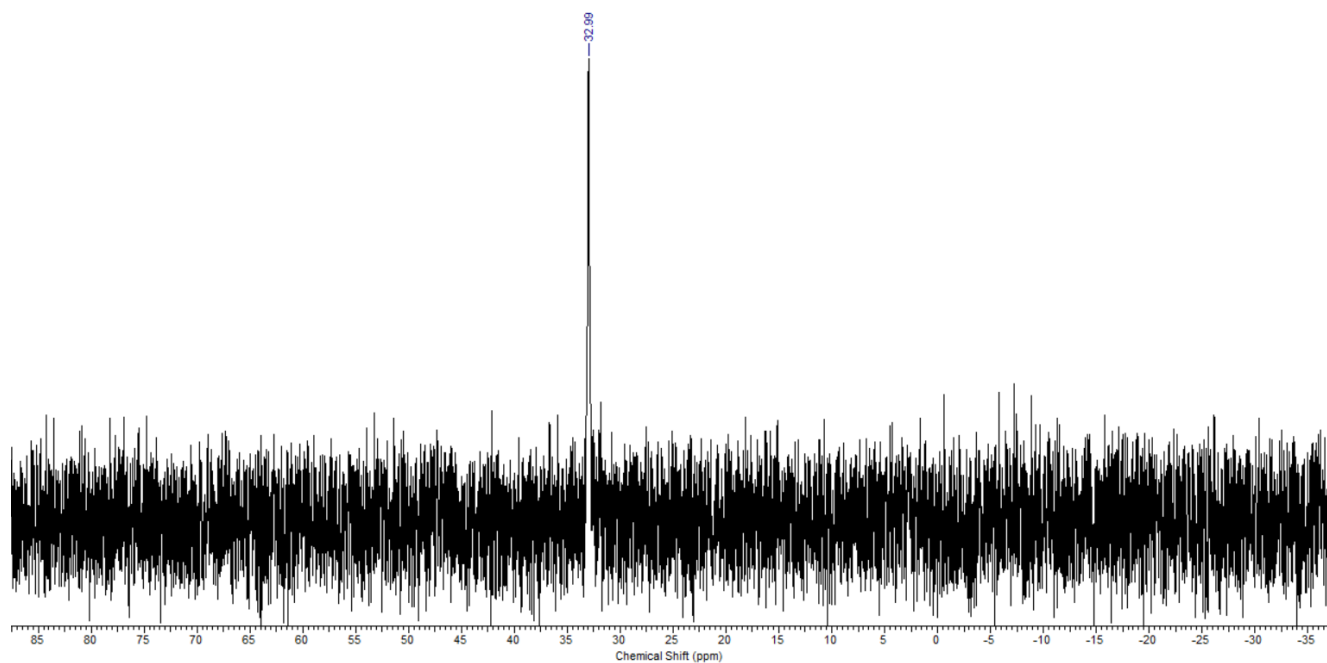
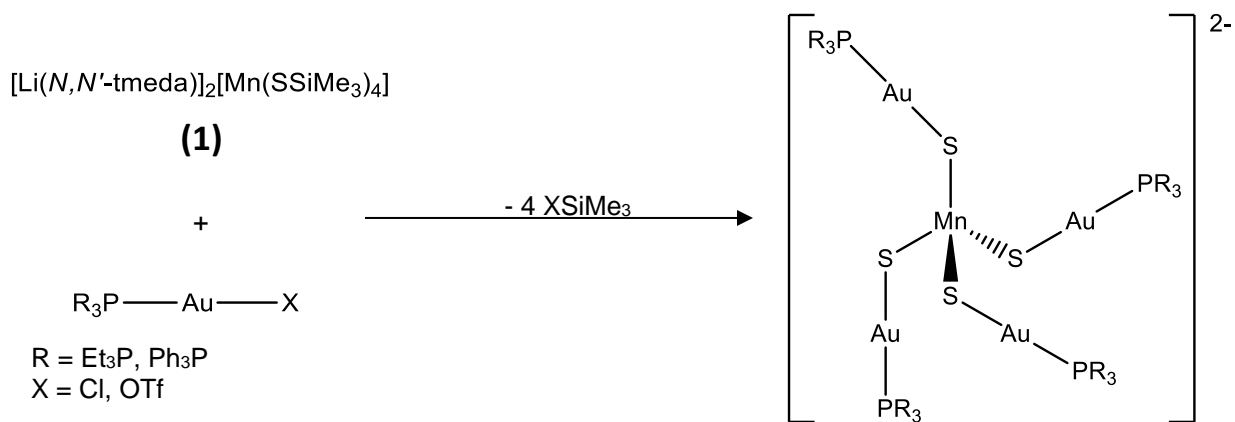


Figure 3.4. $^{31}\text{P}\{^1\text{H}\}$ NMR spectrum of the reaction solution for Scheme 3.1.

The reaction mixture was also studied using NMR spectroscopy. Due to the paramagnetism of the manganese(II) containing species within the mixture, only $^{31}\text{P}\{^1\text{H}\}$ NMR studies produced an acceptable signal (Figure 3.4). The singlet at 33.0 ppm is assigned to the phosphorus center of the triphenylphosphine ligands for the complex $[\text{S}(\text{AuPPh}_3)_3]^+$, which correlates closely with the literature reported value of ~ 33.4 ppm for the same cluster stabilized by different anions.^{29,30} If there were any other compounds present in the reaction solution, they may not be visible due to sufficient broadening of their signals by manganese(II). The $^{31}\text{P}\{^1\text{H}\}$ NMR spectrum shows there is only one phosphorus environment present in the reaction mixture, indicating that manganese(II) ditriflate likely does not interact favourably with the thiolate ligand of the $[\text{Ph}_3\text{PAuSSiMe}_3]$ precursor to produce the desired complex, at least not under the room temperature reactions conditions explored.



Scheme 3.2. Proposed reaction of $[\text{R}_3\text{PAuCl}]$ with $[\text{Li}(\text{N},\text{N}'\text{-tmeda})]_2[\text{Mn}(\text{SSiMe}_3)_4]$.

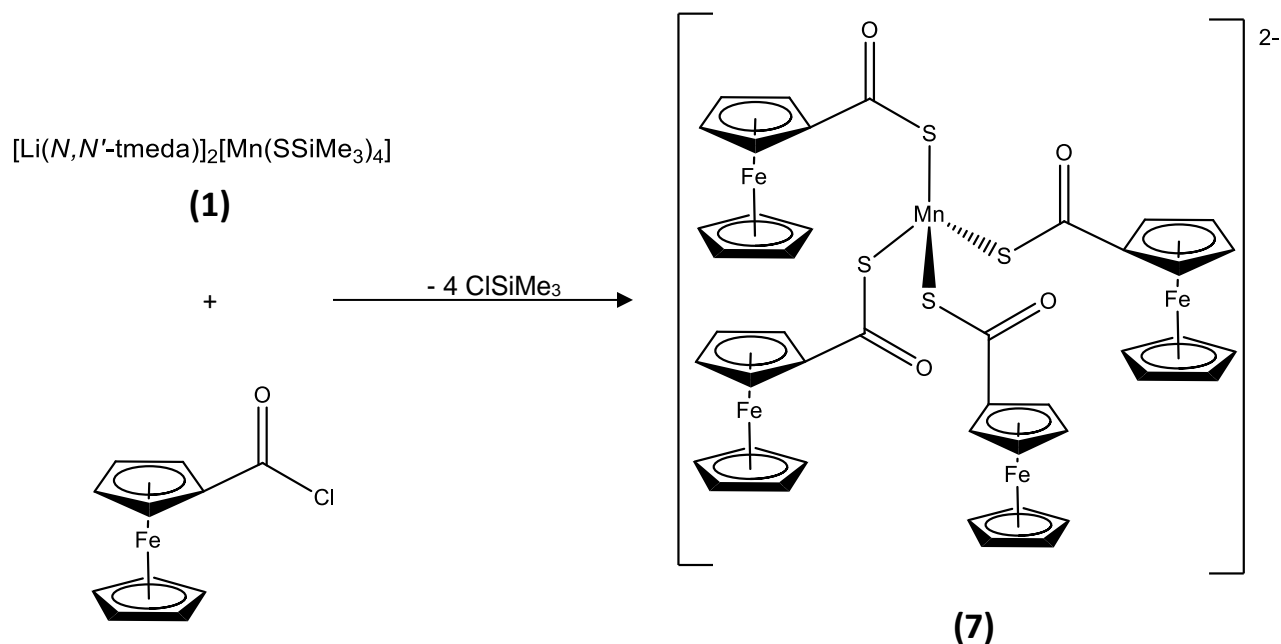
The manganese thiolate precursor $[\text{Li}(\text{N},\text{N}'\text{-tmeda})]_2[\text{Mn}(\text{SSiMe}_3)_4]$ **1** was also used in an attempt to synthesize a heterometallic complex, namely $[\text{Mn}(\text{SAuPR}_3)_4]^{2-}$ from R_3PAuX ($\text{R} = \text{Et}_3\text{P}$, Ph_3P ; $\text{X} = \text{Cl}$, OTf) (Scheme 3.2). Aside from the formation of a small amount of colourless precipitate during these reactions, there were no observable colour change present. Unfortunately, crystals were not produced for any of these reactions, and paramagnetism within the reaction mixture inhibited the use of NMR spectroscopy studies to monitor reaction progress.

3.3.2 Reaction of $[\text{Li}(\text{N},\text{N}'\text{-tmeda})]_2[\text{Mn}(\text{SSiMe}_3)_4]$ with $[\text{FcC}\{\text{O}\}\text{Cl}]$

In general, silylated chalcogen reagents have proven to be very effective for the formation of metal-chalcogenolate and chalcogenide clusters and coordination complexes.^{5, 6, 31-33} Previous work has proven the ability to produce thioester linkages by the reaction of the silylated ferrocenoyl chalcogenide reagent $[\text{FcC}\{\text{O}\}\text{ESiMe}_3]$ ($\text{E} = \text{S}$, Se , Te) with the ligand stabilized salt $[(\text{PPh}_3)\text{MOAc}]$.²⁶ The driving force of these reactions is the production of AcOSiMe_3 .

Attempts were made to prepare the manganese(II) thiolate complex $[\text{Mn}(\text{Fc}(\text{C}\{\text{O}\}\text{S}))_4]^{2-}$ **7** by reaction of the metal chalcogenolate precursor $[\text{Li}(\text{N},\text{N}'\text{-tmeda})]_2[\text{Mn}(\text{SSiMe}_3)_4]$ **1** with the complex $[\text{FcC}\{\text{O}\}\text{Cl}]$ (Scheme 3.3). The precursor ferrocenoyl chloride is prepared through the

addition of oxalyl chloride to a solution of ferrocene carboxylic acid in CH_2Cl_2 at $0\text{ }^\circ\text{C}$. The reaction proceeds upon increasing the temperature of the mixture to room temperature.²⁰ A solution of the chalcogenolate complex $[\text{Li}(\text{N,N}'\text{-tmeda})]_2[\text{Mn}(\text{SSiMe}_3)_4]$ **1** dissolved in THF was introduced to a solution of ferrocenoyl chloride in THF at room temperature. A dark brown precipitate was immediately produced and the reaction was left to progress for 3 hours.



Scheme 3.3. Proposed reaction of ferrocenoyl chloride with $[\text{Li}(\text{N,N}'\text{-tmeda})]_2[\text{Mn}(\text{SSiMe}_3)_4]$.

After filtering the brown precipitate, the reaction solvent was removed *in vacuo* until the product began to precipitate. Following an additional filtration, a crystallization was performed by addition of pentane in a 3:1 volume ratio to the remaining deep red solution. After the counter solvent was seen to disperse fully within the medium, only very small red crystals were observed, in addition to a pale orange non-crystalline solid. The reaction was placed in a $-25\text{ }^\circ\text{C}$ freezer to stimulate crystal growth. The pale red crystals obtained were studied by X-ray diffraction analysis, and found to match the unit cell of diferrocenoyl-disulfide $[(\text{FcC}\{\text{O}\}\text{S})_2]$.²⁴ The presence of this complex was also observed in the ^1H NMR spectrum analysis of the reaction solution.

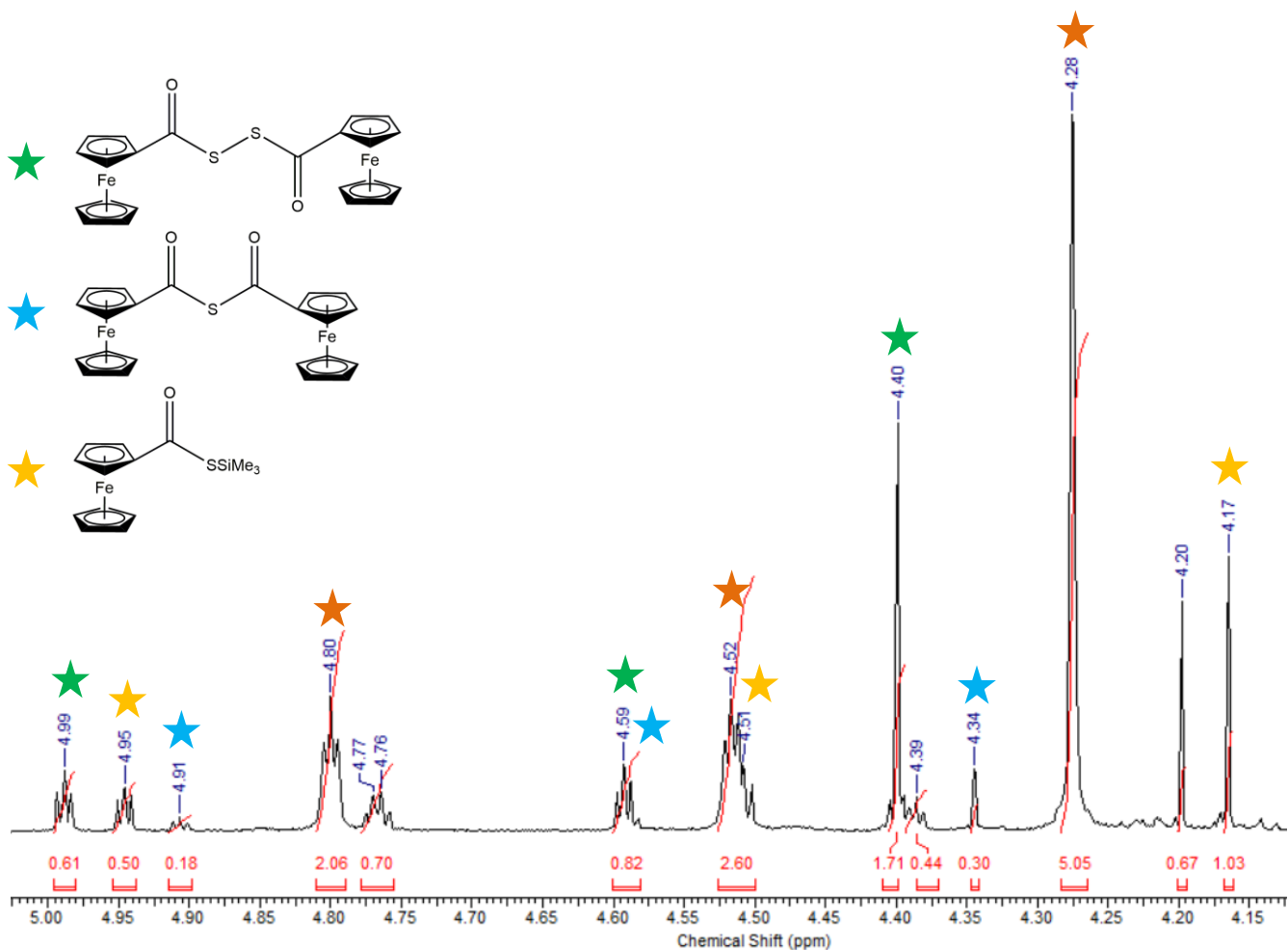


Figure 3.5. Partial ^1H NMR spectrum of the reaction solution outlined in Scheme 3.2.

The ^1H NMR spectrum of the reaction solution shows the presence of three known ferrocene containing compounds (Figure 3.5). Four signals at 4.95, 4.51, 4.17 and 0.48 ppm are assigned to the compound $[\text{FcC}\{\text{O}\}\text{SSiMe}_3]$, with the signals at 4.95, 4.51 and 4.17 ppm assigned to the protons of the ferrocene cyclopentadienyl rings and the signal at 0.48 ppm assigned to the protons of the $-\text{SiMe}_3$. These signals correlate closely with literature values of 4.95, 4.51, 4.16 and 0.48 ppm respectively.²⁶ This indicates that the chalcogenolate precursor $[\text{Li}(\text{N},\text{N}'\text{-tmeda})]_2[\text{Mn}(\text{SSiMe}_3)_4]$ is acting as a delivery agent to transfer $[\text{SSiMe}_3]^-$ to ferrocenoyl chloride,

similar to $\text{Li}[\text{SSiMe}_3]$, likely resulting in the formation of manganese(II) chloride and/or lithium chloride.

Reaction of remaining ferrocenoyl chloride with the generated $[\text{FcC}\{\text{O}\}\text{SSiMe}_3]$ would produce $[(\text{FcC}\{\text{O}\})_2\text{S}]$ as well as ClSiMe_3 . Three signals at 4.91, 4.59 and 4.34 ppm are assigned to the protons of the cyclopentadienyl rings for this compound, which correspond closely to literature reported peaks of 4.92, 4.61 and 4.36 ppm respectively.²⁵ There is no signal to assign to the ClSiMe_3 byproduct because the sample was left under vacuum prior to running the ^1H NMR experiment, which would remove this volatile compound. The third byproduct $[(\text{FcC}\{\text{O}\}\text{S})_2]$ is also formed, with three signals at 4.99, 4.59 and 4.40 ppm assigned to the protons of the cyclopentadienyl rings, which correspond closely to literature reported peaks of 5.00, 4.60 and 4.41 ppm respectively.²⁴ The mechanism of formation of this molecule is less obvious, since there is no direct path by which it can be formed from the starting materials present in the mixture. However, the presence of these ^1H NMR signals, in addition to the unit cell of the crystal formed provide unequivocal evidence for its formation.

Additionally, there are also three strong signals at 4.80, 4.52 and 4.28 ppm which are not assigned. It is proposed that these peaks correspond to a manganese containing product expected, as shown in the reaction (Scheme 3.3). Mass spectroscopy was performed on the reaction mixture in the negative ion polarity mode, which showed the presence of a major molecular fraction at 789.9 m/z (Figure 3.6a). The m/z value of this signal closely matches the theoretical value of 790.0 m/z for the molecular ion $[\text{Mn}(\text{Fc}(\text{C}\{\text{O}\}\text{S}))_3]^-$. The experimental spectrum shows ten isotopes corresponding to the molecular ion, with relative percentage abundances of 1.25%, 0.65%, 19.38%, 9.13%, 100%, 46.19%, 25.52%, 8.12%, 2.33% and 0.80% (Figure 3.6b). These isotopic abundances are in close agreement to those that were calculated for the model of the spectrum. There is no signal in the 1035 m/z area that would correspond to the expected main ion $[\text{Mn}(\text{Fc}(\text{C}\{\text{O}\}\text{S}))_4]^{2-}$. The ion may be unstable, and thus incapable of remaining intact during the ESI experiment or else it is simply not formed.

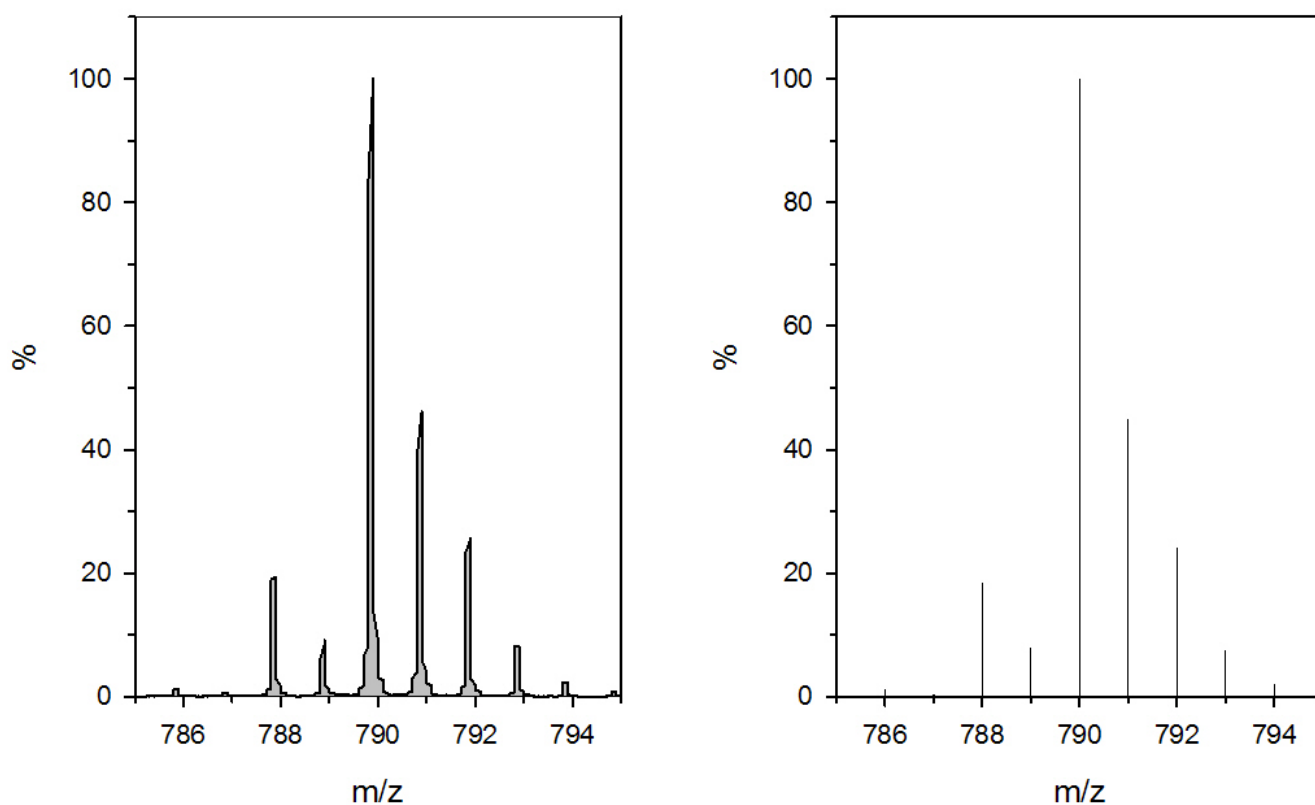


Figure 3.6. (a) Experimental mass spectrum for reaction Scheme 3.3 (b) Calculated mass spectrum for $[\text{Mn}(\text{Fc}(\text{C}\{\text{O}\}\text{S}))_3]^-$.

Unfortunately, although there is evidence for the presence of the target molecule, it was not further characterized as additional attempts at crystallization were not successful. The presence of the many side products likely interfered with the crystallization process, making it difficult to produce the single crystals necessary for use in X-ray crystallography to confirm its structure. Also, since the paramagnetism of manganese(II) makes it difficult to observe NMR signals from nuclei near the manganese centre, it is possible that there are species in solution that are not visible in the ^1H NMR spectrum due to their proximity to unpaired electrons. No new complexes were observed through ^1H NMR spectroscopy when the same experiment was run at 0°C .

3.4 Conclusion

The reaction of the gold(I) chalcogenolate $[\text{Ph}_3\text{PAuSSiMe}_3]$ precursor with manganese(II) ditriflate was performed and found to produce the stable sulfide centered gold cluster $[\text{S}(\text{AuPPh}_3)_3]\text{Cl}$ **6**. The compound was analyzed through SEM, EDX and $^{31}\text{P}\{^1\text{H}\}$ NMR which found this cluster to be the only major product of the reaction. MS ESI was performed on the compound and the resulting spectrum matched the calculated spectrum both in m/z units and isotopic distribution. The reaction of the manganese(II) chalcogenolate $[\text{Li}(\text{N,N}'\text{-tmeda})]_2[\text{Mn}(\text{SSiMe}_3)_4]$ with ferrocenoyl chloride was performed and found to produce a ferrocene containing manganese sulfide cluster, however the exact structure of the product was not determined. MS ESI was performed on the material, and the experimental spectrum for $[\text{Mn}(\text{Fc}(\text{C}\{\text{O}\}\text{S}))_3]^-$ was found to match the m/z value and isotopic distribution of the calculated spectrum. This ion was determined to be the major molecular ion in the sample. The structure of multiple side products from the reaction were characterized using ^1H NMR spectroscopy and single crystal X-ray diffraction.

3.5 References

1. J. Choi, S. Yoon, F.S. Kim, and N. Kim; *Journal of Alloys and Compounds*, **2016**. 671: p. 360-365.
2. R. Buonsanti and D.J. Milliron; *Chemistry of Materials*, **2013**. 25(8): p. 1305-1317.
3. J. Yang, R. Fainblat, S.G. Kwon, F. Muckel, J.H. Yu, H. Terlinden, B.H. Kim, D. Iavarone, M.K. Choi, I.Y. Kim, I. Park, H.K. Hong, J. Lee, J.S. Son, Z. Lee, K. Kang, S.J. Hwang, G. Bacher, and T. Hyeon; *Journal of the American Chemical Society*, **2015**. 137(40): p. 12776-12779.
4. A. Eichhöfer, O. Hampe, S. Lebedkin, and F. Weigend; *Inorganic Chemistry*, **2010**. 49(16): p. 7331-7339.
5. C.B. Khadka, A. Eichhofer, F. Weigend, and J.F. Corrigan; *Inorganic Chemistry*, **2012**. 51(5): p. 2747-2756.
6. C.B. Khadka, D.G. Macdonald, Y.H. Lan, A.K. Powell, D. Fenske, and J.F. Corrigan; *Inorganic Chemistry*, **2010**. 49(16): p. 7289-7297.
7. J. Olkowska-Oetzel, P. Sevillano, A. Eichhofer, and D. Fenske; *European Journal of Inorganic Chemistry*, **2004**. 2004(5): p. 1100-1106.
8. A. Sladek and H. Schmidbaur; *Zeitschrift für Naturforschung B*, **1997**. 52(2): p. 301-303.
9. X. Chen, M. Strange, and H. Hakkinen; *Physical Review B*, **2012**. 85(8): p. 5.
10. J.U. Reveles, P.A. Clayborne, A.C. Reber, S.N. Khanna, K. Pradhan, P. Sen, and M.R. Pederson; *Nature Chemistry*, **2009**. 1(4): p. 310-315.
11. J. Akola, K.A. Kacprzak, O. Lopez-Acevedo, M. Walter, H. Grönbeck, and H. Häkkinen; *The Journal of Physical Chemistry C*, **2010**. 114(38): p. 15986-15994.
12. A. Labande, J. Ruiz, and D. Astruc; *Journal of the American Chemical Society*, **2002**. 124(8): p. 1782-1789.
13. R.C. Mulrooney, N. Singh, N. Kaur, and J.F. Callan; *Chemical Communications*, **2009**(6): p. 686-688.

14. Y. Liu, B. Khalili Najafabadi, M. Azizpoor Fard, and J.F. Corrigan; *Angewandte Chemie*, **2015**. 127(16): p. 4914–4917.
15. S. Onaka and Y. Katukawa; *Journal of Coordination Chemistry*, **1996**. 39(2): p. 135-146.
16. A.B. Pangborn, M.A. Giardello, R.H. Grubbs, R.K. Rosen, and F.J. Timmers; *Organometallics*, **1996**. 15(5): p. 1518-1520.
17. D. Taher, A.I. Wallbank, E.A. Turner, H.L. Cuthbert, and J.F. Corrigan; *European Journal of Inorganic Chemistry*, **2006**. 2006(22): p. 4616-4620.
18. P. Braunstein, H. Lehner, D. Matt, K. Burgess, and M.J. Ohlmeyer, *A Platinum-Gold Cluster: Chloro-1κCl-Bis(Triethylphosphine-1κP)Bis(Triphenyl- Phosphine)-2κP, 3κP-Triangulo-Digold-Platinum(1 +) Trifluoromethanesulfonate*, in *Inorganic Syntheses*. John Wiley & Sons, Inc. **2007**; p. 218-221.
19. B. Breit and D. Breuning; *Synthesis-Stuttgart*, **2005**(16): p. 2782-2786.
20. A. Aguilar-Aguilar, A.D. Allen, E.P. Cabrera, A. Fedorov, N. Fu, H. Henry-Riyad, J. Leuninger, U. Schmid, T.T. Tidwell, and R. Verma; *The Journal of Organic Chemistry*, **2005**. 70(23): p. 9556-9561.
21. P.J. Riedel, N. Arulsamy, and M.P. Mehn; *Inorganic chemistry communications*, **2011**. 14(5): p. 734-737.
22. G. Sheldrick; *Acta Crystallographica Section A*, **2008**. 64(1): p. 112-122.
23. C. Kowala and J. Swan; *Australian Journal of Chemistry*, **1966**. 19(4): p. 547-554.
24. C. Imrie, L. Cook, and D.C. Levendis; *Journal of Organometallic Chemistry*, **2001**. 637–639: p. 266-275.
25. C. Imrie, E.R.T. Elago, N. Williams, C.W. McClelland, and P. Engelbrecht; *Journal of Organometallic Chemistry*, **2005**. 690(21-22): p. 4959-4966.
26. D.G. MacDonald and J.F. Corrigan; *Dalton Transactions*, **2008**. 2008(37): p. 5048-5053.
27. A.M. Polgar, C.B. Khadka, M. Azizpoor Fard, B. Nikkel, T. O'Donnell, T. Neumann, K. Lahring, K. Thompson, C. Cadogan, F. Weigend, and J.F. Corrigan; *Chemistry – A European Journal*, **2016**. 22(51): p. 18378-18382.
28. M.C. Gimeno and A. Laguna; *Chemical Society Reviews*, **2008**. 37(9): p. 1952-1966.

29. M. Preisenberger, P. Pyykkö, A. Schier, and H. Schmidbaur; *Inorganic Chemistry*, **1999**. 38(25): p. 5870-5875.
30. F. Canales, C. Gimeno, A. Laguna, and M.D. Villacampa; *Inorganica Chimica Acta*, **1996**. 244(1): p. 95-103.
31. D.G. MacDonald and J.F. Corrigan; *Philosophical Transactions of the Royal Society A: Mathematical Physical and Engineering Sciences*, **2010**. 368(1915): p. 1455-1472.
32. C.E. Anson, A. Eichhofer, I. Issac, D. Fenske, O. Fuhr, P. Sevillano, C. Persau, D. Stalke, and J. Zhang; *Angewandte Chemie-International Edition*, **2008**. 47(7): p. 1326-1331.
33. T. Niebel, D.G. MacDonald, C.B. Khadka, and J.F. Corrigan; *Zeitschrift Fur Anorganische Und Allgemeine Chemie*, **2010**. 636(6): p. 1095-1099.

Chapter Four

Conclusions and Future Work

4.1. Conclusions

Trimethylsilyl functionalized chalcogenolate (RE^-) and chalcogenide (E^{2-}) reagents have been shown to be powerful precursors for the synthesis of binary (ME) and ternary (MM'E) metal chalcogenide clusters.¹⁻³ It has also been shown that compounds of varying structure and elemental composition are achievable for metal chalcogenide systems, giving rise to a wide array of applications for these materials.⁴⁻⁶ For many of these applications, strict control over the structure and elemental composition is imperative. The research described in this thesis is focused around ternary metal chalcogenide cluster synthesis, particularly ternary manganese(II) metal sulfide structures. Trimethylsilyl functionalized metal thiolate reagents ($M-ESiMe_3$) were used as a reactive precursor toward these ternary metal sulfide systems.

Chapter 2 describes the reaction of $[(dppp)PdCl_2]$ with $[Li(N,N'-tmeda)]_2[Mn(SSiMe_3)_4]$ **1** in a 2:1 ratio to give $[MnCl_2(\mu-S)_2Pd_2(dppp)_2]$ **2** in relatively good yield and under mild reaction conditions. Similar reactions with an increased ratio of $[(dppp)PdCl_2]:[Mn(SSiMe_3)_4]^{2+}$ only produced **2**, even if $[(dppp)Pd(OAc)_2]$ is used with non-chlorinated solvents. In order to completely avoid contact with chlorine, the new trimethylsilyl chalcogenolate $[(dppp)Pd(SSiMe_3)_2]$ **3** was synthesized by reaction of $Li[SSiMe_3]$ with $[(dppp)Pd(OAc)_2]$ in a 2:1 ratio. The reactivity of this complex is tested through a reaction with $[(CH_3CN)_2Mn(OTf)_2]$, yielding the new complex $[Mn(OTf)(thf)_2(\mu-S)_2Pd_2(dppp)_2]OTf$ **4**. Although the lack of chlorine led to the synthesis of a new coordination complex, differing Pd:Mn ratio complexes (1:1, 3:1) were still unattainable. X-ray crystallographic characterization of these complexes reveals

differing coordination geometries around the manganese(II) centre for **2** (distorted tetrahedral) and **4** (distorted trigonal bipyramidal). Since steric crowding of the dppp ligand with the triflate and thf ligands were shown to distort geometry, it is possible that the phenyl groups of dppp restrict the growth of the complex from containing a higher Pd:Mn ratio.

Chapter 3 describes the reactivity of $[\text{Li}(\text{N},\text{N}'\text{-tmeda})]_2[\text{Mn}(\text{SSiMe}_3)_4]$ **1** with various phosphine gold chlorides and gold triflates with no success. The reaction of the gold(I) chalcogenolate $[\text{Ph}_3\text{PAuSSiMe}_3]$ with manganese(II) ditriflate was performed and found to produce the stable sulfide centered gold cluster $[\text{S}(\text{AuPPh}_3)_3]\text{Cl}$ **6**. The compound was analyzed through SEM, EDX, MS ESI and $^{31}\text{P}\{^1\text{H}\}$ NMR which found this cluster to be the only major product of the reaction. The reaction of the $[\text{Li}(\text{N},\text{N}'\text{-tmeda})]_2[\text{Mn}(\text{SSiMe}_3)_4]$ **1** with ferrocenoyl chloride was performed and the structure of multiple side products from the reaction were characterized using ^1H NMR spectroscopy and single crystal X-ray diffraction. MS ESI was performed on the material, and a ferrocene containing manganese sulfide cluster was found to be produced. The experimental spectrum for $[\text{Mn}(\text{Fc}(\text{C}\{\text{O}\}\text{S}))_3]^-$ was found to match the m/z value and isotopic distribution of the calculated spectrum. This ion was determined to be the major molecular ion in the sample. Unfortunately the complex was not able to be purified and characterized further.

4.2 Future Work

The use of $[\text{Li}(\text{N},\text{N}'\text{-tmeda})]_2[\text{Mn}(\text{SSiMe}_3)_4]$ **1** as a precursor towards the formation of ternary metal sulfide systems proved to be successful with the synthesis of $[\text{MnCl}_2(\mu\text{-S})_2\text{Pd}_2(\text{dppp})_2]$ **3**. However, the presence of chlorine as LiCl in crystals of **1** likely inhibits the formation of diverse palladium-manganese-sulfide systems. The synthesis of **1** from a different manganese(II) salt rather than manganese(II) chloride may inhibit the LiX salt from being carried over into the product. The lack of chlorine may allow all four reactive ligands of

$[\text{Mn}(\text{SSiMe}_3)_4]^{2-}$ to be utilized for the formation of structurally diverse manganese(II) metal sulfide systems.

The reaction of $[\text{Li}(N,N'\text{-tmeda})]_2[\text{Mn}(\text{SSiMe}_3)_4]$ **1** with ferrocenoyl chloride likely produces a novel manganese(II) ferrocene containing manganese sulfide cluster, however the exact structure of the product was not determined. Further work should be done to explore this reaction and determine the structure of the product. It would be interesting if the manganese(II) centre maintains coordination to all four sulfide ligands in this reaction, while only maintaining coordination to two sulfide ligands in the palladium reactions as seen in **2** and **4**. Ferrocene containing manganese chalcogenide systems have yet to be explored, and the combination of the redox properties of ferrocene with the paramagnetic properties of manganese(II) may be interesting and worth pursuing.

The formation of Au-S-Mn bonding interactions proved to be quite difficult for reactions with $[\text{Li}(N,N'\text{-tmeda})]_2[\text{Mn}(\text{SSiMe}_3)_4]$ **1** as well as reactions with $[\text{Ph}_3\text{PAuSSiMe}_3]$ **5** as precursors with various metal salts. Gold(I) sulfide systems are unique since they exhibit aurophilic Au-Au interactions which allow for greater structural diversity.⁷ Other members of the group 11 coinage metals also exhibit similar properties (argentophilic interactions for Ag and cuprophilic interactions for Cu).⁸ The reactivity of **1** with copper(I) and silver(I) salts (e.g. CuOAc and AgOAc) may prove to be more successful than the reactions with gold(I) salts, since the intermetallic M-M bonding in copper(I) and silver(I) systems will be weaker than the M-M bonding in gold(I) systems.⁹ The resulting complexes may exhibit interesting structures as a result of the weak M-M bonding interactions. Manganese(II) is often used as a paramagnetic dopant in larger metal chalcogenide systems and the success of these reactions with complex **1** may prove to be a useful synthetic alternative towards doped metal chalcogenide systems.

4.3 References

1. D.G. MacDonald and J.F. Corrigan; *Dalton Transactions*, **2008**. 2008(37): p. 5048-5053.
2. J. Olkowska-Oetzel, P. Sevilano, A. Eichhofer, and D. Fenske; *European Journal of Inorganic Chemistry*, **2004**. 2004(5): p. 1100-1106.
3. C.B. Khadka, A. Eichhofer, F. Weigend, and J.F. Corrigan; *Inorganic Chemistry*, **2012**. 51(5): p. 2747-2756.
4. S.L. Li, K. Tsukagoshi, E. Orgiu, and P. Samori; *Chemical Society Reviews*, **2016**. 45(1): p. 118-151.
5. A. Klein; *Journal of Physics-Condensed Matter*, **2015**. 27(13): p. 24.
6. Y.J. Feng, A. Gago, L. Timperman, and N. Alonso-Vante; *Electrochimica Acta*, **2011**. 56(3): p. 1009-1022.
7. M.C. Gimeno and A. Laguna; *Chemical Society Reviews*, **2008**. 37(9): p. 1952-1966.
8. H. Schmidbaur and A. Schier; *Angewandte Chemie International Edition*, **2015**. 54(3): p. 746-84.
9. H. Schmidbaur and A. Schier; *Chemical Society Reviews*, **2012**. 41(1): p. 370-412.

Appendices

A. Supporting Information for Chapter 2

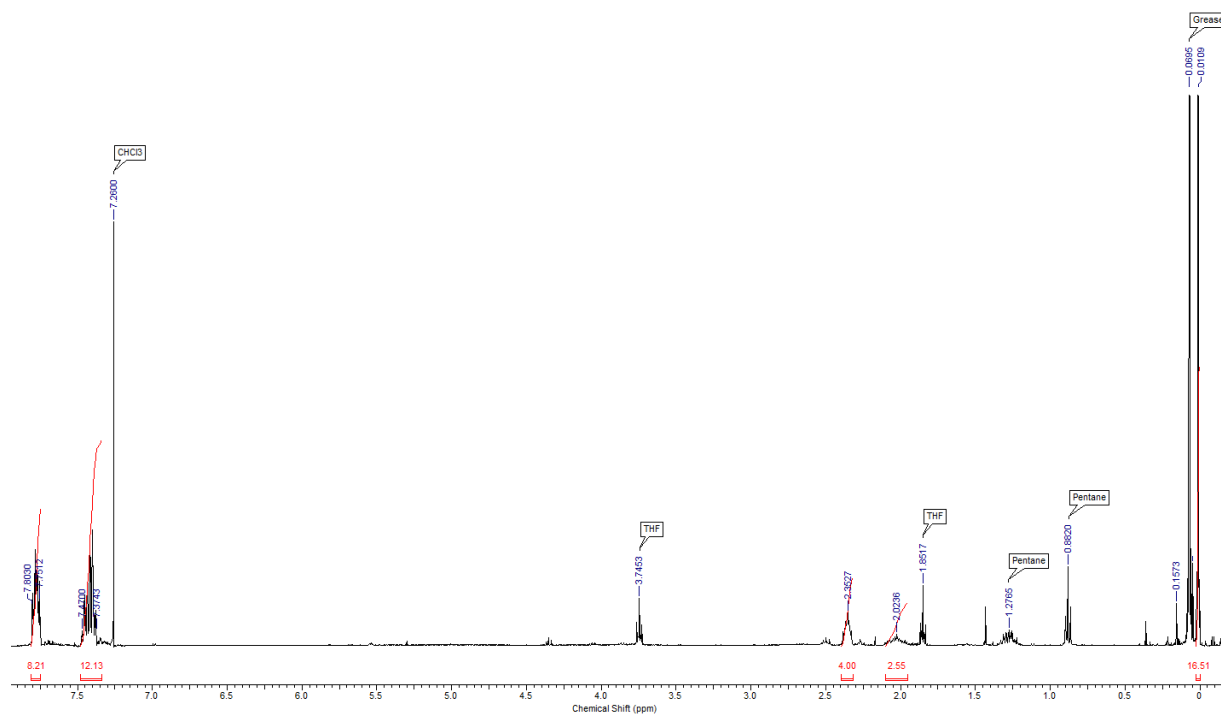


Figure A.1. ^1H NMR spectrum of **3** in CHCl_3 .

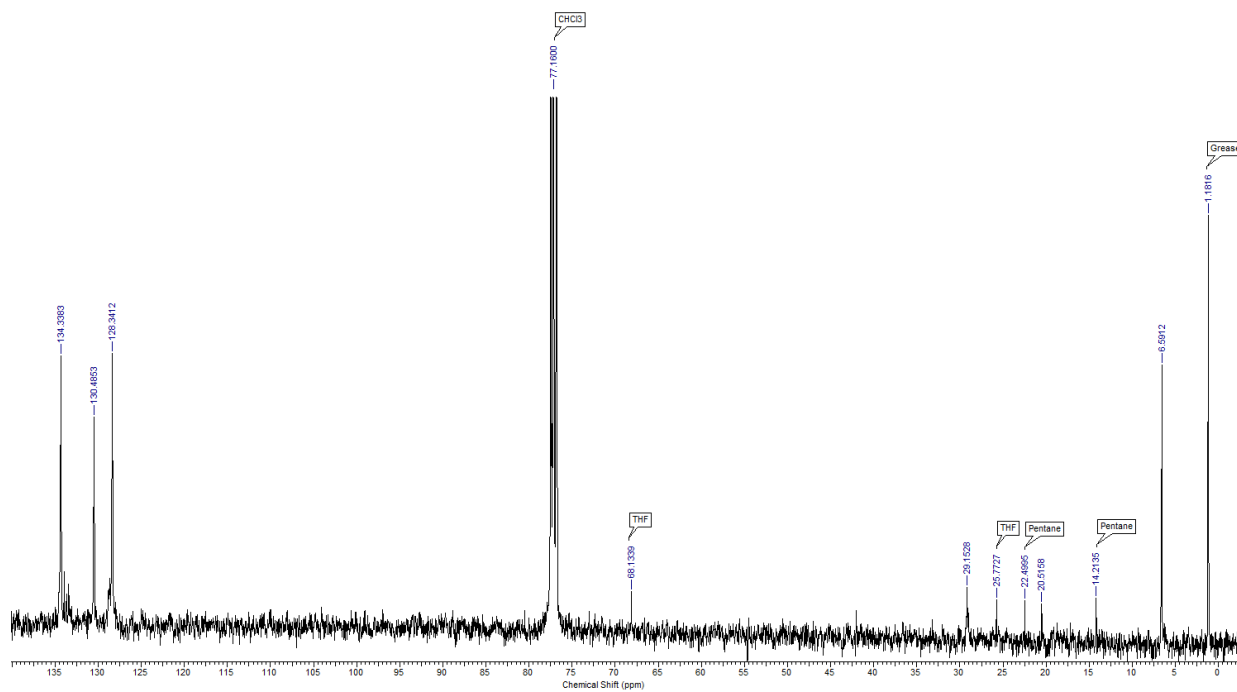


Figure A.2. $^{13}\text{C}\{^1\text{H}\}$ NMR spectrum of **3** in CHCl_3 .

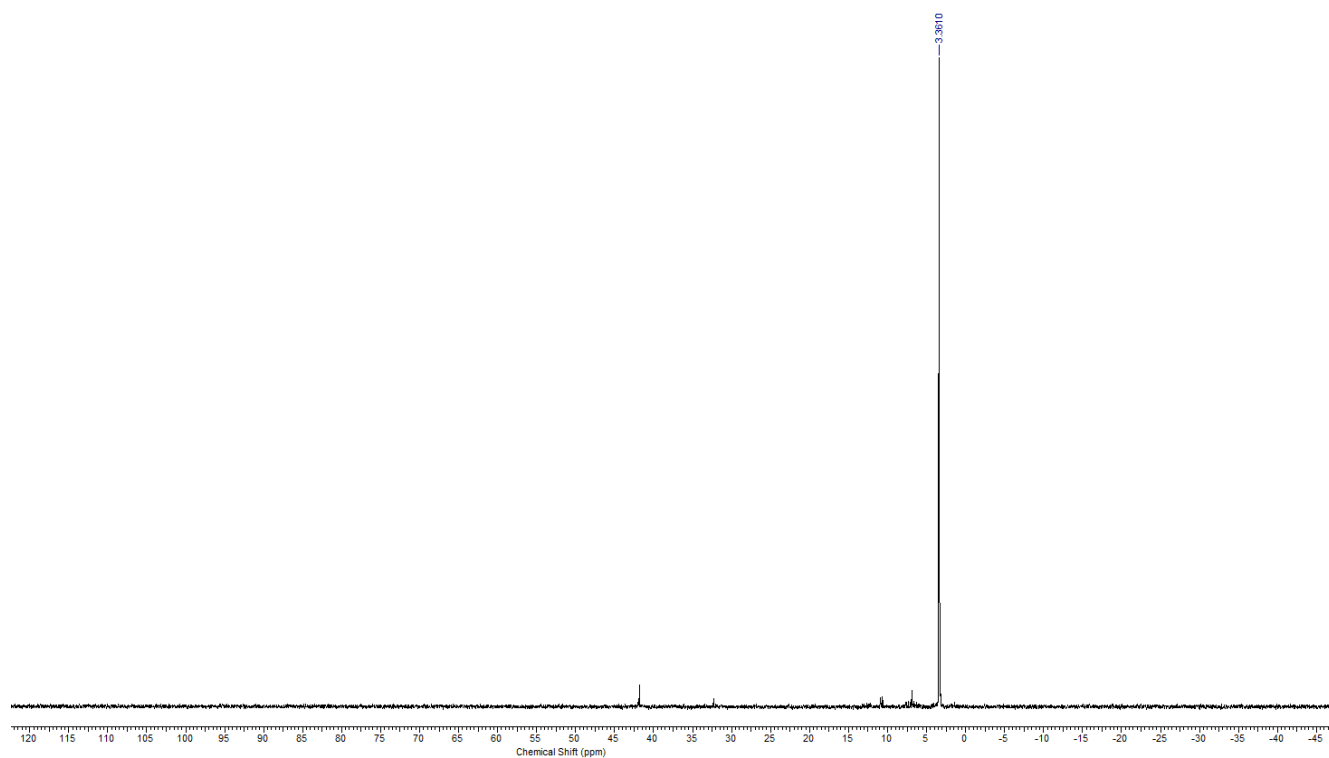


Figure A.3. $^{31}\text{P}\{^1\text{H}\}$ NMR spectrum of **3** in CHCl_3 .

B. X-ray Crystallographic Data Parameters for Compounds 2, 3 and 4

Table B.1. Summary of Crystal Data for **2**

Formula	C ₅₅ H ₅₂ Cl ₄ MnP ₄ Pd ₂ S ₂
Formula Weight (g/mol)	1310.50
Crystal Dimensions (mm)	0.128 × 0.052 × 0.032
Crystal Color and Habit	orange needle
Crystal System	monoclinic
Space Group	P 2 ₁ /m
Temperature, K	110
a, Å	9.759(4)
b, Å	15.934(7)
c, Å	17.569(7)
α, °	90
β, °	90.129(19)
γ, °	90
V, Å ³	2732.0(19)
Number of reflections to determine final unit cell	6869
Min and Max 2θ for cell determination, °	5.42, 52.98
Z	2
F(000)	1318
ρ (g/cm)	1.593
λ, Å, (MoKα)	0.71073
μ, (cm ⁻¹)	1.305
Diffraction Type	Bruker Kappa Axis Apex2
Scan Type(s)	phi and omega scans
Max 2θ for data collection, °	61.186
Measured fraction of data	0.998
Number of reflections measured	98505
Unique reflections measured	8631
R _{merge}	0.1249
Number of reflections included in refinement	8631
Cut off Threshold Expression	I > 2σ(I)
Structure refined using	full matrix least-squares using F ²
Weighting Scheme	w=1/[σ ² (F _o ²)+(0.0683P) ² +0.5841P]] where P=(F _o ² +2F _c ²)/3
Number of parameters in least-squares	329
R ₁	0.0532
wR ₂	0.1138
R ₁ (all data)	0.0886
wR ₂ (all data)	0.1307
GOF	1.049
Maximum shift/error	0.000
Min & Max peak heights on final ΔF Map (e ⁻ /Å)	-2.164, 1.087

Table B.2. Atomic Coordinates for **2**

Atom	x	y	z	U _{iso} /equiv
Pd1	0.12576(6)	0.7500	0.19393(3)	0.01878(12)
Pd2	0.23230(5)	0.7500	0.36376(3)	0.01592(12)
Mn1	-0.08332(11)	0.7500	0.31433(7)	0.0239(3)
Cl1	-0.1839(2)	0.7500	0.43493(13)	0.0328(4)
Cl2	-0.2591(3)	0.7500	0.22139(15)	0.0493(6)
S1	0.10707(13)	0.65063(7)	0.29267(7)	0.0191(2)
P1	0.13239(16)	0.64793(8)	0.10375(8)	0.0230(3)
P2	0.33767(13)	0.64466(8)	0.42846(7)	0.0189(3)
C1	0.0808(6)	0.5432(3)	0.1340(3)	0.0247(11)
C2	-0.0538(7)	0.5297(4)	0.1579(3)	0.0330(13)
C3	-0.0929(7)	0.4516(4)	0.1834(4)	0.0376(14)
C4	0.0000(7)	0.3872(3)	0.1868(3)	0.0349(13)
C5	0.1318(8)	0.3997(4)	0.1642(4)	0.0397(15)
C6	0.1741(6)	0.4784(3)	0.1382(4)	0.0319(12)
C7	0.2997(6)	0.6339(3)	0.0616(3)	0.0283(12)
C8	0.4146(7)	0.6477(4)	0.1063(4)	0.0391(15)
C9	0.5454(7)	0.6383(4)	0.0771(4)	0.0472(18)
C10	0.5612(8)	0.6157(5)	0.0032(4)	0.0492(18)
C11	0.4507(9)	0.6006(5)	-0.0423(4)	0.052(2)
C12	0.3184(7)	0.6087(4)	-0.0139(3)	0.0374(15)
C13	0.0145(7)	0.6685(4)	0.0250(3)	0.0332(13)
C14	0.0400(10)	0.7500	-0.0198(5)	0.035(2)
C15	0.3935(5)	0.5600(3)	0.3668(3)	0.0233(10)
C16	0.4908(6)	0.5779(4)	0.3119(3)	0.0333(13)
C17	0.5330(8)	0.5157(5)	0.2617(4)	0.0451(17)
C18	0.4796(9)	0.4357(5)	0.2666(4)	0.055(2)
C19	0.3821(8)	0.4173(4)	0.3204(3)	0.0409(15)
C20	0.3395(6)	0.4794(3)	0.3706(3)	0.0299(12)
C21	0.2262(5)	0.5993(3)	0.5001(3)	0.0197(10)
C22	0.2711(6)	0.5359(3)	0.5505(3)	0.0269(11)
C23	0.1811(6)	0.5037(4)	0.6041(3)	0.0322(13)
C24	0.0500(6)	0.5334(4)	0.6092(3)	0.0304(13)
C25	0.0062(6)	0.5962(4)	0.5600(3)	0.0316(13)
C26	0.0925(6)	0.6280(3)	0.5059(3)	0.0247(11)
C27	0.4934(5)	0.6695(3)	0.4806(3)	0.0246(11)
C28	0.4869(8)	0.7500	0.5283(4)	0.0265(16)
Cl1S	0.6725(3)	0.2500	0.19049(17)	0.0788(10)
Cl2S	0.8133(4)	0.2820(2)	0.3311(2)	0.0539(9)
C1S	0.6974(16)	0.2096(10)	0.2857(8)	0.055(4)
H2	-0.1183	0.5743	0.1565	0.040
H3	-0.1849	0.4423	0.1988	0.045

H4	-0.0276	0.3337	0.2050	0.042
H5	0.1953	0.3546	0.1660	0.048
H6	0.2666	0.4872	0.1236	0.038
H8	0.4034	0.6640	0.1579	0.047
H9	0.6233	0.6475	0.1086	0.057
H10	0.6508	0.6104	-0.0173	0.059
H11	0.4641	0.5843	-0.0937	0.063
H12	0.2415	0.5973	-0.0456	0.045
H13A	0.0194	0.6207	-0.0110	0.040
H13B	-0.0799	0.6702	0.0455	0.040
H14A	0.1361	0.7500	-0.0377	0.042
H14B	-0.0199	0.7500	-0.0653	0.042
H16	0.5287	0.6327	0.3086	0.040
H17	0.5989	0.5284	0.2237	0.054
H18	0.5104	0.3933	0.2327	0.066
H19	0.3440	0.3625	0.3232	0.049
H20	0.2726	0.4666	0.4080	0.036
H22	0.3624	0.5154	0.5478	0.032
H23	0.2109	0.4605	0.6376	0.039
H24	-0.0108	0.5113	0.6463	0.036
H25	-0.0845	0.6173	0.5638	0.038
H26	0.0605	0.6702	0.4721	0.030
H27A	0.5151	0.6219	0.5149	0.030
H27B	0.5696	0.6748	0.4439	0.030
H28A	0.4007	0.7500	0.5579	0.032
H28B	0.5640	0.7500	0.5650	0.032

Table B.3. Summary of Crystal Data for **3**

Formula	C ₃₃ H ₄₄ P ₂ PdS ₂ Si ₂
Formula Weight (g/mol)	729.32
Crystal Dimensions (mm)	0.640 × 0.500 × 0.374
Crystal Color and Habit	orange block
Crystal System	monoclinic
Space Group	P 2 ₁ /n
Temperature, K	110
a, Å	16.012(3)
b, Å	12.9746(19)
c, Å	34.994(5)
α, °	90
β, °	102.538(7)
γ, °	90
V, Å ³	7096.8(19)
Number of reflections to determine final unit cell	9442
Min and Max 2θ for cell determination, °	5.66, 133.22
Z	8
F(000)	3024
ρ (g/cm)	1.365
λ, Å, (CuKα)	1.54178
μ, (cm ⁻¹)	6.971
Diffractometer Type	Bruker Kappa Axis Apex2
Scan Type(s)	phi and omega scans
Max 2θ for data collection, °	133.614
Measured fraction of data	0.980
Number of reflections measured	84037
Unique reflections measured	12362
R _{merge}	0.0364
Number of reflections included in refinement	12362
Cut off Threshold Expression	I > 2sigma(I)
Structure refined using	full matrix least-squares using F ²
Weighting Scheme	w=1/[sigma ² (Fo ²)+(0.0346P) ² +7.6144P] where P=(Fo ² +2Fc ²)/3
Number of parameters in least-squares	721
R ₁	0.0283
wR ₂	0.0704
R ₁ (all data)	0.0293
wR ₂ (all data)	0.0710
GOF	1.103
Maximum shift/error	0.004
Min & Max peak heights on final ΔF Map (e ⁻ /Å)	-0.675, 0.622

Table B.4. Atomic Coordinates for **3**

Atom	x	y	z	U _{iso} /equiv
Pd2	0.30530(2)	0.11698(2)	0.60098(2)	0.01114(5)
Pd1	0.80192(2)	0.60152(2)	0.64600(2)	0.01256(5)
S4	0.35012(3)	0.09077(4)	0.67015(2)	0.01450(11)
S3	0.20195(3)	-0.01862(4)	0.59271(2)	0.01511(11)
P4	0.39816(3)	0.25265(4)	0.61237(2)	0.01344(11)
S1	0.66937(3)	0.52277(4)	0.64576(2)	0.01936(12)
P2	0.92889(3)	0.67608(4)	0.64310(2)	0.01513(12)
S2	0.76755(4)	0.62383(4)	0.57717(2)	0.01662(12)
P3	0.26469(4)	0.13918(4)	0.53482(2)	0.01561(12)
P1	0.84754(4)	0.57410(5)	0.71198(2)	0.01725(12)
Si4	0.24030(4)	0.12744(5)	0.69213(2)	0.01610(13)
Si3	0.27438(4)	-0.15450(5)	0.60930(2)	0.01796(13)
Si1	0.57604(4)	0.63812(5)	0.62674(2)	0.01966(14)
Si2	0.75327(4)	0.47179(5)	0.55366(2)	0.01954(13)
C22	0.98742(14)	0.60771(17)	0.61207(7)	0.0167(5)
C60	0.57142(15)	0.28346(19)	0.64651(7)	0.0217(5)
C59	0.65542(15)	0.2517(2)	0.65984(8)	0.0253(5)
C35	0.39674(17)	0.2820(2)	0.53186(7)	0.0260(5)
C53	0.38893(18)	0.4300(2)	0.70879(7)	0.0268(6)
C23	1.02777(15)	0.5149(2)	0.62547(7)	0.0235(5)
C38	0.09848(17)	0.10673(19)	0.48756(7)	0.0225(5)
C17	0.99112(16)	0.8689(2)	0.62492(7)	0.0236(5)
C49	0.37085(14)	0.34897(17)	0.64552(7)	0.0161(5)
C58	0.67617(16)	0.1482(2)	0.65928(8)	0.0247(5)
C18	0.98332(16)	0.9730(2)	0.61565(8)	0.0261(6)
C37	0.14878(15)	0.15118(17)	0.52075(7)	0.0180(5)
C20	0.83168(16)	0.9623(2)	0.61008(7)	0.0244(5)
C57	0.61308(16)	0.07633(19)	0.64515(7)	0.0228(5)
C54	0.41268(16)	0.35541(18)	0.68450(7)	0.0209(5)
C64	0.17584(16)	0.0121(2)	0.69984(7)	0.0243(5)
C10	0.76818(15)	0.5437(2)	0.74038(7)	0.0212(5)
C43	0.29739(16)	0.04066(19)	0.50383(7)	0.0221(5)
C39	0.00992(17)	0.1175(2)	0.47994(8)	0.0274(6)
C16	0.91924(14)	0.81028(18)	0.62708(7)	0.0170(5)
C50	0.30339(15)	0.41724(19)	0.63138(8)	0.0222(5)
C4	0.91985(15)	0.46444(19)	0.72019(7)	0.0212(5)
C19	0.90350(17)	1.01964(19)	0.60856(7)	0.0256(5)
C27	0.98745(15)	0.63981(18)	0.57422(7)	0.0193(5)
C21	0.83954(15)	0.85748(19)	0.61932(7)	0.0203(5)
C25	1.06716(15)	0.48944(19)	0.56383(7)	0.0234(5)
C55	0.50724(14)	0.21147(17)	0.63254(6)	0.0157(4)
C62	0.26939(17)	-0.2010(2)	0.65931(8)	0.0278(6)

C42	0.10972(17)	0.20846(19)	0.54571(7)	0.0249(5)
C56	0.52900(15)	0.10752(18)	0.63196(7)	0.0188(5)
C26	1.02779(16)	0.5816(2)	0.55045(7)	0.0238(5)
C24	1.06715(16)	0.4564(2)	0.60132(8)	0.0257(5)
C63	0.38807(16)	-0.1354(2)	0.60655(9)	0.0306(6)
C65	0.27866(17)	0.1905(2)	0.74106(7)	0.0288(6)
C52	0.32289(17)	0.49723(19)	0.69444(8)	0.0268(6)
C2	0.96891(18)	0.7414(2)	0.72093(8)	0.0320(6)
C40	-0.02792(17)	0.1737(2)	0.50518(8)	0.0299(6)
C11	0.70053(18)	0.6110(2)	0.73879(8)	0.0310(6)
C36	0.41216(16)	0.33597(19)	0.57142(7)	0.0222(5)
C31	0.81248(19)	0.3716(2)	0.58711(8)	0.0322(6)
C51	0.27986(16)	0.49093(19)	0.65567(8)	0.0261(6)
C1	0.90639(18)	0.6804(2)	0.74032(7)	0.0272(6)
C13	0.64222(17)	0.5034(2)	0.78225(8)	0.0317(6)
C41	0.02202(17)	0.2201(2)	0.53788(8)	0.0299(6)
C15	0.77204(16)	0.4549(2)	0.76319(7)	0.0242(5)
C3	1.00617(15)	0.6851(2)	0.68995(7)	0.0235(5)
C44	0.3553(2)	0.0617(3)	0.48041(9)	0.0393(7)
C48	0.26640(19)	-0.0596(2)	0.50380(8)	0.0296(6)
C12	0.63756(18)	0.5906(2)	0.75932(8)	0.0356(7)
C66	0.16699(16)	0.2172(2)	0.65919(8)	0.0277(6)
C28	0.48992(18)	0.6118(2)	0.65392(10)	0.0361(7)
C32	0.64002(18)	0.4292(2)	0.53851(9)	0.0345(7)
C14	0.70931(17)	0.4357(2)	0.78428(8)	0.0298(6)
C34	0.30192(17)	0.25814(19)	0.51639(7)	0.0244(5)
C30	0.61736(17)	0.7716(2)	0.63853(10)	0.0352(7)
C61	0.22824(19)	-0.2609(2)	0.57495(8)	0.0314(6)
C5	0.90608(19)	0.3859(2)	0.69284(8)	0.0303(6)
C9	0.9865(2)	0.4550(3)	0.75285(10)	0.0453(8)
C7	1.0246(2)	0.2914(3)	0.73015(11)	0.0486(9)
C46	0.3502(2)	-0.1140(2)	0.45850(9)	0.0412(8)
C29	0.5278(2)	0.6342(3)	0.57323(9)	0.0396(7)
C6	0.9586(2)	0.2992(2)	0.69758(10)	0.0423(8)
C45	0.3816(2)	-0.0162(3)	0.45819(9)	0.0474(8)
C33	0.7992(2)	0.4733(2)	0.50888(8)	0.0381(7)
C47	0.2924(2)	-0.1357(2)	0.48136(9)	0.0411(8)
C8	1.0379(2)	0.3685(3)	0.75758(13)	0.0581(10)
H60A	0.5578	0.3531	0.6469	0.026
H59A	0.6979	0.3000	0.6692	0.030
H35A	0.4292	0.2183	0.5344	0.031
H35B	0.4169	0.3256	0.5132	0.031
H53A	0.4178	0.4344	0.7348	0.032
H23A	1.0282	0.4923	0.6507	0.028

H38A	0.1240	0.0697	0.4704	0.027
H17A	1.0448	0.8379	0.6297	0.028
H58A	0.7324	0.1269	0.6684	0.030
H18A	1.0316	1.0114	0.6142	0.031
H20A	0.7781	0.9934	0.6049	0.029
H57A	0.6272	0.0069	0.6445	0.027
H54A	0.4568	0.3098	0.6945	0.025
H64A	0.2117	-0.0360	0.7167	0.036
H64B	0.1298	0.0332	0.7116	0.036
H64C	0.1529	-0.0202	0.6751	0.036
H39A	-0.0238	0.0868	0.4579	0.033
H50A	0.2741	0.4130	0.6054	0.027
H19A	0.8984	1.0896	0.6028	0.031
H27A	0.9602	0.7009	0.5648	0.023
H21A	0.7910	0.8190	0.6203	0.024
H25A	1.0935	0.4500	0.5476	0.028
H62A	0.2107	-0.2108	0.6607	0.042
H62B	0.2996	-0.2651	0.6645	0.042
H62C	0.2953	-0.1508	0.6784	0.042
H42A	0.1431	0.2391	0.5678	0.030
H56A	0.4868	0.0589	0.6227	0.023
H26A	1.0285	0.6045	0.5253	0.029
H24A	1.0937	0.3947	0.6104	0.031
H63A	0.3907	-0.1116	0.5809	0.046
H63B	0.4139	-0.0853	0.6257	0.046
H63C	0.4183	-0.1996	0.6117	0.046
H65A	0.3164	0.1444	0.7581	0.043
H65B	0.3086	0.2528	0.7378	0.043
H65C	0.2305	0.2063	0.7523	0.043
H52A	0.3073	0.5467	0.7108	0.032
H2A	0.9395	0.8024	0.7089	0.038
H2B	1.0162	0.7644	0.7414	0.038
H40A	-0.0871	0.1804	0.5002	0.036
H11A	0.6973	0.6706	0.7238	0.037
H36A	0.3731	0.3938	0.5696	0.027
H36B	0.4699	0.3633	0.5773	0.027
H31A	0.8713	0.3917	0.5954	0.048
H31B	0.7875	0.3647	0.6096	0.048
H31C	0.8091	0.3069	0.5736	0.048
H51A	0.2352	0.5361	0.6459	0.031
H1A	0.8650	0.7285	0.7466	0.033
H1B	0.9385	0.6525	0.7649	0.033
H13A	0.6002	0.4903	0.7963	0.038
H41A	-0.0035	0.2590	0.5545	0.036

H15A	0.8167	0.4083	0.7643	0.029
H3A	1.0235	0.6163	0.6992	0.028
H3B	1.0567	0.7215	0.6861	0.028
H44A	0.3765	0.1282	0.4796	0.047
H48A	0.2275	-0.0755	0.5192	0.035
H12A	0.5919	0.6359	0.7576	0.043
H66A	0.1981	0.2775	0.6546	0.042
H66B	0.1441	0.1835	0.6347	0.042
H66C	0.1210	0.2368	0.6713	0.042
H28A	0.5137	0.6135	0.6816	0.054
H28B	0.4461	0.6633	0.6474	0.054
H28C	0.4657	0.5450	0.6468	0.054
H32A	0.6079	0.4795	0.5212	0.052
H32B	0.6376	0.3641	0.5253	0.052
H32C	0.6161	0.4220	0.5612	0.052
H14A	0.7127	0.3770	0.7998	0.036
H34A	0.2910	0.2543	0.4881	0.029
H34B	0.2685	0.3150	0.5231	0.029
H30A	0.6427	0.7763	0.6660	0.053
H30B	0.6596	0.7872	0.6237	0.053
H30C	0.5710	0.8198	0.6320	0.053
H61A	0.1695	-0.2716	0.5761	0.047
H61B	0.2316	-0.2425	0.5488	0.047
H61C	0.2600	-0.3232	0.5824	0.047
H5A	0.8612	0.3910	0.6710	0.036
H9A	0.9965	0.5071	0.7716	0.054
H7A	1.0600	0.2338	0.7335	0.058
H46A	0.3676	-0.1654	0.4434	0.049
H29A	0.5058	0.5664	0.5661	0.059
H29B	0.4820	0.6834	0.5672	0.059
H29C	0.5706	0.6508	0.5588	0.059
H6A	0.9493	0.2470	0.6789	0.051
H45A	0.4210	-0.0013	0.4430	0.057
H33A	0.8578	0.4950	0.5158	0.057
H33B	0.7961	0.4053	0.4978	0.057
H33C	0.7672	0.5202	0.4900	0.057
H47A	0.2707	-0.2021	0.4817	0.049
H8A	1.0821	0.3625	0.7796	0.070

Table B.5. Summary of Crystal Data for 4

Formula	C ₇₂ H ₈₄ F ₆ MnO ₁₀ P ₄ Pd ₂ S ₄
Formula Weight (g/mol)	1743.25
Crystal Dimensions (mm)	0.913 × 0.186 × 0.105
Crystal Color and Habit	red block
Crystal System	triclinic
Space Group	P -1
Temperature, K	110
a, Å	12.949(4)
b, Å	14.113(4)
c, Å	21.576(6)
α, °	99.293(10)
β, °	102.330(15)
γ, °	100.494(12)
V, Å ³	3704(2)
Number of reflections to determine final unit cell	9233
Min and Max 2θ for cell determination, °	6.7, 69.98
Z	2
F(000)	1782
ρ (g/cm)	1.563
λ, Å, (MoKα)	0.71073
μ, (cm ⁻¹)	0.919
Diffractometer Type	Bruker Kappa Axis Apex2
Scan Type(s)	phi and omega scans
Max 2θ for data collection, °	70.292
Measured fraction of data	0.996
Number of reflections measured	121637
Unique reflections measured	32403
R _{merge}	0.0410
Number of reflections included in refinement	32403
Cut off Threshold Expression	I > 2sigma(I)
Structure refined using	full matrix least-squares using F ²
Weighting Scheme	w=1/[sigma ² (Fo ²)+(0.0885P) ² +2.16 83P] where P=(Fo ² +2Fc ²)/3
Number of parameters in least-squares	887
R ₁	0.0465
wR ₂	0.1283
R ₁ (all data)	0.0767
wR ₂ (all data)	0.1537
GOF	1.021
Maximum shift/error	0.001
Min & Max peak heights on final ΔF Map (e ⁻ /Å)	-1.323, 1.774

Table B.6. Atomic Coordinates for **4**

Atom	x	y	z	U _{iso} /equiv
Pd1	0.61216(2)	0.37268(2)	0.32056(2)	0.01675(4)
Pd2	0.70417(2)	0.22978(2)	0.22732(2)	0.01754(4)
Mn1	0.65467(3)	0.18121(3)	0.35417(2)	0.02210(7)
S1	0.53822(4)	0.21509(4)	0.25523(3)	0.01972(10)
S2	0.77819(4)	0.32114(4)	0.33529(3)	0.01935(10)
S3	0.44135(5)	0.18272(5)	0.41534(3)	0.02522(12)
P1	0.45755(5)	0.42371(5)	0.28334(3)	0.01957(11)
P2	0.67930(5)	0.50712(4)	0.40406(3)	0.01978(11)
P3	0.60671(5)	0.14856(4)	0.12580(3)	0.01923(11)
P4	0.87121(5)	0.24890(5)	0.20703(3)	0.02099(11)
F1S	0.4182(2)	0.02831(18)	0.46662(14)	0.0618(7)
F2S	0.31522(17)	0.12611(17)	0.48803(11)	0.0483(5)
F3S	0.4859(2)	0.1656(2)	0.53646(11)	0.0673(8)
O1S	0.78209(15)	0.16197(15)	0.43382(10)	0.0283(4)
O2S	0.63302(16)	0.02575(14)	0.32265(10)	0.0300(4)
O3S	0.55318(15)	0.17406(15)	0.41877(10)	0.0286(4)
O4S	0.36293(18)	0.12242(18)	0.35865(11)	0.0378(5)
O5S	0.4304(2)	0.28120(16)	0.43459(12)	0.0391(5)
C1	0.3985(2)	0.4817(2)	0.34548(14)	0.0279(5)
C1S	0.8975(2)	0.1916(3)	0.44064(16)	0.0353(6)
C2	0.4785(2)	0.5697(2)	0.39315(14)	0.0302(5)
C2S	0.9433(3)	0.1122(3)	0.47009(18)	0.0451(8)
C3	0.5717(2)	0.54367(19)	0.43931(13)	0.0255(5)
C3S	0.8721(3)	0.0919(3)	0.51566(18)	0.0436(8)
C4	0.6823(2)	0.09876(19)	0.07032(12)	0.0240(4)
C4S	0.7616(2)	0.0970(2)	0.47714(16)	0.0339(6)
C5	0.7875(2)	0.1711(2)	0.07240(13)	0.0264(5)
C5S	0.7083(2)	-0.0170(2)	0.29181(17)	0.0352(6)
C6	0.8800(2)	0.1741(2)	0.13121(13)	0.0253(5)
C6S	0.6541(3)	-0.1246(2)	0.26440(16)	0.0354(6)
C7	0.34411(19)	0.33248(18)	0.22783(12)	0.0221(4)
C7S	0.5620(3)	-0.1421(2)	0.2977(2)	0.0486(9)
C8	0.3179(2)	0.3286(2)	0.16112(13)	0.0276(5)
C8S	0.5305(3)	-0.0431(2)	0.30520(18)	0.0401(7)
C9	0.2344(2)	0.2540(2)	0.11955(15)	0.0330(6)
C9S	0.4152(3)	0.1230(3)	0.48048(17)	0.0388(7)
C10	0.1776(2)	0.1825(2)	0.14420(16)	0.0334(6)
C11	0.2037(2)	0.1847(2)	0.21017(16)	0.0326(6)
C12	0.2872(2)	0.2594(2)	0.25196(14)	0.0264(5)
C13	0.4879(2)	0.51811(17)	0.23776(12)	0.0219(4)
C14	0.4083(2)	0.5632(2)	0.20863(15)	0.0313(6)
C15	0.4322(3)	0.6304(2)	0.17051(16)	0.0344(6)

C16	0.5368(3)	0.6549(2)	0.16245(15)	0.0325(6)
C17	0.6172(2)	0.6133(2)	0.19260(14)	0.0292(5)
C18	0.5925(2)	0.54431(18)	0.22916(12)	0.0237(4)
C19	0.7570(2)	0.61866(18)	0.38971(12)	0.0243(4)
C20	0.7421(3)	0.7120(2)	0.41289(16)	0.0344(6)
C21	0.8011(3)	0.7947(2)	0.39868(19)	0.0428(8)
C22	0.8749(3)	0.7854(2)	0.36196(17)	0.0380(7)
C23	0.8918(3)	0.6938(2)	0.33995(17)	0.0365(6)
C24	0.8327(2)	0.6098(2)	0.35299(14)	0.0297(5)
C25	0.7650(2)	0.47942(18)	0.47446(12)	0.0231(4)
C26	0.7233(2)	0.3972(2)	0.49724(13)	0.0284(5)
C27	0.7825(3)	0.3740(2)	0.55206(14)	0.0340(6)
C28	0.8851(3)	0.4327(3)	0.58454(14)	0.0360(6)
C29	0.9269(2)	0.5130(3)	0.56130(14)	0.0345(6)
C30	0.8672(2)	0.5371(2)	0.50646(13)	0.0283(5)
C31	0.5392(2)	0.22921(18)	0.08170(12)	0.0231(4)
C32	0.4597(2)	0.1888(2)	0.02382(13)	0.0289(5)
C33	0.4094(3)	0.2494(2)	-0.01147(14)	0.0347(6)
C34	0.4402(3)	0.3508(2)	0.01045(15)	0.0387(7)
C35	0.5175(3)	0.3913(2)	0.06811(16)	0.0415(8)
C36	0.5671(3)	0.3311(2)	0.10350(14)	0.0317(6)
C37	0.49705(19)	0.04428(17)	0.12061(11)	0.0206(4)
C38	0.5147(2)	-0.05116(19)	0.11512(13)	0.0252(5)
C39	0.4293(2)	-0.1302(2)	0.11041(15)	0.0306(5)
C40	0.3271(2)	-0.1152(2)	0.11252(14)	0.0297(5)
C41	0.3100(2)	-0.0204(2)	0.11949(14)	0.0287(5)
C42	0.3938(2)	0.05886(19)	0.12332(13)	0.0260(5)
C43	0.96964(19)	0.2149(2)	0.26827(13)	0.0250(5)
C44	0.9624(2)	0.1152(2)	0.26851(14)	0.0282(5)
C45	1.0342(3)	0.0861(3)	0.31568(16)	0.0361(6)
C46	1.1136(2)	0.1569(3)	0.36299(16)	0.0402(7)
C47	1.1205(2)	0.2559(3)	0.36292(15)	0.0376(7)
C48	1.0489(2)	0.2855(2)	0.31596(14)	0.0306(5)
C49	0.9291(2)	0.3733(2)	0.20167(14)	0.0280(5)
C50	1.0322(2)	0.3978(2)	0.18984(18)	0.0375(7)
C51	1.0714(3)	0.4915(3)	0.1815(2)	0.0538(10)
C52	1.0091(3)	0.5620(3)	0.1845(3)	0.0626(12)
C53	0.9080(3)	0.5395(3)	0.1968(3)	0.0557(11)
C54	0.8686(2)	0.4452(2)	0.20571(18)	0.0376(7)
S1S	0.85199(6)	-0.15723(6)	0.15975(4)	0.03149(14)
F4S	1.0128(2)	-0.2040(2)	0.11393(15)	0.0659(7)
F5S	0.8974(2)	-0.1544(2)	0.04749(11)	0.0654(7)
F6S	1.01123(19)	-0.05060(17)	0.12714(13)	0.0575(6)
O6S	0.7936(2)	-0.25796(18)	0.13438(13)	0.0451(6)

O7S	0.78977(19)	-0.08459(18)	0.14657(13)	0.0421(5)
O8S	0.9208(2)	-0.1365(2)	0.22435(12)	0.0518(7)
C10S	0.9479(3)	-0.1407(2)	0.10954(17)	0.0384(7)
O9S	0.2188(4)	-0.1166(4)	0.2661(2)	0.1042(14)
C11S	0.1859(7)	-0.1259(4)	0.3263(3)	0.0912(19)
C12S	0.1868(6)	-0.2222(5)	0.3394(3)	0.0344(13)
C16S	0.2355(8)	-0.1949(7)	0.3525(5)	0.052(2)
C13S	0.2598(5)	-0.2580(4)	0.3061(2)	0.0710(14)
C14S	0.2499(4)	-0.2150(4)	0.2461(2)	0.0599(11)
O10S	0.1921(4)	0.5700(4)	0.0703(3)	0.0463(11)
C17S	0.2042(10)	0.4756(8)	0.0416(6)	0.071(3)
C18S	0.1775(10)	0.4655(9)	-0.0295(6)	0.074(3)
C19S	0.1748(8)	0.5651(7)	-0.0417(5)	0.062(2)
C20S	0.2145(6)	0.6348(5)	0.0320(3)	0.1086(18)
O11S	0.2145(6)	0.6348(5)	0.0320(3)	0.1086(18)
C21S	0.2670(11)	0.5632(9)	0.0005(7)	0.085(3)
C22S	0.2129(11)	0.4752(10)	0.0071(8)	0.085(3)
C23S	0.0973(13)	0.4915(11)	0.0126(8)	0.105(4)
C24S	0.1202(11)	0.6093(9)	0.0255(7)	0.086(3)
H1A	0.3344	0.5039	0.3239	0.033
H1B	0.3734	0.4321	0.3698	0.033
H1SA	0.9280	0.2573	0.4697	0.042
H1SB	0.9135	0.1939	0.3980	0.042
H2A	0.4379	0.6054	0.4194	0.036
H2B	0.5097	0.6153	0.3681	0.036
H2SA	0.9357	0.0527	0.4366	0.054
H2SB	1.0205	0.1367	0.4938	0.054
H3A	0.5405	0.4892	0.4582	0.031
H3B	0.6054	0.6014	0.4754	0.031
H3SA	0.8966	0.1423	0.5565	0.052
H3SB	0.8714	0.0259	0.5260	0.052
H4A	0.7002	0.0375	0.0818	0.029
H4B	0.6356	0.0816	0.0255	0.029
H4SB	0.7203	0.0308	0.4523	0.041
H4SC	0.7194	0.1235	0.5064	0.041
H5A	0.7733	0.2379	0.0738	0.032
H5B	0.8104	0.1518	0.0322	0.032
H5SB	0.7778	-0.0104	0.3239	0.042
H5SC	0.7232	0.0167	0.2567	0.042
H6A	0.9500	0.2008	0.1220	0.030
H6B	0.8795	0.1060	0.1372	0.030
H6SA	0.7053	-0.1673	0.2750	0.043
H6SB	0.6260	-0.1370	0.2167	0.043
H7SA	0.5007	-0.1954	0.2705	0.058

H7SB	0.5869	-0.1590	0.3403	0.058
H8A	0.3572	0.3772	0.1439	0.033
H8SA	0.4845	-0.0358	0.2640	0.048
H8SB	0.4913	-0.0347	0.3397	0.048
H9A	0.2166	0.2523	0.0743	0.040
H10A	0.1206	0.1319	0.1159	0.040
H11A	0.1647	0.1354	0.2271	0.039
H12A	0.3053	0.2602	0.2971	0.032
H14A	0.3372	0.5477	0.2150	0.038
H15A	0.3773	0.6596	0.1500	0.041
H16A	0.5531	0.7005	0.1361	0.039
H17A	0.6892	0.6320	0.1883	0.035
H18A	0.6474	0.5143	0.2487	0.028
H20A	0.6915	0.7190	0.4384	0.041
H21A	0.7904	0.8582	0.4144	0.051
H22A	0.9141	0.8421	0.3518	0.046
H23A	0.9443	0.6878	0.3157	0.044
H24A	0.8438	0.5467	0.3369	0.036
H26A	0.6538	0.3569	0.4751	0.034
H27A	0.7535	0.3183	0.5675	0.041
H28A	0.9257	0.4173	0.6223	0.043
H29A	0.9971	0.5523	0.5829	0.041
H30A	0.8964	0.5929	0.4911	0.034
H32A	0.4397	0.1194	0.0084	0.035
H33A	0.3544	0.2215	-0.0503	0.042
H34A	0.4080	0.3925	-0.0143	0.046
H35A	0.5367	0.4607	0.0835	0.050
H36A	0.6206	0.3595	0.1430	0.038
H38A	0.5848	-0.0622	0.1146	0.030
H39A	0.4412	-0.1951	0.1057	0.037
H40A	0.2693	-0.1695	0.1092	0.036
H41A	0.2405	-0.0096	0.1217	0.034
H42A	0.3810	0.1235	0.1278	0.031
H44A	0.9083	0.0669	0.2364	0.034
H45A	1.0292	0.0181	0.3156	0.043
H46A	1.1627	0.1372	0.3952	0.048
H47A	1.1746	0.3041	0.3952	0.045
H48A	1.0540	0.3537	0.3164	0.037
H50A	1.0749	0.3499	0.1876	0.045
H51A	1.1413	0.5079	0.1737	0.065
H52A	1.0363	0.6259	0.1780	0.075
H53A	0.8658	0.5878	0.1991	0.067
H54A	0.7995	0.4298	0.2147	0.045
H11B	0.2361	-0.0757	0.3629	0.109

H11C	0.1120	-0.1138	0.3224	0.109
H11D	0.2088	-0.0616	0.3573	0.109
H11E	0.1060	-0.1478	0.3170	0.109
H12B	0.2119	-0.2186	0.3865	0.041
H12C	0.1134	-0.2657	0.3232	0.041
H16B	0.3029	-0.1604	0.3858	0.063
H16C	0.1866	-0.2326	0.3739	0.063
H13A	0.2403	-0.3309	0.2942	0.085
H13B	0.3350	-0.2368	0.3336	0.085
H13C	0.2090	-0.3232	0.2964	0.085
H13D	0.3345	-0.2667	0.3212	0.085
H14B	0.1931	-0.2589	0.2094	0.072
H14C	0.3197	-0.2043	0.2335	0.072
H17B	0.1551	0.4231	0.0536	0.085
H17C	0.2798	0.4693	0.0575	0.085
H18B	0.1062	0.4198	-0.0497	0.088
H18C	0.2333	0.4396	-0.0477	0.088
H19A	0.1006	0.5686	-0.0637	0.075
H19B	0.2251	0.5847	-0.0685	0.075
H20B	0.2930	0.6655	0.0432	0.130
H20C	0.1734	0.6873	0.0361	0.130
H21B	0.2592	0.5658	-0.0458	0.102
H21C	0.3451	0.5759	0.0224	0.102
H22B	0.2508	0.4562	0.0465	0.102
H22C	0.2063	0.4230	-0.0312	0.102
H23B	0.0758	0.4660	0.0492	0.125
H23C	0.0408	0.4606	-0.0280	0.125
H24B	0.0794	0.6313	-0.0117	0.103
H24C	0.0992	0.6361	0.0651	0.103

KYLE NICHOLAS WILLIAM ROZIC

EDUCATION

M.Sc., Inorganic Chemistry

The University of Western Ontario, London, ON, Canada. Jan. 2014 – Present
Area of Study: Low Nuclearity Metal-Chalcogen Cluster Synthesis.

H.B.Sc., Chemistry

Lakehead University, Thunder Bay, ON, Canada. Sept. 2008 – Sept. 2013
Area of Study (H.B.Sc. thesis): Electrochemical Study of TiO₂ Nanotubes Modified with RuO₂ and IrO₂.

AWARDS AND HONOURS

❖ Dean's List – Lakehead University 2013

PROFESSIONAL EXPERIENCE

Teaching Assistant

The University of Western Ontario, London, ON, Canada. Jan. 2014 – Present

Responsibilities/Area of Focus:

- ❖ Laboratory
 - Supervising of laboratories
 - Demonstrating and explaining the procedures of experiments
 - Setting up experiments
- ❖ Grading
 - Prelab reports
 - Video exercises
 - Lab reports
- ❖ Proctoring
 - Tests, midterms and quizzes

COURSE EXPERIENCE

- ❖ Chem 9541B Crystallography I 80
- ❖ Chem 9531Q Molecular Energy Conversion 83
- ❖ Chem 9503S Advanced NMR Spectroscopy 72
- ❖ Chem 9658Y Graduate Seminar 84